US Army Corps of Engineers

MISCELLANEOUS PAPER CERC-88-12

COASTAL PROCESSES AT SEA BRIGHT TO OCEAN TOWNSHIP, NEW JERSEY

VOLUME I: MAIN TEXT AND APPENDIX A

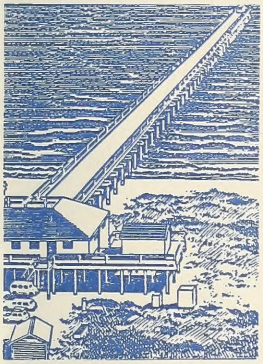

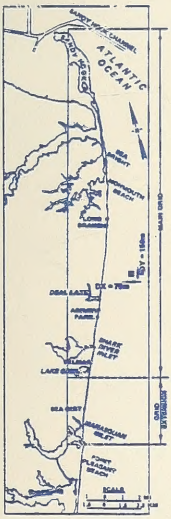

by

Nicholas C. Kraus, Norman W. Scheffner, Hans Hanson
Lucia W. Chou, Mary A. Cialone, Jane M. Smith, Thomas A. Hardy

Coastal Engineering Research Center

DEPARTMENT OF THE ARMY
Waterways Experiment Station, Corps of Engineers
PO Box 631, Vicksburg, Mississippi 39181-0631

August 1988
Final Report

Approved For Public Release; Distribution Unlimited

Prepared for US Army Engineer District, New York
26 Federal Plaza
New York, New York 10278-0090

Destroy this report when no longer needed. Do not return it to the originator.

The findings in this report are not to be construed as an official Department of the Army position unless so designated by other authorized documents.

The contents of this report are not to be used for advertising, publication, or promotional purposes. Citation of trade names does not constitute an official endorsement or approval of the use of such commercial products.

Unclassified
SECURITY CLASSIFICATION OF THIS PAGE

REPORT DOCUMENTATION PAGE

Form Approved
OMB No. 0704-0188
Exp. Date: Jun 30, 1986

1a. REPORT SECURITY CLASSIFICATION
Unclassified

1b. RESTRICTIVE MARKINGS

2a. SECURITY CLASSIFICATION AUTHORITY

3. DISTRIBUTION/AVAILABILITY OF REPORT
Approved for public release; distribution unlimited.

2b. DECLASSIFICATION/DOWNGRADING SCHEDULE

4. PERFORMING ORGANIZATION REPORT NUMBER(S)
Miscellaneous Paper CERC-88-12

5. MONITORING ORGANIZATION REPORT NUMBER(S)

6a. NAME OF PERFORMING ORGANIZATION
USAEWES, Coastal Engineering Research Center

6b. OFFICE SYMBOL (If applicable)

7a. NAME OF MONITORING ORGANIZATION

6c. ADDRESS (City, State, and ZIP Code)
PO Box 631
Vicksburg, MS 39181-0631

7b. ADDRESS (City, State, and ZIP Code)

8a. NAME OF FUNDING/SPONSORING ORGANIZATION
US Army Corps of Engineers

8b. OFFICE SYMBOL (If applicable)

9. PROCUREMENT INSTRUMENT IDENTIFICATION NUMBER

8c. ADDRESS (City, State, and ZIP Code)
Washington, DC 20314-1000

10. SOURCE OF FUNDING NUMBERS

PROGRAM ELEMENT NO.	PROJECT NO.	TASK NO.	WORK UNIT ACCESSION NO

11. TITLE (Include Security Classification)
Coastal Processes at Sea Bright to Ocean Township, New Jersey; Volume I: Main Text and Appendix A; Volume II: Appendixes B-G

12. PERSONAL AUTHOR(S)
See reverse.

13a. TYPE OF REPORT	13b. TIME COVERED	14. DATE OF REPORT (Year, Month, Day)	15. PAGE COUNT
Final report	FROM Jan 85 TO Aug 86	August 1988	297

16. SUPPLEMENTARY NOTATION
See reverse.

17. COSATI CODES		
FIELD	GROUP	SUB-GROUP

18. SUBJECT TERMS (Continue on reverse if necessary and identify by block number)
Beach erosion
Coastal processes
New Jersey
Sand transport
Sandy Hook
Sea Bright
Shoreline change

19. ABSTRACT (Continue on reverse if necessary and identify by block number)

This report describes a study of coastal processes along the Atlantic Coast from Sea Bright to Ocean Township, New Jersey. Predictive tools were developed and a data analysis made to assist in evaluation and implementation of comprehensive shore protection plans for this highly utilized stretch of coastline. The study was divided into four broad areas as: (1) deepwater wave climate analysis and nearshore wave refraction, (2) numerical modeling of long-term shoreline change, (3) numerical modeling of storm-induced beach erosion, and (4) development of stage-frequency relations for the back bay and ocean coast. A literature review of previous studies and results of the four tasks are given in Volume I of the report. Volume II contains listings and interpretations of coastal processes data assembled in the study, including data on profiles, shoreline change, sediment sizes, and incident waves. The study represents an integrated attempt to quantitatively evaluate long and short-term coastal processes on a regional scale for use in engineering design.

20. DISTRIBUTION/AVAILABILITY OF ABSTRACT
☒ UNCLASSIFIED/UNLIMITED ☐ SAME AS RPT. ☐ DTIC USERS

21. ABSTRACT SECURITY CLASSIFICATION
Unclassified

22a. NAME OF RESPONSIBLE INDIVIDUAL

22b. TELEPHONE (Include Area Code)

22c. OFFICE SYMBOL

DD FORM 1473, 84 MAR

83 APR edition may be used until exhausted.
All other editions are obsolete.

SECURITY CLASSIFICATION OF THIS PAGE
Unclassified

12. PERSONAL AUTHOR(S) (Continued).

Kraus, Nicholas C.; Scheffner, Norman W.; Hanson, Hans; Chou, Lucia W.; Cialone, Mary A.; Smith, Jane M.; Hardy, Thomas (Volume I). Kraus, Nicholas C.; Gravens, Mark B.; Mark, David J. (Volume II).

16. SUPPLEMENTARY NOTATION (Continued).

Volume II (Appendixes B-G) was published under separate cover. Copies of Volume I (main text and Appendix A) and Volume II are available from National Technical Information Service, 5285 Port Royal Road, Springfield, VA 22161.

PREFACE

The coastal processes study reported herein was requested by US Army Engineer District, New York (NAN) as part of a comprehensive plan of shore protection for Sea Bright to Ocean Township, New Jersey. This investigation was conducted by personnel of the US Army Engineer Waterways Experiment Station (WES) Coastal Engineering Research Center (CERC) during the period January 1985 to August 1986. Messrs. Silvio Calisi and James C. Urbelis were NAN Technical Monitors during the study, and Mr. Joseph Vietri and Ms. Lynn M. Koeth were Technical Monitors during the final review and publication phase of the report.

Results are contained in two volumes. Volume I presents the main narrative, including problem statement, background information, procedures, and principal results. Volume II contains data sets that were processed and/or generated in the course of the study, including offshore and nearshore wave information, shoreline change statistics, and plots of beach profiles.

Volume I was written by Dr. Nicholas C. Kraus, Dr. Norman W. Scheffner, Dr. Hans Hanson, Ms. Lucia Chou, Ms. Mary A. Cialone, Ms. Jane M. Smith, and Mr. Thomas A. Hardy. Dr. Hanson, Lecturer, Department of Water Resources Engineering, University of Lund, Sweden, was visiting researcher in Research Division, CERC, during the period August 1985 to February 1986. Volume II was written by Dr. Nicholas C. Kraus, Mr. Mark B. Gravens, and Mr. David J. Mark. Ms. Kathryn J. Gingerich assisted in preparation of the final draft of the report. Work performed in this study was under the general supervision of Mr. H. Lee Butler, former Chief, Coastal Processes Branch, Research Division and presently Chief, Research Division; Dr. Steven A. Hughes, former Chief, Coastal Processes Branch; Dr. Edward F. Thompson, Chief, Oceanography Branch; and Dr. James R. Houston and Mr. Charles C. Calhoun, Jr., Chief and Assistant Chief, CERC, respectively.

Commander and Director of WES during publication of this report was COL Dwayne G. Lee, EN. Dr. Robert W. Whalin was Technical Director.

CONTENTS

* Appendixes B-G (Volume II) were published under separate cover. Copies are available from National Technical Information Service, 5285 Port Royal Road, Springfield, VA 22161.

LIST OF TABLES

LIST OF FIGURES

CONVERSION FACTORS, NON-SI TO SI (METRIC)
UNITS OF MEASUREMENT

Non-SI units of measurement used in this report can be converted to SI (metric) units as follows:

Multiply	By	To Obtain
cubic yards	0.7646	cubic metres
cubic yards per year	0.7646	cubic metres per year
feet	0.3048	metres
feet per second	0.3048	metres per second
inches	2.54	centimetres
knots (international)	0.5144444	metres per second
miles (US statute)	1.6093	kilometres
miles (nautical)	1.8520	kilometres
yards	0.9144	metres

VOLUME 1: MAIN TEXT AND APPENDIX A

PART I: INTRODUCTION

Scope of Work

1. The US Army Engineer Waterways Experiment Station (CEWES), Coastal Engineering Research Center (CERC) was requested to provide technical assistance to the US Army Engineer District, New York (CENAN), in an engineering study of coastal processes along the Atlantic Coast from Sea Bright to Ocean Township, New Jersey. The study was funded by a series of four DA Form 2544 "Intra-Army Orders for Reimbursable Services" dated 21 February 1985, 22 March 1985, 2 January 1986, and 4 June 1986.

2. The purpose of the study is to provide predictive tools and interpret data to assist in evaluation and implementation of CENAN's comprehensive shore protection plan for this highly utilized stretch of coastline. Stage-frequency relationships for the study site are also generated for the back-bay and ocean coast.

3. A preliminary shore protection plan is contained in the report "Reanalysis of the Federally Authorized Project Atlantic Coast of New Jersey Sandy Hook to Barnegat Inlet with Emphasis on Sea Bright to Monmouth Beach" (Corps of Engineers (CE) 1984). The 1984 report reanalyzes and describes modifications to shore protection plans for the north New Jersey coast that had been the subject of a previous but now dated comprehensive and unified CENAN study entitled "Atlantic Coast of New Jersey, Sandy Hook to Barnegat Inlet, Beach Erosion Control Report on Cooperative Study (Survey)" (CE 1954).

4. Technical portions of the present study were accomplished as four interconnected tasks. The individual tasks are:

a. Wave refraction analysis.

b. Numerical modeling of long-term shoreline change.

c. Numerical modeling of storm-induced beach erosion.

d. Development of stage-frequency relationships.

The main results and narrative for these four tasks are presented in this

volume. Volume 2 (Kraus, Gravens, and Mark 1988) contains the associated appendices with supplementary analyses and data.

5. The wave refraction study (Task a) encompassed a hindcast of the wave climate and refraction analyses for the existing bathymetry and hypothetical bathymetries as modified by possible beach fill borrow dredging in the offshore. Task b involved development of a numerical model of long-term shoreline change, based on longshore sand transport rates calculated by use of wave information from Task a. The shoreline change model allows inclusion of numerous groins and a seawall already located on the coast, as well as additional groins, removal and modification of existing groins, and placement of beach fill.

6. The beach erosion numerical model developed in Task c permits an estimation of storm-induced erosion of material placed to protect the seawall at the study site. This model was specifically adapted for the present study and incorporates a boundary condition to account for the presence of the seawall. Recession-recurrence curves were calculated through use of storm statistics available from Task d. Task d involved the addition of storm ensemble enhancements to a previous CERC study, the "Fire Island to Montauk Point Storm Surge Study (FIMP)" (Prater, Hardy, and Butler in preparation; Prater, Butler, and Hardy in preparation; Butler and Prater 1987), and computation of stage-frequency relationships for tidal and storm events in the Navesink and Shrewsbury Rivers.

Organization of this Report

7. This report is divided into six parts. Part I gives an introduction. Part II provides a short review of related literature, summarizes important previous work, and describes present conditions at the project site. Parts III - VI respectively present the results of the four individual study tasks listed in paragraph 4. Appendices given in Volume 2 contain supplementary information on the wave hindcast statistics (Appendix B), representative wave refraction patterns (Appendix C), historical shoreline and beach profile change (Appendix D), open-ocean borrow sites (Appendix E), wave refraction changes at borrow sites (Appendix F), and back-bay stage-frequency curves (Appendix G). The appendices contain considerable background data and

additional results and explanation of the various analyses performed in this study.

Units of Measurement

8. In conformance with the trend in the United States to employ SI (metric) units of measurement in engineering and science, calculations and data analyses associated with numerical models newly developed in this study were performed and reported in metric units. Most historical engineering work for the north New Jersey coast has been done in American customary units, whereas in the related scientific literature dealing with this coast numerical values are given in metric form. For tasks a, b, and c, numerical values have usually been expressed in metric form; however, certain tables and citations contain customary unit conversions. In particular, customary units were employed in discussion of previous engineering results and design specifications in order to provide continuity and ease of cross reference. A table containing conversion factors is given on page 7.

PART II: HISTORICAL AND EXISTING CONDITIONS

9. This chapter gives a review of previous work to provide a summary of independent results and data pertinent to the study, as well as to identify sources of supplementary information. Detailed and comprehensive background information, as well as the original authorized plan, can be found in two CE reports (CE 1954, 1984). These reports should be consulted for the history and design of the project.

Orientation to the Study Area

10. The study area is located on the northern coast of New Jersey (Figure 1). The authorized project concerns the approximately 51-mile*-long (82 km) stretch of coast from Sea Bright to Barnegat Inlet (CE 1954). In the original improvement plan, the northern portion of this stretch is divided into four regions: Sandy Hook, Sea Bright to Ocean Township, Asbury Park to Manasquan, and Point Pleasant Beach to Seaside Park (CE 1954, p 2 and Table D-1 therein). Ocean Township does not typically appear on maps, but it is a political entity located broadly in the vicinity of Deal and Asbury Park.

11. The reanalysis of the authorized project (CE 1984) focused on the approximately 8-mile-long (12.8 km) section of shoreline along the adjoining boroughs of Sea Bright and Monmouth, both located in Monmouth County. The width of this section of the barrier spit varies from approximately 100 to 400 m, and the elevation varies between approximately 1 and 4 m above mean low water (MLW). The wave refraction, long-term shoreline change, and storm-induced beach erosion tasks of the present study were specifically done for the Sea Bright to Ocean Township section. However, neighboring areas were also considered since they had to be incorporated in the boundary conditions of the modeling. An added major task of this study, not directly addressed in the 1954 and 1984 CE reports, deals with storm surge and inundation in the back-bay areas of the Navesink and Shrewsbury Rivers.

12. The ocean-fronting coast from Sea Bright to Ocean Township is heavily structured, including an almost continuous, massive rubble mound stone

---

* A table of factors for converting non-SI units of measurement to SI (metric) units is presented on page 7.

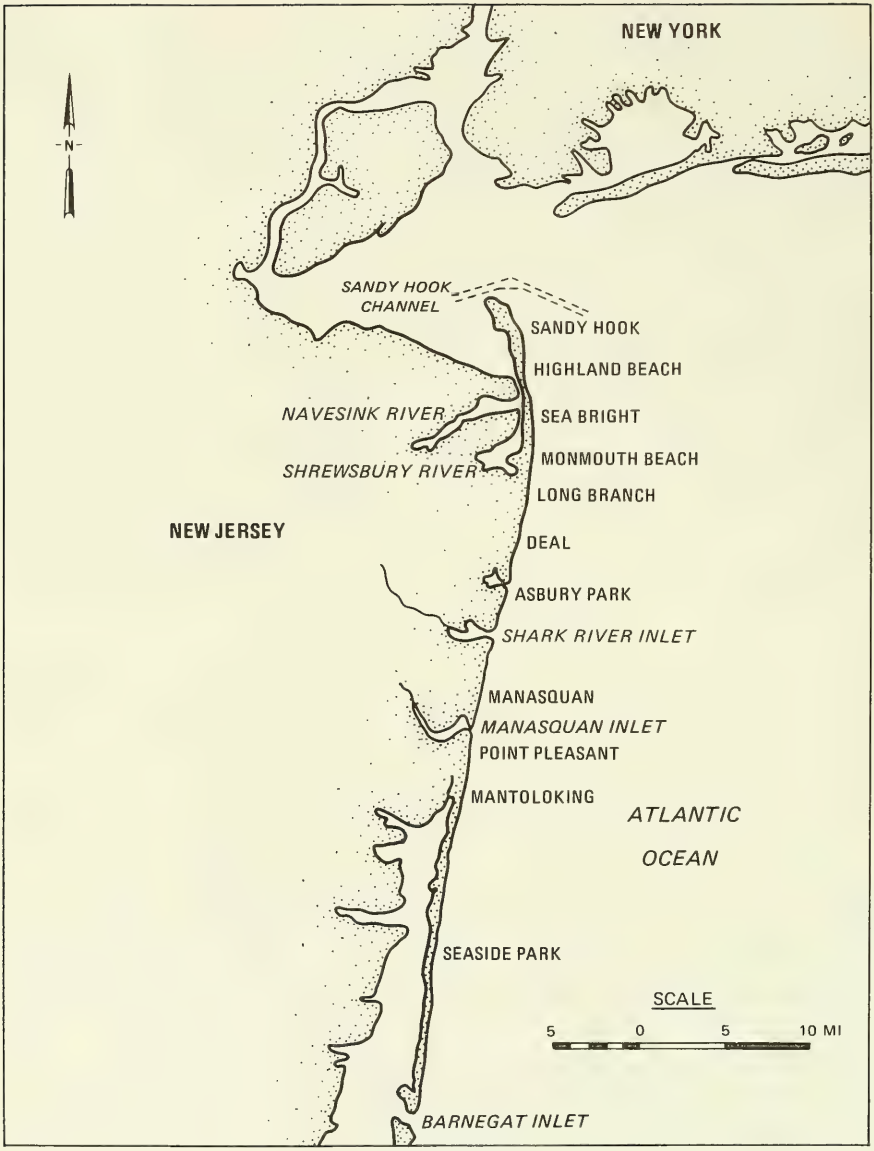

Figure 1. Location map for the study area

seawall built in sections in 1898, 1947, and the 1950s (Figures 2 and 3). This ocean coast has been suffering from chronic shoreline erosion for more than a century. Numerous groins have been constructed since about 1910 to maintain the beach (Figures 4 and 5), and beachfills have been placed by local interests, State Government, and Federal Government. Depletion of the sandy beach reduces the integrity of the seawall, increasing the risk of catastrophic failure of the wall during a storm.

Review of Previous Studies

13. A comprehensive annotated bibliography on the coastal literature of the northern New Jersey coast is given in a CERC report (Gorman 1988) companion to this project. The work of Kondolf (1978), Gares (1981), and Heritage Studies (1985) may also be consulted for general historical and geological information.

14. Many coastal geology and geomorphology studies have been made for Sandy Hook. In contrast, few published geologic or coastal engineering studies can be found for the highly structured coast to the south of Sandy Hook, which includes the present project area, Sea Bright to Ocean Township.

15. One of the most well-known applied studies in the field of coastal engineering was the budget analysis performed by Caldwell (1966) for the New Jersey coast. This paper introduced and refined basic techniques that have been incorporated in virtually all subsequent coastal budget analyses. Other pertinent coastal processes-related studies of the area are the wave hindcast of Saville (1954), the visually observed breaking wave conditions at Monmouth Beach compiled by Helle (1958), and the wave hindcast and sediment transport analysis of Fairchild (1966).

16. The literature on Sandy Hook will be introduced, followed by a critical review of general engineering and coastal processes literature on the north New Jersey coast.

Sandy Hook

17. Sandy Hook is one of the most famous spits in the world. It is approximately 10 miles long (16 km) and projects northward from the New Jersey barrier island chain into the New York Bight. Sandy Hook Lighthouse serves as a reliable landmark for intercomparison of numerous shoreline maps available from the 18th century to present. Shoreline change at Sandy Hook figured

Figure 2. Seawall and groins along Highland Beach looking north toward Sandy Hook

Figure 3. Seawall and groin at Sandy Hook (looking south)

Figure 4. Aerial view of groin field at North Long Branch

Figure 5. Impoundment at functioning groin in study area

prominently in the sediment budget analysis of Caldwell (1966), and the morphology and dynamics of the spit have been extensively studied by researchers associated with Rutgers, The State University of New Jersey (e.g., Allen 1981a,b; Allen and Nordstrom 1977a; Nordstrom et al. 1982; Phillips, Psuty, and McCluskey 1984). Kondolf (1978) and Gares (1981) present accounts of the history and geology of Sandy Hook. The annotated bibliography by Gorman (1988) contains a comprehensive list of references on Sandy Hook.

18. By definition, as a spit, Sandy Hook is an accretionary feature. Numerous researchers have concluded that the majority of sediment originally forming the spit was derived from erosion of the northern 30 km of the New Jersey barrier island shore, along which the predominant longshore drift is to the north (CE 1954, Caldwell 1966). Sandy Hook Lighthouse, originally built 30 m from the northern tip in 1764 (cf. Kondolf 1978, p 35), now lies some 2 km inland. Allen (1981a) performed budget analyses for the time intervals 1953-1976 and 1971-1978 and concluded, on the basis of aerial photographs, that Sandy Hook had an average material loss of 270,000 cu m/year in the interval 1971-1978.

19. Removal of potential updrift sources of littoral material due to seawall and revetment construction is probably the major cause of erosion along Sandy Hook. An additional factor may be convergence of wave energy due to refraction (Allen 1981a). Caldwell (1966) assumed that groins have caused limited sand starvation at Sandy Hook. However, it should be noted that groins have a finite trapping capacity; once the limit of trapping of a groin field is reached, sand transported alongshore is expected to pass through the field.

20. Researchers at Rutgers University have termed the 2-km-long region of Sandy Hook just north of Sea Bright (more precisely, north of Highland Beach) the "critical zone," because of its susceptibility to erosion. The critical zone is of interest to the present project since the numerical model of shoreline change had to be calibrated for this area (cf. Part IV). Nordstrom et al. (1982, p 6) state that the average shoreline recession rate along the critical zone for the period 1943-1972 was 5.3 m/year and for 1973-1982, 30 m/year obtained mainly on the basis of aerial photograph interpretation. Survey data available in the present study give a recession rate of 8.2 m/year with a standard deviation of 0.97 m for the interval 1971-1982. Both data sets indicate significant erosion. Differences in recession rates

may be explained by the different methods of analysis and somewhat different time periods. In response to the threat of breaching caused by severe erosion along this stretch of shoreline, 1,824,000 cu m of fill were emplaced on the critical zone between November 1982 and August 1983. A monitoring study of the fill was made by Phillips, Psuty, and McCluskey (1984) (see also Slezak et al. 1984).

21. Process characteristics. Data on visually measured breaking wave characteristics (wave height, direction, and period), longshore currents, sediment grain size, and shoreline and beach profile change at various locations along Sandy Hook have been published in a number of reports and articles (e.g., Nordstrom 1975, Nordstrom et al. 1982, Allen 1985). Of particular relevance to the wave refraction task (Part III) are the breaking wave conditions, for which the aforementioned reports contain data spanning several hundred measurement days. Typical values of breaking wave height are in the range 0.1-0.8 m; wave period in the range 3-9 sec; and breaking wave angle 5-15 deg, where a positive angle corresponds to waves out of the south. Measured waves were generally out of the south with relatively large breaking angles. Longshore sand transport rates in the aforementioned reports were estimated through either changes in shoreline position or from predictive formulas based on breaking wave data. The erosion rate obtained for the critical zone for recent times (1971-1978) is given as 270,000 cu m/year (Allen 1981a) or about 70 percent of the transport rate determined by Caldwell (1966), discussed below.

22. Allen and Nordstrom (1977b) report preliminary results of a numerical modeling study that involved wave refraction and shoreline modeling of the critical zone of Sandy Hook. A wave ray refraction model was coupled to a shoreline change model. Final results do not appear to have been published. In their preliminary work, it can be inferred that some interpretation problems arose in the refraction modeling due to caustics and the irregular spacing of wave rays alongshore. No shoreline change model results are given, but the large alongshore grid spacing (100-1000 m) and long time step (1 year) would produce results of questionable accuracy and validity in the statistical sense. In the present study, an advanced refraction model allowed calculation of wave refraction at a fixed interval alongshore (150 m), and the shoreline model incorporated a finer alongshore grid spacing of 50 m and a time step of 6 hr. These specifications are appropriate to the length and time scale of

naturally occurring wave and shoreline change. The refraction model is described in Part III, and the shoreline change model is described in Part IV.

Project area

23. In contrast to the considerable literature on Sandy Hook, few published studies are available on the coastal processes along the heavily structured shoreline from Sea Bright to Shark River Inlet. A catalogue of selected structures along the New Jersey coast contains clear photographs, dating from the 1920's to 1961, of groins and seawall sections along Deal, Monmouth, Sea Bright, and neighboring beaches (CE 1964). The location and condition of modern groins from Sea Bright to Asbury Park are described in an unpublished collection of groin inspection sheets (Coastal Planning and Engineering, undated, Circa 1985) prepared under contract for CENAN.

24. Wave data. Helle (1958, pp 6 and A-7 therein) compiled monthly statistics on visual observations of breaking waves off Monmouth Beach Lifeboat Station from 1954-1957. Wave height, direction (point on the compass), and period were averaged for 10 significant waves at 4-hr intervals during daylight hours. Fifty percent of the breaking wave heights in the observation period were less than 3 ft (0.9 m), 85 percent were less than 4 ft (1.2 m), and less than 5 percent were greater than 5.5 ft (1.7 m). Breaking wave heights larger than 6 ft (1.8 m) occurred rarely, and no waves higher than 10 ft (3.0 m) were recorded. Average wave periods were typically in the 5-9 sec range. For 36 months of the 37-month observation period, the majority of the waves were out of the southeast and east; during 1 month waves were mainly out of the northeast. Very rare occurrences of waves out of the north and south were reported.

25. The report of Saville (1954) presents results of a hindcast made for four stations along the north Atlantic coast. Two of the stations are relevant to this report: New York Harbor, north of Sandy Hook, and Cape May, at the end of the New Jersey barrier island chain. The hindcast was performed by hand using techniques that have been superceded in the CE by automated techniques employed in the present report (Part III).

26. Fairchild (1966) interpolated values of wave parameters from the 1954 hindcast (Saville 1954) to obtain wave heights and angles "at the shoreline" along the north New Jersey coast, including the vicinity of the project area. His procedure and results, although pioneering, are somewhat ambiguous due to the hybrid methodology employed. The shoreward limit of the refraction

calculation, made by the wave ray method, was at the 30-ft contour, after which the wave angle at the shoreline apparently was obtained by a straight line extension of the wave ray to the shoreline. Limitations of the procedure were recognized by the original author. Yearly averages of the longshore component of wave energy flux at the shoreline were calculated by use of the wave refraction results. Longshore sediment transport rates available from the study of Caldwell (1966) described below were correlated with the calculated energy fluxes. A positive correlation was found among widely scattered data. The trend in longshore sediment transport direction, to the north at Sandy Hook and to the south at Cape May, was qualitatively discussed based on differences in local wave energy distributions related to shadowing by Long Island. This result agrees with the generally held conceptual model of bifurcation of the longshore current on the New Jersey coast (cf., e.g., Ashley, Halsey, and Buteux 1986) and can be considered a milestone in coastal processes modeling.

27. Long-term Shoreline Change and Longshore Sediment Transport. The article of Caldwell (1966) has served as the basis for most subsequent sediment transport work on the New Jersey coast and will be described in detail. The transport rates calculated through shoreline change mapping appear to be based in great part on work done in the 1954 CE report, supplemented by additional data such as impoundment rates at the north jetty at Cold Springs Inlet at Cape May Harbor. Caldwell made a budget analysis using historic shoreline change data available from 1838 to 1953. These data are presented in chart form in the 1954 CE report and were digitized in the present study. Properties and interpretation of these and more recent shoreline and beach profile data are given in Appendix D. There are minor discrepancies in dates of shoreline surveys in comparison of the CE 1954 report and Caldwell (1966). Three of the earlier surveys were taken over a period of several years, namely, 1836-1839, 1964-1874, and 1875-1899 according to topographic sheets included in CE 1954. CE 1954, Caldwell (1966), and the present report assign an average or representative year to these survey intervals which may slightly differ between sources. Also, Table 11 in the CE 1954 report gives a transport rate for the interval 1933-1951, but no survey for the year 1951 could be located in the present work. Caldwell (1966) used the year 1953, for which shoreline position data are available in CE 1954, as described in Appendix D.

28. Caldwell (1966, p 154) inferred local average yearly longshore

sediment transport rates or "littoral drift" mainly from areal changes between shoreline surveys. Four shoreline reaches in the project area were examined by this method. The bifurcation or nodal point in the longshore transport rate was located at Dover Township, between Manasquan Inlet to the north and Barnegat Inlet to the south. North of Dover Township the net transport rate was found to be directed to the north, increasing from 0 at the section Mantolokung to Manasquan, to 74,000 cu yd/year between Manasquan and Asbury Park, 319,000 cu yd/year from Asbury Park to the base of Sandy Hook, and 493,000 cu yd/year along Sandy Hook (Figure 6). The transport rate along Sandy Hook during the approximate 50-year interval 1899-1953 was 12 percent lower than that for the previous approximate 60-year interval (1838-1899). This decrease was attributed to active groin and jetty construction. However, this conclusion cannot be applied to long-term changes since the beach in a groin field may eventually reach a filled state and thereafter bypass sand. Also, errors in measurement and interpretation of shoreline position and beach profiles are probably larger than 10 percent, making firm conclusions about a 12 percent change in transport rate doubtful. Additional seawall construction in the compared time interval may have reduced the transport rate by eliminating sources of sand that might otherwise be transported north.

29. In order to compute volumetric beach change based on shoreline data, not only change in shoreline position but also associated profiles for the compared dates must be available. Caldwell did not specifically address this critical third dimension in his paper. For the 1885 and 1933 surveys, profiles were compared to "about the 30-foot mean low water contour" (CE 1954, p 44). The budget analysis technique requires the compared profiles to match at a pinch-off depth or depth of closure. Even with modern ocean survey techniques, pinch-off depth is a difficult quantity to determine, and inspection of profiles shown in Appendix D reveals some lack in achievement of pinch-off. The shape of the active profile also changes according to season, with large volumes of sediment translating on-offshore. Volume differences between complex and varied profiles are difficult to calculate by hand. Therefore, some subjectivity entered Caldwell's analysis, but has gone undocumented. However, because of the long time periods involved, over which considerable shoreline change occurred, the order of magnitude of Caldwell's results (also CE 1954) is probably reliable.

30. In this paragraph, a short summary is given of the shoreline change

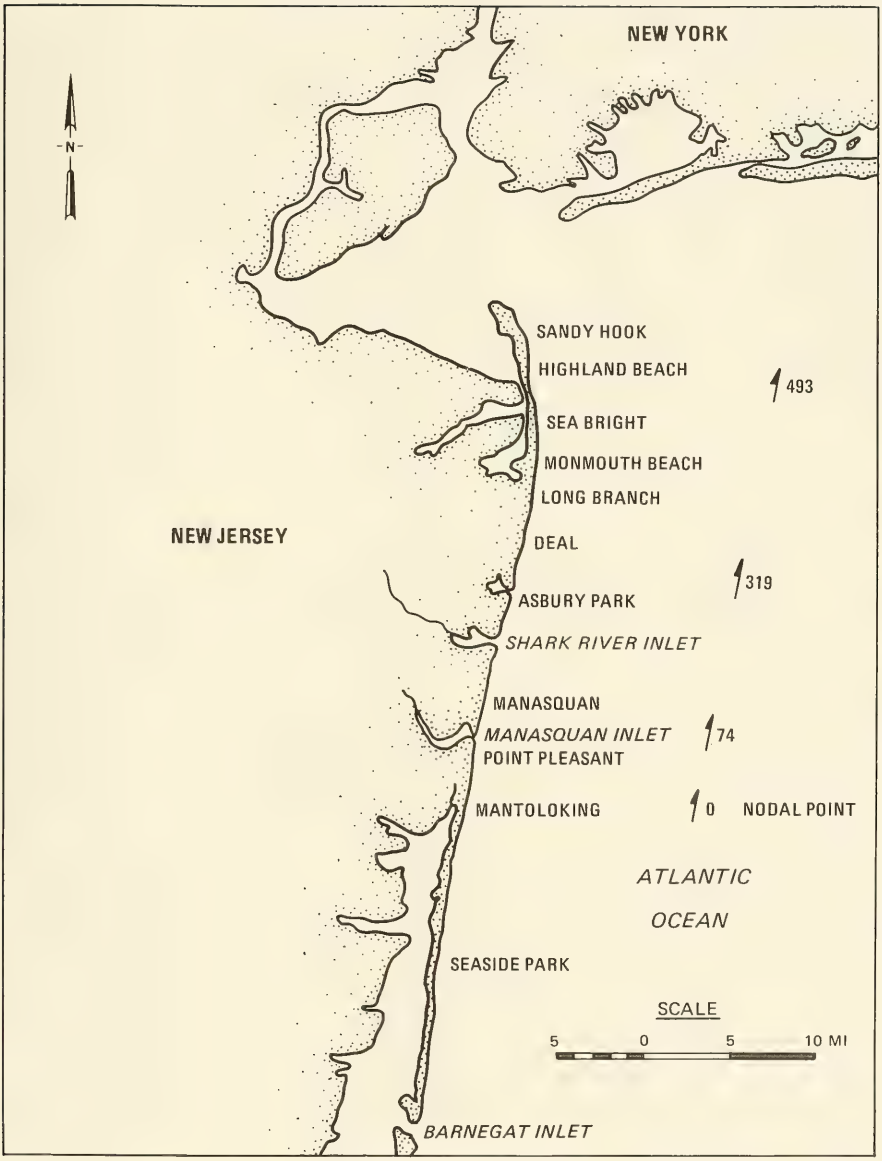

Figure 6. Historical longshore sediment transport rates (thousands of cubic yards/year) (after Caldwell 1966)

data and interpretations contained in Appendix D. In recent years, the rate of shoreline change on this highly protected coast has been low, but exhibiting a tendency for erosion. As an example, the average recession rate along the project reach in the time interval 1953-1985 was 0.17 m/year (Table D-18). The recession rate is low because the beach has effectively retreated to the seawall along much of the reach. For specific sections with existing sandy beaches, such as the northern portion of Sea Bright and north Long Branch, the recession rates in the same time interval were 0.84 and 1.18 m/year, respectively. These rates of shoreline retreat are comparable to historic rates existing prior to the modern era of significant shore protection. For example, Table D-7 shows that the average shoreline recession rate for the period 1836-1932 was 0.85 m/year, with several sections of the coast experiencing rates twice the average. Based on these and other data contained in Appendix D, the potential rate of shoreline recession can estimated to be on the order of 1 m/year. The potential rate applies to a sandy beach; for the numerous areas where the beach has eroded to the seawall, the recession rate will approach zero.

31. Other reports. Two unpublished reports (PRC Harris, Inc. 1980; Farrell 1981) also contain longshore sediment transport rate analyses. PRC Harris developed longshore transport rate estimates for Manasquan Inlet using four methods: adoption of best known rate at a nearby site, historical changes in topography, wave energy flux, and an empirical predictive method. Although some lower transport rates were obtained, most calculations for various time periods resulted in rates of 300,000-400,000 cu yd/year, and this range of values was recommended for sand bypassing design.

32. The report of Farrell (1981), based on original analysis of pre- and post-survey dredged volumes measured during the interval 1968-1980 for Manasquan Inlet and Shark River Inlet, presents longshore sediment transport rates much lower than other estimates. The annual rate for the recent 13-year period is 22,200 cu yd/year. Farrell compared his results with those of PRC Harris (1980) and discussed possible reasons for the order of magnitude difference. It is noted that transport rates calculated using the shoreline change numerical model developed in the present report (Part IV) lie between the rates determined by Caldwell (1966) and Farrell (1981)

33. Sea level rise. The scope of this study did not include an investigation of sea level rise. Based on data from the Sandy Hook tide gage

for 1940-1980, the rate of sea level rise in the study area has been estimated at 4.0-5.0 mm/year (Hicks 1978; Hicks, Debaugh, and Hickman 1983). Sea level rise will result in an apparent shore recession (e.g., Bruun 1962). The subject of sea level rise in the project area is discussed further by Gorman (1988), and a general discussion of the potential economic consequences of sea level rise has been given by Weggel (1986).

PART III: WAVE REFRACTION ANALYSIS

34. This chapter describes procedures and results of the wave refraction task of the study. The wave refraction task consisted of three steps. As a first step, the Wave Information Study (WIS) technique (Jensen 1983) was used to generate a 20-year hindcast time series of wave height, direction, and period. In the second step, a numerical model of wave refraction was applied to obtain a time series of representative wave conditions at fixed points alongshore. The resultant wave heights and directions provided the principal input to drive the shoreline change model, described in Part IV. The third step was an evaluation of refraction over two potential open-ocean beach fill borrow sites.

Wave Hindcast

35. As discussed in Part II, there are no long-term wave measurements available for the vicinity of the project. Therefore, the required wave information was generated by means of the WIS hindcast technique. WIS provides a 20-year hindcast for the US Atlantic Ocean coast for the years 1956-1975. Phase II of this hindcast includes a 20-year time series of wave height, wave direction, and wave period at 3-hr intervals for both sea and swell components at a point off the north New Jersey coast. This Phase II point (Station 23) is located about 30 km offshore and is shown on Figure 7. For the purpose of the present study, the time series of wave characteristics at this point was used as wave input to the Phase III transformation technique. This technique involves transformation of the deepwater wave conditions to a specified water depth, taking into account the effects of wind-wave interaction, refraction and shoaling over straight and parallel bottom contours, and the sheltering of wave energy by Long Island. Bottom features on a horizontal scale less than 18.5 km are not incorporated in the Phase III transformation, i.e., grid cell dimensions in the WIS technique are on the order of 18.5 km.

36. Although WIS Phase III information for the area of the project site is available at Station 54, which lies off the project area at a depth of 10 m, a special Phase III run was made to compute the hindcast wave time series at the depth of the seaward boundary of the nearshore refraction grid.

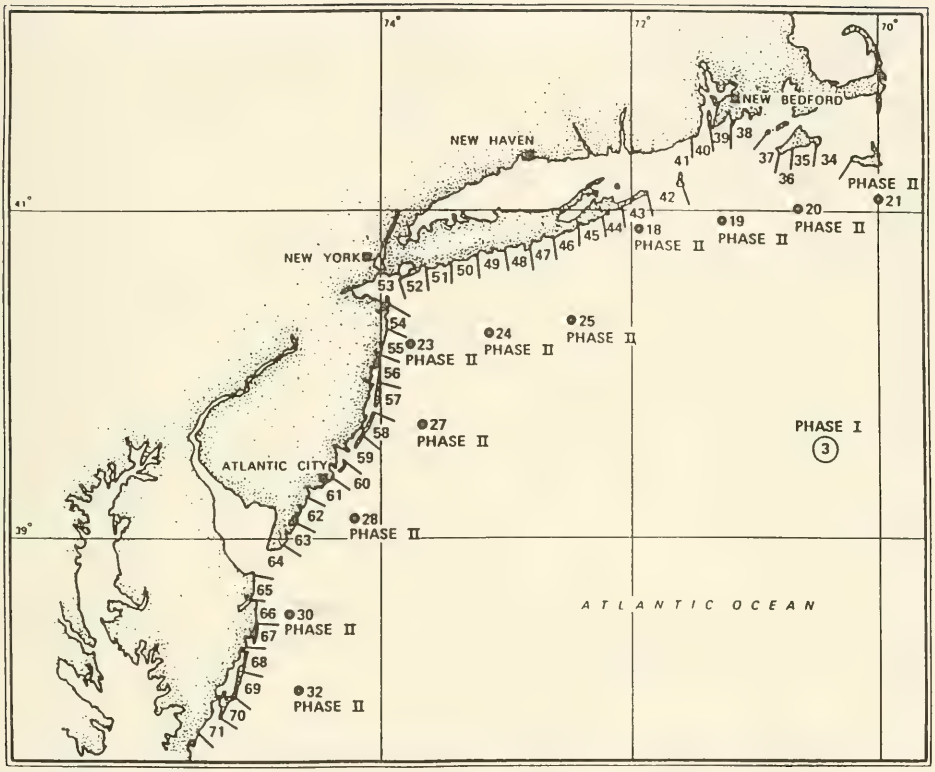

Figure 7. Locations of phase stations for shallow-water wave information along the Atlantic coast, Region Z

The WIS transformation was therefore halted at a depth of 18.29 m (60 ft) MLW. Since the Phase III technique does not adequately describe wave propagation and transformation over irregular and greatly varying nearshore bathymetry, a fine-meshed nearshore grid and wave refraction model were employed to bring the waves into shallower water, with the WIS hindcast providing the input.

Characteristics of the
wave hindcast data set

37. Each year of the hindcast contains values of significant wave height, peak spectral period, and peak spectral direction for both sea and swell (6 values) at 3-hr intervals for a total of 17,520 values per year. (More precisely, WIS provides an estimate of an energy-based wave height called H_{mo}*; however, for deep water, H_{mo} is effectively equivalent to the significant wave height, H_s, which is defined as the average wave of the highest one-third of the waves in the record or observation.) General statistics for each year of the WIS Phase III hindcast (Appendix B) were compiled as given in Tables 1 and 2. Table 1 gives a comparative summary of the significant wave height and peak spectral period by year, and Table 2 summarizes characteristics of the hindcast according to wave direction. The orientation of the coast is shown in Figure 8. In Table 1, the column labeled "Events" gives the ordinal number of the 62 largest storms occurring in the 20-year hindcast for the associated year. The column labeled "Greater than H_{savg}" marks those years with an average significant wave height greater than the 20-year average. The right-hand column contains general observations resulting from the comparison of yearly statistics. A more detailed summary of the statistics determined in the hindcast can be found in Appendix B.

38. The 200 largest wave heights from the 20-year WIS hindcast were identified for use in possible future work along this coast. The 200 highest waves occurred in 62 storms ("Events" in Table 1). Appendix B gives a table of the 200 largest wave heights ranked in descending order, together with the corresponding date, wave period, and wave direction measured from the south. The largest wave height in each storm is preceded by a line containing asterisks and the ranking of the storm, based on the largest wave height it contained.

---

* For convenience, symbols and abbreviations are listed in the Notation, Appendix A.

Table 1

Summary of Selected Yearly Statistics and Properties of the WIS Hindcast for the North New Jersey Coast

Year	H_{savg} (m)	T_p (sec)	H_{smax} (m)	Events	Greater than H_{savg}	General Comments
1956	0.50	7	3.35	15,54	Yes	Many long periods
1957	0.45	7	3.25	37	-	Typical year
1958	0.44	7	3.31	30,31,53	-	Typical year
1959	0.39	7	3.34	29,51	-	Some long periods
1960	0.45	8	3.63	10,17,18,36,52	-	Typical year
1961	0.48	8	3.40	16,55	Yes	Many long periods
1962	0.48	4,7	6.87	1,11,20,41,42, 60,61,62	Yes	Very skewed toward high waves
1963	0.40	7	2.88	62	-	Lacks 9 & 10-sec waves
1964	0.46	7	3.63	12,21,22,40,59	Yes	Lacks long periods
1965	0.39	7	3.29	23,39	-	None > 9 sec
1966	0.40	7	3.68	5	-	Lacks long periods
1967	0.49	8	3.18	38,43,44	Yes	Typical year
1968	0.41	7	3.26	24,25,57,58	-	Typical year
1969	0.50	7	3.61	13,19,45	Yes	Many long periods
1970	0.43	7	3.49	14,46,56	-	Typical year
1971	0.46	7	3.30	26,48	Yes	Lacks long periods
1972	0.49	7	4.57	2,27,28,34,47,49	Yes	Lacks long periods
1973	0.47	6	4.14	4,9,32,35	Yes	Typical year
1974	0.45	7	4.17	3,8,33,50	-	Typical year
1975	0.43	8	3.66	6,7	-	Typical year
AVG	0.45	7	3.70			

Notation: H_{savg}, H_{smax} denote average and maximum significant wave height, respectively; T_p denotes the peak spectral wave period.

Table 2

Summary of Frequency of Occurrence and Wave Height Characteristics from the WIS Hindcast for the North New Jersey Coast

	N	NNE	NE	ENE	E	ESE	SE	SSE	S
Percent Occur.	0.0	0.0	0.0	7.7	15.0	9.9	10.8	27.9	13.3
Average H_s (m)	0.00	0.00	0.00	0.37	0.83	0.62	0.61	0.49	0.24
Maximum H_s (m)	0.00	0.00	0.00	2.37	6.87	4.60	4.14	3.09	1.10

Notation: H_s denotes significant wave height.

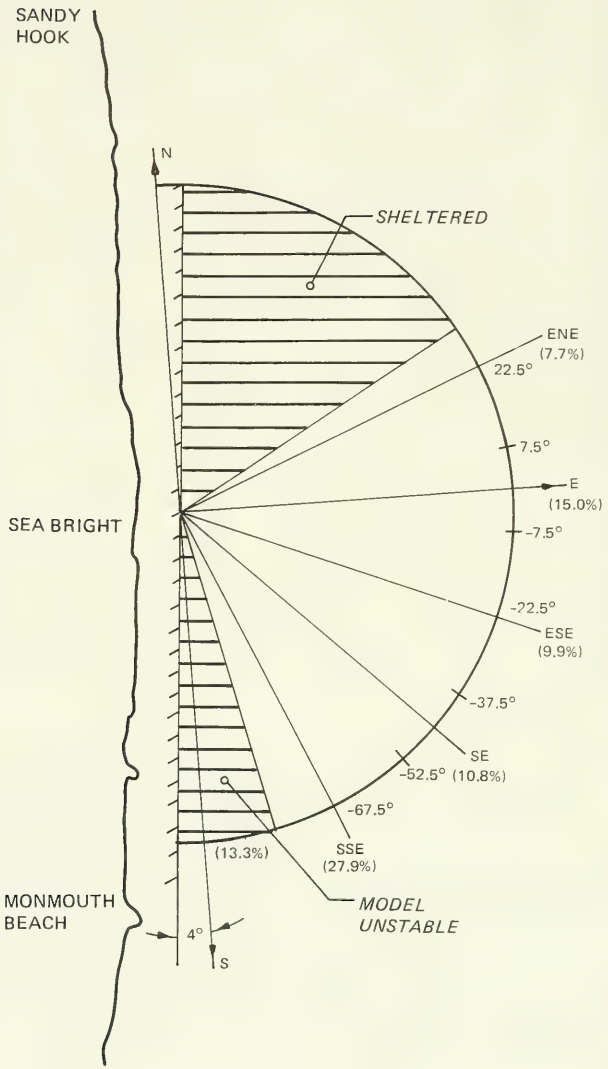

Figure 8. Wave angle bands defined by WIS relative to the shoreline trend along Sea Bright to Ocean Township

39. From Table 1 it is seen that the average significant wave height is 0.45 m and the average maximum yearly significant wave height is 3.70 m. The largest wave height, 6.87 m, which defines Event 1, occurred during the notorious 3 March 1962 "5-High" storm, which had a duration that lasted through 5 high tides.

40. Table 2 (see also Figure 8) shows that 61.9 percent of the hindcast waves originated out of the southern sector (from S through ESE), 15 percent were out of the east, and 7.7 percent were out of the east-northeast. The total is 84.6 percent. The remainder, 15.4 percent, represents the occurrence of completely calm wave conditions, for which neither sea nor swell existed. The zero occurrences in Table 2 for most of the northern sector are a result of wave sheltering by Long Island, New York, discussed in the next paragraph. Due to the bias for waves to originate from the south, the predominant direction of longshore sediment transport at the project area is expected to be from south to north. This is in general agreement with the commonly accepted direction of transport along this coast. The local orientation of the shoreline and wave refraction over the irregular bottom must be incorporated for more quantitative discussion of longshore sediment transport.

41. Wave Sheltering. The WIS Phase III wave generation technique allows for wave sheltering by large land masses. In the present case, Long Island restricts the fetch of winds and propagation of waves out of the north directed toward the north New Jersey coast. The directional distribution of the potential wave population is modified in two ways if sheltering enters the hindcast. For wind seas, the energy within discrete direction bands is removed (zeroed) if the orientation of the sheltering land body would preclude propagation of waves in the band. For the swell component, all energy in the geometric shadow zone of the land mass is removed. For the north New Jersey coast, the sheltering effect of Long Island is greatest at Sandy Hook and decreases with distance to the south. The single WIS hindcast specifically performed for this study was assumed to be valid for the project reach; i.e., the differential effect of shadowing with distance along the coast was assumed to be negligible.

Selection of representative wave conditions

42. The shoreline model (described in Part IV) requires input of representative wave conditions. Since the purpose of the model is to simulate

shoreline change occurring over several years, unusually high wave energy and low wave energy years in the hindcast were avoided. The consequences of severe storm events are treated with the beach erosion model, discussed in Part V.

43. The representative wave data set is to be used for both calibration and verification of historical (measured) shoreline change and prediction of future shoreline change. Since wave data are not available in either case, a deterministic interpretation of the input wave data set is not possible. However, one can obtain a representative data set with which certain parameters can be varied to estimate the range of variability given by the model (the wave and shoreline models). To keep computer file sizes within manageable limits, 3 years of data were selected from among the 20 years of available hindcast data to produce the representative wave data set.

44. From consideration of Table 1, the consecutive years 1973 through 1975 were judged to be suitable to represent the total data set. The average significant wave height for these 3 years is equal to the average wave height for the 20-year total. One year, 1973, has an average significant wave height above the 20-year average, and each of the selected 3 years contains two of the highest ten wave energy events occurring among the 20 years. The average peak spectral period for these years ranges from 6-8 sec, which gives a spread of values around the commonly occurring 7-sec peak period. Since wave refraction and shoaling are to a large extent controlled by wave period, this spread is a desirable feature.

45. As mentioned above, the chosen 3-year wave set possesses an average wave height equal to the average of the available 20 years of hindcast data, a characteristic compatible with the function of the shoreline change model. A complementary characteristic is that the data set includes slightly more high-wave energy events than average to account for realistic stormier conditions. It is noted that the 3-year record employed is much longer than records typically reported in shoreline modeling literature, in which only a small number of representative conditions, such as seasonal averages, are repeated numerous times over the simulation period.

Nearshore Refraction Simulation

Wave transformation model

46. An estimation of wave transformation from the nominal 18.29-m (60 ft) depth to the nominal 3-m depth (10 ft) along the coast was made by application of the Regional Coastal Processes Wave Model, RCPWAVE (Ebersole, Prater, and Cialone 1986). RCPWAVE was specifically designed for use in projects with large spatial extent, such as in the present case. This model is superior to classical wave ray refraction procedures in that energy propagation along wave crests due to irregular bathymetry is accounted for in addition to energy propagation in the direction of ray travel. The model is also more efficient than wave ray models since the governing equations are solved directly on a user-specified depth grid in the horizontal plane (by an iterative finite-difference solution scheme) rather than by ray shooting and interpolation to the grid.

47. Basic assumptions used in RCPWAVE are:

a. Mild bottom slopes

b. Linear, monochromatic, and irrotational waves

c. Negligible wave reflection

d. Negligible energy losses due to bottom friction or wave breaking outside the surf zone

48. These assumptions are common to most numerical models used for engineering application. Results from the model are expected to be adequate for estimating longshore sand transport rates.

49. Model Grid and Boundary Conditions. The main model grid (Figure 9) is rectangular with a mesh of 106 cells across-shore (positive x-axis directed offshore) and 240 cells alongshore (positive y-axis directed north). The cell spacing alongshore was set at 150 m; the cross-shore cell spacing was 75 m. This grid spacing is fine-meshed for wide-area modeling, but it was considered the minimum necessary to resolve any systematic irregularities in the breaking wave pattern that might be induced by unusual bottom features in the area.

50. The main grid covers the coast from Sandy Hook navigation channel on the north to a point just beyond Lake Como. Across-shore, the grid extends from inland of the present shoreline seaward to approximately the 20-m contour. The grid was extended well outside the Sea Bright to Ocean Township project area to eliminate possible contamination from the lateral boundary conditions.

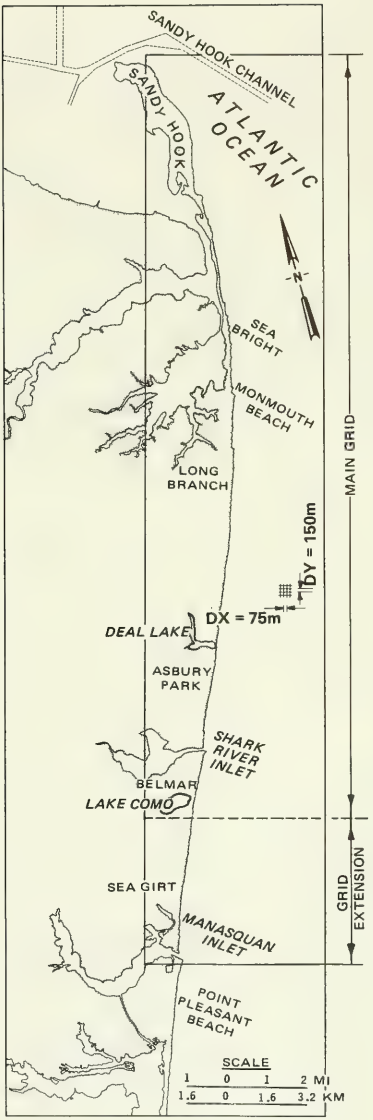

Figure 9. Grid used in the nearshore refraction calculation

51. At a later stage in this study, the grid was extended on the south to permit simulations of refraction over potential beachfill borrow sites located off the township of Belmar. The 106 by 39 grid cell extension began at Lake Como and ended at Manasquan Inlet. This extension made possible the incorporation of three profile lines from the 1985 survey not located on the main (original) grid. Revision of the original grid to incorporate the 1985 profile survey information is described below.

52. The grid was overlaid on National Oceanic and Atmospheric Administration (NOAA) nautical chart No. 12324 (Edition 22, dated January 1984) to assign an average depth to each cell, interpolating as necessary. The depths at the centers of grid cells were transferred to a computer file for use as model input. A 3-dimensional plot was made of the bathymetry to provide a visual check (Figure 10).

53. Wave height, direction, and period as determined from the Phase III WIS hindcast provided the required offshore boundary values for RCPWAVE. The default lateral boundary condition is a "no-flow" condition equivalent to specifying a plane beach at the sides. RCPWAVE was modified to save values of a transformation coefficient related to wave height (described further below) and wave direction at fixed points alongshore at a nominal 3-m depth for input to the local wave refraction and breaking simulation routine employed by the shoreline change model.

Model runs

54. Test runs were made to verify proper operation of the model. During the testing phase, it was noted that on some runs, waves propagating northward, approximately parallel to shore (out of the south, Table 2), caused model instability. Examination of this condition indicated these waves would refract offshore at certain locations, a possibility not accommodated by RCPWAVE and of no physical significance. In order to represent waves from the south without concern for rare exceptions producing model instability, input Phase III waves out of the south were reassigned to the southeast sector.

55. Production refraction model runs were made in an innovative way to eliminate the expense of making a computer run for each offshore wave condition in the WIS 3-year time series. Direct use of the time series of wave height, direction, and period at 6-hr intervals would require 8,760 runs (sea and swell). The cost to make this enormous number of runs and to store the results would be prohibitive. The procedure would also be misleading since

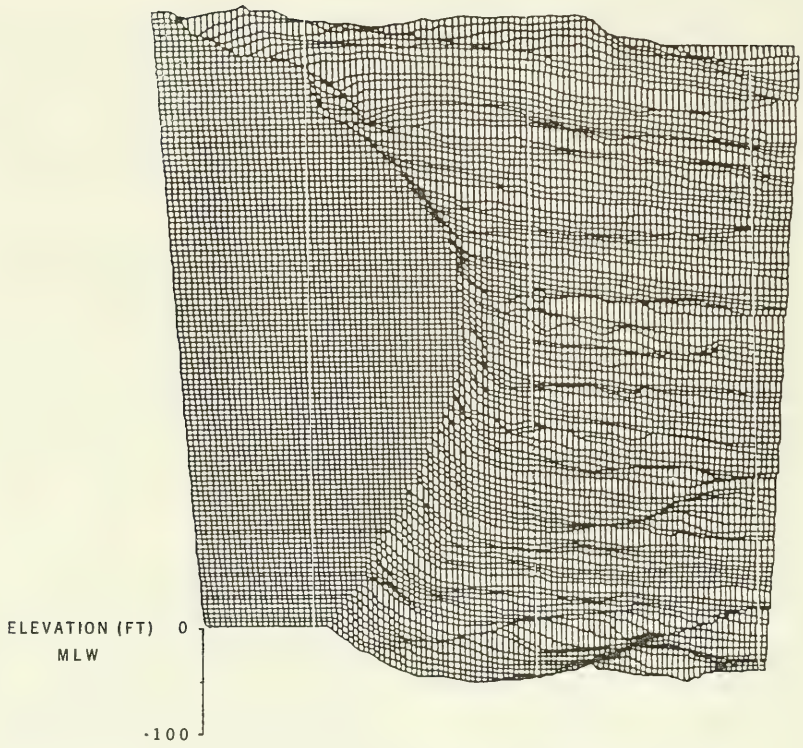

Figure 10. Nearshore bathymetry based on NOAA nautical chart No. 12324 (Edition 22, dated January 1984)

the accuracy of the shoreline change model is not compatible with such detailed information. Instead, 56 deepwater wave conditions were selected to represent the wave climate. The 56 conditions are defined by all possible combinations of wave periods and directions given in Table 3. The directions given in Table 3 are with respect to an imaginary line normal to the trend of the shoreline. Thus, a wave direction of 0 deg would correspond to waves incident normal to the coast.

Table 3
Selected Deepwater Wave Periods and Directions

Period (sec)	Direction (deg)
4.0	22.5
6.0	7.5
7.5	-7.5
8.5	-22.5
9.5	-37.5
10.5	-52.5
11.5	-67.5
12.5	

Note: Directions defined in Figure 8.

56. A unit (1-m) wave height was used for each calculation period and direction combination. Since the model RCPWAVE is based on linear wave theory, the transformed unit wave height can be interpreted as the product of combined refraction, diffraction, and shoaling coefficients (called a transformation coefficient here). The actual value of the wave height at a particular grid point is obtained as the product of the transformation coefficient and the deepwater wave height in the WIS time series. Thus, although deepwater wave period and direction were described by a limited number (56) of combinations, the wave height appearing in each wave condition in the 3-year time series was utilized.

57. The output of the production runs consists of the transformation coefficient and wave direction at the nominal 3-m depth at each of the 240 longshore grid lines. In linear wave theory, employed by RCPWAVE, the wave

period does not vary in the refraction process. The results from all model runs were compiled into one random access file keyed on input wave period and direction. Knowledge of the deepwater wave height associated with each set of WIS wave conditions allows rapid calculation of nearshore wave properties. Plots showing the results of selected refraction model runs were made to further verify proper operation of the model and to give a visualization of the results. Selected plots are contained in Appendix C.

Time series processing

58. A program was developed to link the 3-year time series of the hindcast wave results at the 18.29-m depth to the results of the wave model runs to create a time series of wave height, period, and direction at the 3-m depth at each longshore grid line. The program reads one record of WIS data (height, direction, and period of sea and swell components) and defines a key, based on input period and direction, for both the sea and swell component. The keys are then used to enter the random access file and extract transformed wave conditions. The transformed wave height at each grid line at the 3-m depth is obtained as the product of the transformation coefficient and the deepwater wave height in the WIS record. The sea component is limited by the calculated TMA limit (Hughes 1984), which is the maximum wind sea that can occur at a given depth and period. (The acronym "TMA" derives from locations of field experiments used to verify the theory.)

59. The shoreline change model requires input wave conditions at 6-hr intervals. Therefore, every other record of the hindcast time series was analyzed. To conserve computer memory and file space, only the component (sea or swell) with the greater energy flux per unit length of shoreline was saved in the output file. If both components had wave heights of less than 20 cm (0.66 ft) at the seaward boundary of the grid, no results were saved because neither component is expected to have sufficient energy to produce significant longshore sediment transport. In the shoreline model, this condition was treated as a calm wave condition of effective zero wave height. This technique of imposing a threshold, although somewhat arbitrary, resulted in a significant reduction in calculation time. Analysis of the original and processed time series showed that the energy flux of the processed series was 24 percent less than that of the original series due to the removal of the numerous low wave energy events. Field experiments performed by CERC subsequent to the present study support the concept of a threshold in longshore sediment

transport of the magnitude employed in the model (Kraus and Dean 1987).

60. The final output from this program is a sequential file that contains a 3-year time series of effective wave heights, periods, and directions at 6-hr intervals at the nominal 3-m depth for each of the 240 longshore grid lines. This file constitutes the principal wave input for the numerical model of shoreline change.

Revision of nearshore bathymetry and additional refraction runs

61. At the request of CENAN, in May and June, 1985, staff of CERC's Field Research Facility (FRF) in Duck, North Carolina, made beach profile surveys in the project and neighboring beach area. Many of the control points used in the 1953 (CE 1954) and 1961 surveys were reestablished. In coordination with CENAN and CERC personnel involved in the numerical modeling tasks, profile surveys were made at a density of approximately four lines per mile of shoreline in the stretch between the north end of Sea Bright and the south side of Shark River Inlet. In all, 68 lines were surveyed by the FRF in 1985. These lines extended from the control point well onshore, typically landward of the seawall, to a nominal depth of 9 m (30 ft). Elevations were measured relative to the National Geodetic Vertical Datum (NGVD). Sixty-five of the 68 lines are located on the main refraction grid. The positions of the survey lines were converted from the original Easting and Northing coordinates to latitude and longitude and transferred to NOAA chart No. 12324. Depths from the surveys were read on to the grid and the bathymetry updated. Limited extrapolation and interpolation were done to update grid values immediately adjacent to the survey lines.

62. The 1985 profile data became available after the processed time series and 56 refraction runs had already been generated. In order to determine whether it would be necessary to repeat this considerable effort for the updated bathymetry, five refraction runs were made with unit wave height for the pre-1985 (original) and 1985 (updated) bathymetries. Selected pairs of wave period and direction were 8 sec, -67.5 deg; 10 sec, -52.5 deg; 8 sec, -7.5 deg; 5 sec, -22.5 deg; and 8 sec, -22.5 deg. Wave transformation coefficients and directions for each of these period-direction pairs were output at a nominal 3-m depth for the 240 longshore grid lines of the main grid.

63. Example comparisons of calculated wave height and direction are given in Figure 11a and Figure 11b, respectively. In these figures, the

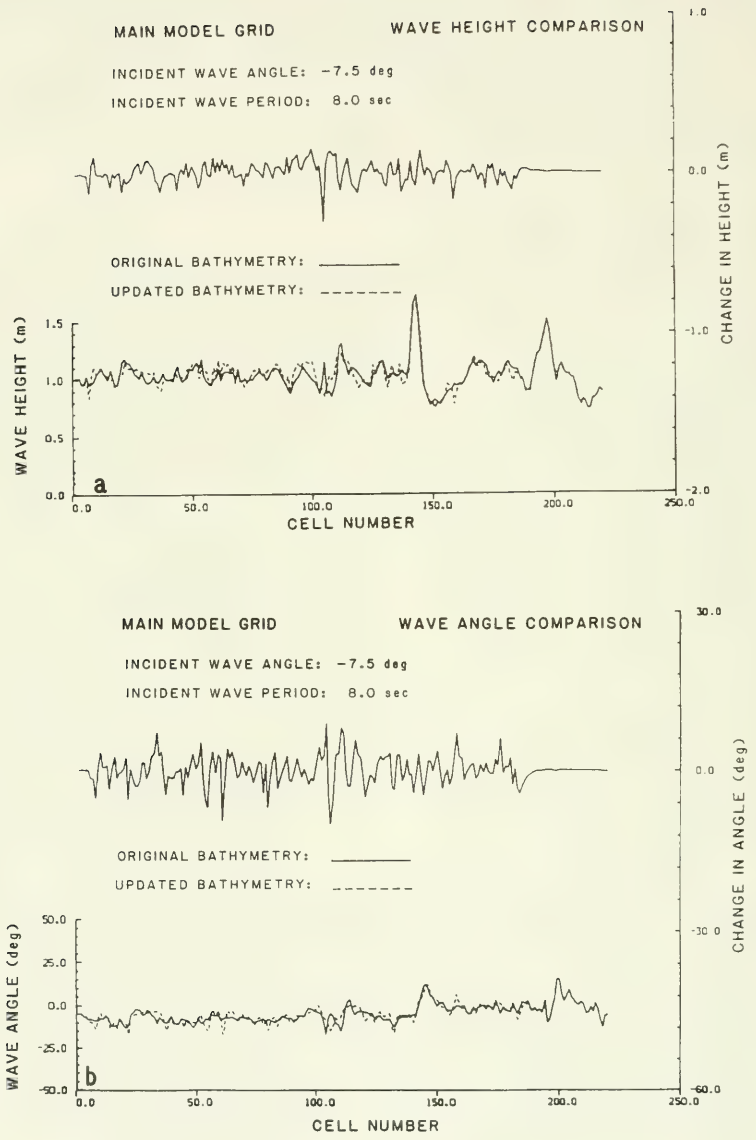

Figure 11. Comparison of calculated (a) wave height and (b) wave direction at the nominal 3-m depth alongshore for original bathymetry and bathymetry updated with 1985 profile surveys

lower plots show actual calculated quantities and the upper plots show the difference in quantities. Since the bathymetry in the study area is irregular and the shoreline jagged, wave height and direction vary appreciably alongshore. However, trends are seen to be similar for the lower plots on each figure and, importantly, the difference in calculated quantities is random, that is, no systematic change in wave properties resulted from the updated bathymetry. Therefore, it was concluded that use of the wave time series and refraction results for the original bathymetry is justified. The updated bathymetry was employed in the later stages of the project for calculating refraction over beach fill borrow sites.

Refraction Over Beach Fill Borrow Sites

64. For an open-ocean coast, breaking wave height and direction are considered to be the primary factors controlling longshore sediment transport and subsequent beach change. The pattern of breaking waves is determined by the properties of the incident waves in deep water (wave height, direction, and period) and the bathymetry over which the waves propagate and transform. Alteration of the nearshore bathymetry due to removal of sediment at an offshore beach fill borrow site may alter the breaking wave characteristics. The sediment transport rate along the beach could, in principle, be modified to such a degree that the naturally occurring evolution of the beach plan shape would be changed by an amount sufficient to have engineering significance.

65. Two open-ocean sites are under active consideration as borrow sources for the project beachfill. The locations and configurations of the potential borrow sites are indicated on Figures 12 and 13. Herein, the borrow area off Sea Bright and Sandy Hook is called the northern site, and the area off Belmar is called the southern site. A description of the two sites and the available deposits is given in Appendix E. The bathymetry in the vicinity of the southern site is highly irregular (Figure 13), whereas regular bottom contours could be drawn for the northern site (Figure 12).

66. The sites lie relatively close to shore and in water depths ranging from approximately 25 ft (8 m) to 60 ft (18 m) MLW. An 8-sec linear wave at these depths has a length of approximately 213 ft (65 m) and 282 ft (86 m), respectively, and the corresponding depth to wavelength ratios are 0.12 and 0.21. These values are much less than 0.5, the ratio at which waves are

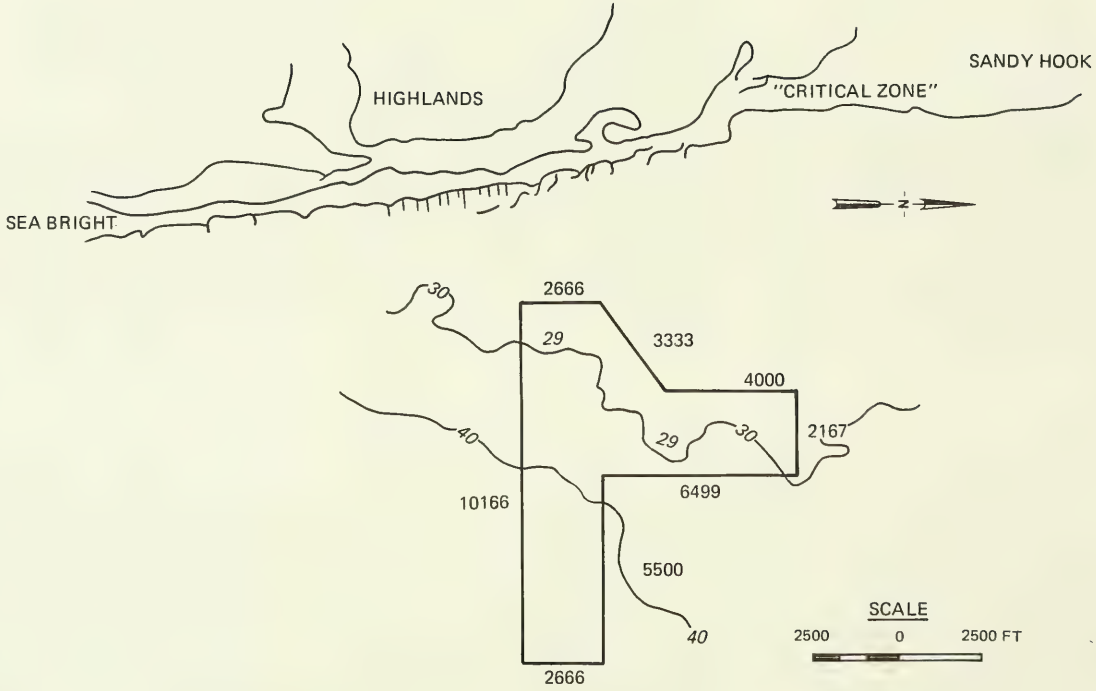

Figure 12. Location and horizontal dimensions of the northern borrow site (depth contours in ft MLW)

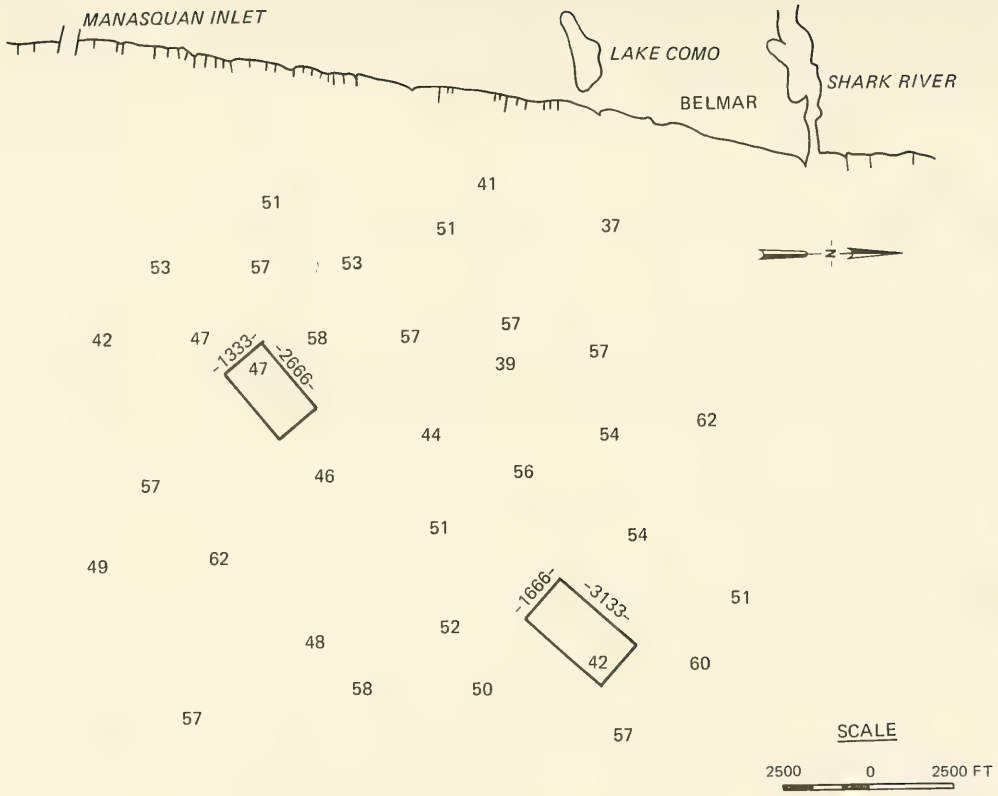

Figure 13. Location and horizontal dimensions of the southern borrow site (depth in ft MLW)

traditionally judged to "feel" the bottom. Therefore, an investigation into the effect of the borrow sites on the wave refraction pattern was made. Emphasis was given to calculations for the northern site as it contains more suitable and more plentiful quantities of usable fill material, and is the probable major source.

67. Previous studies. The phenomenon of wave refraction over dredged holes has received little attention. Only two technical papers could be found (Motyka and Willis 1975; Horikawa, Sasaki, and Sakuramoto 1977) that treat the subject. In addition to investigating wave refraction over dredged holes, both studies employed a simple version of the shoreline model described in Part IV to calculate shoreline change. These studies were of a preliminary nature but do provide some practical guidance. As expected, the refraction pattern was found to notably change with increase in dredged depth at a given water depth and with increase in wave period. Motyka and Willis (1975) state that, at the time of their study, beach mining in the United Kingdom was restricted to depths greater than 18 m (60 ft).

68. Calculation conditions. Two subgrids derived from the main depth grid were used in calculation of refraction over the borrow sites. The subgrid for the northern site ran from Long Branch to Sandy Hook Lighthouse, and the subgrid for the southern area ran from Manasquan Inlet to Deal Lake. Table 4 (northern site) and Table 5 (southern site) list the calculated combinations of deepwater wave conditions and dredged depths.

69. As described in Appendix E, the northern site cannot be dredged uniformly because the usable sediment source lies in irregularly-shaped lenses of varying thicknesses. For greater dredged depths, the borrow hole was "dug" on the grid at allowable depths in the appropriate regions. Three borrow hole configurations were simulated for the northern site and two for the southern site.

Calculation results

70. The 20 refraction run conditions for the northern site are listed in Table 4, and the 15 conditions for the southern site are listed in Table 5. A wave direction of 7.5 deg corresponds to a wave out of the east, the quadrant associated with much higher than average wave heights in the hindcast (Table 2). For this direction, waves of three periods (4, 8, and 12 sec) were run to investigate the effect of wave period. The effect of incident wave direction was investigated by specifying waves out of the east-northeast

Table 4

Northern Beach Fill Borrow Site:

Wave and Bathymetry Conditions for Refraction Runs

Run No.	Wave Angle (deg)	Wave Period (sec)	Dredged Depths (ft)
1	7.5	4	no dredging
2	7.5	4	6, 6, 6
3	7.5	4	6, 10, 10
4	7.5	4	6, 10, 20
5	7.5	8	no dredging
6	7.5	8	6, 6, 6
7	7.5	8	6, 10, 10
8	7.5	8	6, 10, 20
9	7.5	12	no dredging
10	7.5	12	6, 6, 6
11	7.5	12	6, 10, 10
12	7.5	12	6, 10, 20
13	-22.5	8	no dredging
14	-22.5	8	6, 6, 6
15	-22.5	8	6, 10, 10
16	-22.5	8	6, 10, 20
17	22.5	8	no dredging
18	22.5	8	6, 6, 6
19	22.5	8	6, 10, 10
20	22.5	8	6, 10, 20

Table 5

Southern Beach Fill Borrow Site:

Wave and Bathymetry Conditions for Refraction Runs

Run No.	Wave Angle (deg)	Wave Period (sec)	Dredged Depths (ft)
1	7.5	4	no dredging
2	7.5	4	6
3	7.5	4	10
4	7.5	8	no dredging
5	7.5	8	6
6	7.5	8	10
7	7.5	12	no dredging
8	7.5	12	6
9	7.5	12	10
10	-22.5	8	no dredging
11	-22.5	8	6
12	-22.5	8	10
13	22.5	8	no dredging
14	22.5	8	6
15	22.5	8	10

(22.5 deg) and east-southeast (-22.5 deg) for the fixed, average wave period of 8 sec.

71. Full results are displayed in graphical form in Appendix F. Two examples are presented; one for the northern site in Figure 14a,b and one for the southern site in Figure 15a,b. These figures show alongshore distributions of calculated wave height and direction at the nominal 3-m depth. The upper curve in each figure is the difference between the quantities calculated with and without the dredged hole of specified characteristics. The lower curve plots actual values of the quantity for the dredged and original bottom conditions. The horizontal axis is given in local model grid cell numbers. Refraction model cells are 150 m in length. For the northern borrow site, grid cell 1 is at Long Branch and cell 100 is located just north of the critical zone at Sandy Hook. The lateral limits of the northern borrow site are at cell numbers 75 and 93. For the southern borrow site, grid cell 1 is

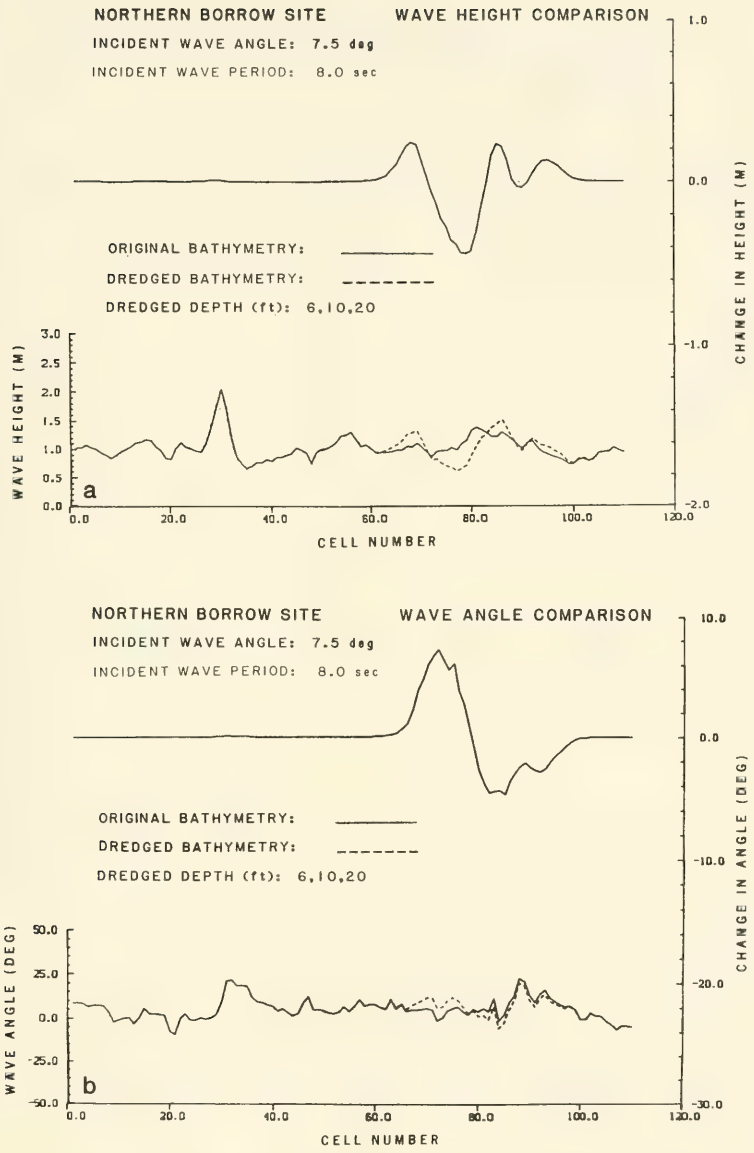

Figure 14. Change in wave properties at the nominal 3-m depth for waves refracting over the northern borrow site: (a) change in wave height, (b) change in wave direction

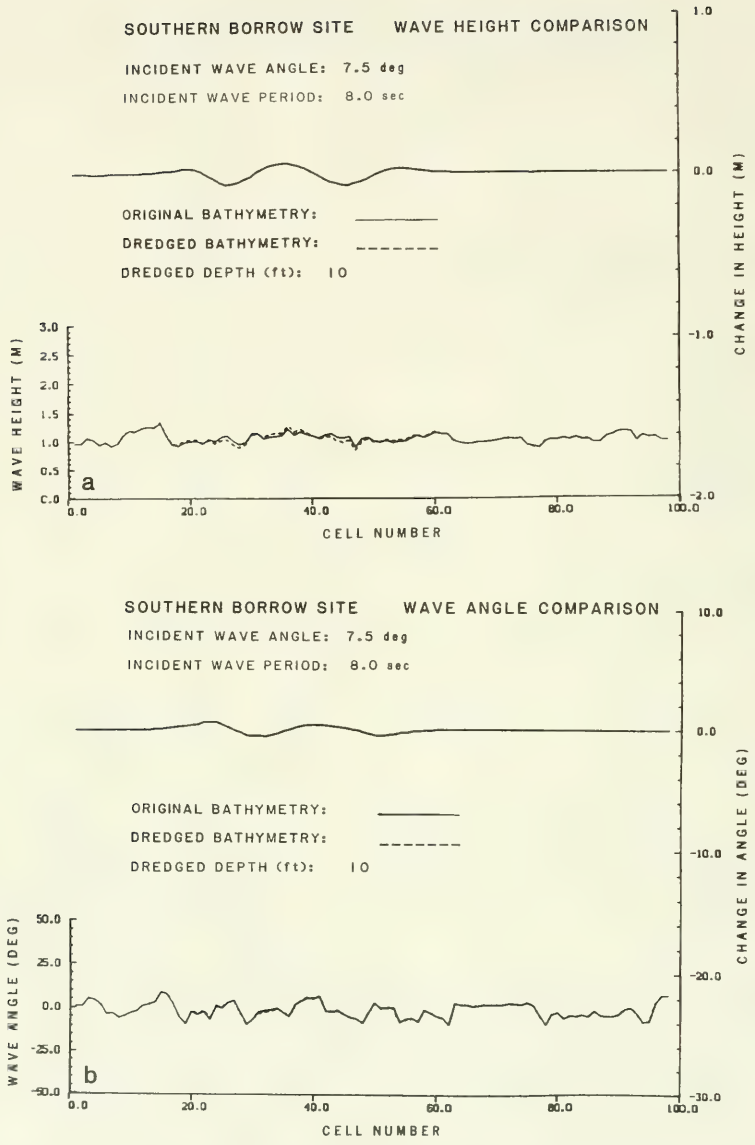

Figure 15. Change in wave properties at the nominal 3-m depth for waves refracting over the southern borrow site: (a) change in wave height, (b) change in wave direction

at Manasquan Inlet and grid cell 100 is at Deal Lake. The lateral limits of southern borrow site holes are at cell numbers 25 and 52.

72. Classical geometrical wave theory predicts waves will diverge behind a hole. Wave height will be lower directly in the shadow of the hole and greater at the sides, where waves that are refracted outward by the hole and waves that are directly incident will combine. Since waves diverge outward from the center line of a hole, the directions of waves that have passed over the hole will be of opposite sign with respect to the center line.

73. The results shown in Figures 14 and 15, and in Appendix F exhibit the general characteristics of refraction over a hole as described in the previous paragraph. In Figure 14a, the change in wave height at the approximate center of the borrow hole has a maximum negative value as expected, and lobes appear on each side. The side toward Sandy Hook has two major lobes caused by the irregular plan shape of the hole. The changes in wave direction at the 3-m depth, given in Figure 14b, show waves positively directed on the south side of the hole and negatively directed on the north side. The lobe with a positive change in direction (on the south side) is higher because the waves are incident out of the east.

74. From Figure 15, it is seen that the two southern holes approximately act as one unit. By comparison to Figure 14, the smaller areal extent and smaller dredged depth of the southern site limit changes in the wave properties near shore. Another mitigating factor is the greater ambient depth in which the southern borrow holes are located.

75. The following list gives a summary of results obtained from the wave refraction analysis:

a. A (divergence) region of lower than average refracted waves exists at a location roughly along the centerline of the borrow site hole(s). A major lobe of higher than average waves exists at both sides of the divergence region. The refracted wave direction goes through zero in the divergence region and is opposite in sign on either side.

b. The region of significant change in refracted wave height and direction is relatively insensitive to deepwater incident wave direction. This region remains localized directly landward of the hole and has lateral (longshore) dimensions of the order of the lateral dimensions of the hole.

c. Changes in refracted wave height and direction are small for short period (4-sec) waves and increase with the wave period. The rate of increase of changes in wave properties decreases as the wave period increases, however. Thus, the change is larger

between 4-sec and 8-sec waves than between 8-sec and 12-sec waves.

d. Changes in refracted wave properties increase with the dredged hole depth. The dependence of the changes on dredged depth is similar to the dependence of changes on wave period, i.e., the change is larger for relatively small dredged depths and thereafter only gradually grows with increases in depth.

76. Discussion. Several hypothetical dredged bottom configurations were examined in this task. For the northern site, the plans with sediment dredging below 6 ft produced notable changes in refraction for waves of periods greater than about 8 sec. However, these plans also contained more beach fill volume than is necessary for the initial proposed beach fill. A smaller dredging area (for a given depth of sediment dredging) would have a less pronounced effect on the nearshore wave pattern. Also, dredging beyond a specified water depth at the deeper contours of the site or seaward of the site would mitigate the influence of the altered bottom topography on the waves.

77. The present study has indicated that random dredging in the shallower portions of the northern borrow site may have an impact on the shoreline. The natural infill sediment transport rate by waves and currents is expected to gradually fill and smooth the borrow pit, reducing influence of the hole with time.

PART IV: LONG-TERM SHORELINE CHANGE

Introduction

78. A central task of this study was to develop a numerical model for simulating long-term shoreline change along Sea Bright to Ocean Township and to apply the model to evaluate alternative plans for protective beachfill configurations. For an open-ocean coast, where wave action typically is the dominant factor producing sediment (sand) movement, shoreline change occurring in the time frame of several years or decades is believed to be controlled by the transport of sediment alongshore. The basic budget analysis technique commonly used in coastal engineering and geology is an arithmetic balance of beach volume changes with inputs and outflows of sediment at the landward, seaward, and lateral boundaries of the region considered. Regardless of the quantity of sediment gained or lost at the onshore and offshore boundaries of the study area, it is the longshore transport of sediment that ultimately determines the long-term plan shape (horizontal pattern) of the beach. A numerical model of shoreline evolution is a highly systemized and quantified implementation of the budget analysis method, in which the change in beach volume is calculated as a function of the time-varying wave conditions.

79. As discussed in Part II, the budget study of Caldwell (1966) as well as subsequent studies have concluded that longshore sediment transport is the dominant process controlling long-term shoreline evolution of the north New Jersey coast. A numerical model of shoreline change for the project area is expected to be a valid extension of previous work, providing a useful tool for examining the course of beach change resulting from proposed shore protection projects.

80. Structure of this chapter. An introduction to the shoreline change numerical model is first given. Representation of structures in the model is discussed in some detail since a long seawall and numerous groins figure prominently in shore protection along this coast. The position of the shoreline is to a significant extent constrained by these coastal structures. Calibration and verification procedures are then presented.

Shoreline Change Numerical Model

Background

81. The introduction of numerical models of shoreline change to applied coastal engineering research and practice began in the mid-1970's in England (Price, Tomlinson, and Willis 1973; Willis and Price 1975; Motyka and Willis 1975) and Japan (Sasaki 1975, Sasaki and Sakuramoto 1978) and, later, in the United States (e.g., Perlin and Dean 1979). Although CE has sponsored development of numerical models of shoreline evolution (Le Mehaute and Soldate 1980, Perlin and Dean 1983), this technology has had limited use in District and Division projects.

82. GENESIS. The numerical modeling effort for this project was jointly carried out with ongoing shoreline change model development activities performed by research work units at CERC. This allowed considerably more resources to be applied than were available for the project alone. As progress was made, the Sea Bright to Ocean Township modeling task became a detailed case study using the recently completed shoreline evolution suite of models called "GENESIS," for GENEralized model for SImulating Shoreline change (Hanson 1987, Hanson and Kraus in preparation). It is anticipated that GENESIS will be released for Corps-wide use in 1989.

83. GENESIS is an integrated set of computer programs developed to calculate wave refraction and diffraction under simplified conditions, breaking wave height and direction, longshore sediment transport rate, and shoreline change. A wide range of boundary conditions, numbers and types of coastal structures, beachfill locations and volumes, and other common situations influencing shoreline change can be simulated with relatively moderate levels of operator effort. Input of wave conditions from an external source (as from data or another computer program such as RCPWAVE as in the present project) is also possible.

One-line model

84. The shoreline change model portion of GENESIS is classified as a "one-line" model. In one-line model theory it is assumed that beach contours remain parallel over the course of the simulation period. Therefore, one line or contour, conveniently taken as the shoreline, can be used to characterize beach plan-shape change. GENESIS was developed from site-specific one-line models that have successfully described long-term shoreline change measured at

long groins, detached breakwaters, and seawalls (Kraus 1983; Kraus and Harikai 1983; Kraus, Hanson, and Harikai 1985; Hanson and Kraus 1986), both in the field and in laboratory physical models.

85. One-line theory assumptions and equations. Principle assumptions in one-line model theory are:

a. Nearshore bottom contours move in parallel.

b. A depth of closure exists beyond which longshore sediment transport does not take place.

c. The volume of beach material in the littoral system, assumed to consist mainly of sand, is conserved.

86. Comparisons of available beach profiles separated by a recent 32-year interval and by shorter time intervals indicate that the slope of the profile along the project site is remarkably stable (cf. Part II, and Appendix D paragraph 14). In general, beach profile slope adjacent to a groin is expected to be milder than average on the updrift side and steeper than average on the downdrift side. However, groins along the project shoreline are not long and sand bypassing can easily occur during episodes of high longshore sediment transport, minimizing the potential offset in slopes. Since the one-line model has been successfully used to simulate beach change at groins of much greater length at other sites, assumption a is considered to be well satisfied. A predictive expression for the depth of closure needed to satisfy assumption b has recently become available and is described below. Assumption c is necessary for quantitative implementation of the budget analysis technique.

87. The basic equation of the one-line model is:

$$\frac{dy}{dt} + \frac{1}{D_c}\frac{dQ}{dx} = 0 \qquad (1)$$

where

y = shoreline position

t = time

D_c = depth of closure

Q = volume rate of longshore sand transport

x = distance alongshore

88. Depth of closure is difficult to determine and becomes, in effect, part of the calibration process. In calibration trials, the depth of

closure, D_c, was either a constant (for example, 6 m or 8 m) or calculated from an expression given by Hallermeier (1979, 1983):

$$D_c = 2.28\, H_s - 10.9\, \frac{H_s^2}{L_s} \tag{2}$$

in which H_s is the significant wave height in deep water and L_s is the deepwater wavelength. Equation 2 was developed for extreme wave conditions; H_s and L_s were originally defined to be the average of the respective quantities for the highest waves occurring during 12 hours in a year. Kraus and Harikai (1983) argued that for use with the one-line model, Equation 2 can be reinterpreted to hold as a function of daily input wave conditions. Numerical values for the depth of closure are given below in discussion of model calibration and verification.

89. The predictive formula for the longshore sediment transport rate is taken to be

$$Q = \frac{H_b^2\, C_{gb}}{16\,(S - 1)(1 - a)}\; K_1 \sin(2\theta_{bs}) - 2\, K_2 \frac{dH_b}{dx} \cot(\beta)\,(\theta_{bs}) \tag{3}$$

where

H_b = breaking wave height

C_{gb} = wave group velocity at breaking

S = ratio of sand density to water density ($S = 2.65$)

a = sand porosity ($a = 0.4$)

θ_{bs} = breaking wave angle to the shoreline

$\tan\beta$ = average nearshore beach slope

The quantities K_1 and K_2 are transport parameters determined in calibration of the model.

90. The first term in Equation 3 corresponds to the CERC formula (Shore Protection Manual (SPM) 1984, Chapter 4) and describes sediment transport produced by obliquely incident breaking waves. The second term describes transport produced by a longshore variation in breaking wave height. The first term is always dominant, but the second term will provide a significant correction if diffraction enters the problem (Ozasa and Brampton 1980, Kraus 1983, Kraus and Harikai 1983).

91. The SPM recommends a value of $K_1 = 0.77$ for root mean square wave height in Equation 3, and the coefficient K_2 has been empirically found to

lie in the range $K_2 = 0.5\ K_1$ to $1.5\ K_1$ (Kraus 1983).

Numerical solution scheme

92. GENESIS allows selection of either an explicit or implicit finite difference solution scheme. Because of the locally jagged nature of the project reach with its numerous, irregularly-shaped revetments, seawall, groins, and other structures, the implicit solution scheme was chosen to be run at 6-hr intervals in order to minimize problems with instability. The program remained stable for all runs.

93. Grid and boundary conditions. An alongshore grid axis was set parallel to the longshore axis of the wave refraction grid. In shoreline modeling, the axis along the trend of the shore is customarily denoted as the "x-axis," and the axis orthogonal to it and pointing positive offshore is denoted as the "y-axis." This convention was maintained. Grid spacing alongshore was set at 50 m, giving three shoreline cells per wave model refraction cell. The finer spacing in the shoreline model is necessary to adequately resolve shoreline features in groin compartments.

94. The grid had to be extended well beyond the project area on both sides to obtain termination points that would provide adequate boundary conditions. The south boundary was placed at Shark River Inlet, and the north boundary was placed at the northern end of the Sandy Hook critical zone (cf., Part II). The south boundary condition did not allow sediment to be transported north across the boundary except under high wave conditions, but did allow sediment to be transported south under those wave conditions indicating transport to the south. This boundary condition represents Shark River Inlet as an almost complete sediment sink.

95. The magnitude of the longshore sediment transport rate within the grid area is controlled in part by the lateral boundary conditions. In the present case, the predominant transport direction is believed to be from south to north, and model results become sensitive to the boundary condition imposed on the south side, i.e., at Shark River Inlet. This boundary condition cannot be specified with certainty, however. Reconnaissance of the site indicated that the inlet does function as a sink of transported sediment due to the channel and jetties.

96. From inspection of available shoreline data, it appeared that the northern end of the Sandy Hook critical zone had moved little over the past 50 years. Therefore, a fixed beach boundary condition was implemented on the

northern end of the grid. This type of boundary condition allows sediment to move freely alongshore across the boundary from either side. The full grid consists of 537 cells and spans a coastal reach of 26.9 km (16.6 miles). This is the longest known extent to be simulated with a shoreline change model.

Representation of
structures in the model

97. As discussed in Part II, a massive seawall and numerous groins have been constructed on the north New Jersey coast in an attempt to reduce erosion and control the position of the shoreline. To accurately simulate shoreline change, the influence of these structures on the longshore sediment transport rate and shoreline position must be represented in the model.

98. Seawall. A seawall functions to prevent landward retreat of the shoreline. Although only portions of the project coastline are backed by an actual seawall, roads and buildings located immediately landward of the present shoreline serve as an effective seawall (transport restrictor) since erosion would not be permitted beyond such facilities. Topographic sheets from the 1985 shoreline survey indicate the position of an effective seawall for the full length of the modeled area. A seawall introduces a constraint on the longshore sediment transport rate, in addition to constraining the possible position of the shoreline. Implementation of the seawall constraint in the model is complex; the report by Hanson and Kraus (1986) should be consulted for further details.

99. The seawall constraint is imposed at the same level of approximation as the assumptions used to derive the one-line model. Wave reflection, scouring, and flanking are not simulated. This description is believed to be reasonable, provided the beach slope in front of the seawall does not appreciably deviate from that of the neighboring beach. This restriction is equivalent to assumption a of the one-line theory.

100. Groins. The positions and lengths of groins were obtained directly from 1985 aerial photographs and corresponding topographic maps. Based on careful inspection of the photographs, 91 groins were placed on the full grid with, for example, 19 groins lying in the 8-mile-long stretch from Sea Bright to Monmouth. Six groins lie to the north, between the project's north terminus and Sandy Hook Gateway Recreation Park. Only groins judged to be efficient at trapping sand were entered in the model; very short groins and nonfunctioning groin remnants were not included. Classification of a groin as

functioning or nonfunctioning was easily determined by visual inspection.

101. Bypassing at groins. If only longshore sediment transport is considered, in principle, a high groin extending seaward well beyond the surf zone will completely block the movement of sediment. In practice, the surf zone often extends beyond the end of a groin, allowing sediment to move past the structure. Rip currents and complex horizontal circulation patterns also act to transport sediment around a groin. During high tide and high wave conditions, suspended sediment moving alongshore may overtop a groin, i.e., the groin will function as a weir. If a groin contains voids, sediment transported alongshore can pass through it. Recent groin inspection (Coastal Planning and Engineering, circa 1985) indicates that most functioning groins in the study area can be considered sediment tight. In the present report, longshore transport of sediment around the end of a groin is called bypassing, and transport of sediment over and through a groin is called transmission. There are no data sets available to directly estimate groin bypassing and transmission.

102. Formally, GENESIS incorporates algorithms to represent sediment bypassing and transmission at groins. Transmission is represented by specifying a "permeability factor" ranging between 0 (no transmission) and 1 (complete transmission). Since the groins in the modeled area are mainly built of heavy, grouted stone, the permeability factor of functioning groins was set to 0. It is recognized that a limited amount of overtopping will occur during high tide and high wave conditions, but specification of that effect is not possible at the present time.

103. Bypassing of groins definitely occurs in the project area and must be represented in the model. In a theoretically complete analysis of the amount of sediment transported around a groin, both the cross-shore distribution of the longshore sediment transport rate (Q in Equation 3) and the horizontal circulation and transport pattern must be known. Knowledge of the latter is beyond the present state of the art. For the former, there is not sufficient field data available to estimate the distribution of the transport rate. Although theoretical expressions exist to predict the cross-shore distribution of the longshore sediment transport rate, all pertain to idealized conditions and none have been verified. In light of these circumstances, the simplest assumption that produces reasonable results is appropriate.

104. In GENESIS, a "bypassing factor" is defined which ranges between

0 and 1. The value 0 describes complete blockage (no bypassing) and the value 1 describes complete bypassing (no groin). The bypassing factor, B , was defined through use of a rectangular distribution of the longshore transport rate and the depth of closure pertaining to the wave conditions at a particular time step:

$$B = \begin{cases} 1 - \dfrac{D_g}{D_c} & , \quad D_c > D_g \\ 0 & , \quad D_c \leq D_g \end{cases} \tag{4}$$

in which D_g is the depth at the seaward end of the groin and D_c is the depth of closure given by Equation 2. A rectangular distribution of the transport rate provides a good approximation to available field data sets (Kraus and Dean 1987) and is also easily calculated.

Summary

105. In summary of the above, three kinds of information are required for shoreline simulation using GENESIS:

a. initial conditions, such as initial position of the shoreline, positions and characteristics of structures, duration of time to be modeled, grid spacing, etc.

b. wave conditions as a function of time to calculate the longshore sediment transport rate.

c. boundary conditions at the lateral ends of the beach.

Model Calibration and Verification

Introduction

106. The general calibration procedure for GENESIS is to determine the transport parameters K_1 and K_2 by reproducing measured shoreline change that occurred at the target site between two surveys. If sufficient data are available, the calibrated model is then run to simulate observed shoreline change that occurred in a time interval not spanned by the calibration, to verify that the calibration constants are independent of the time interval. Since wave data for these time intervals, which may cover years, are rarely available, it is common to use hindcast wave data.

107. As discussed in Part II, considerable shoreline position survey data are available for this coast. However, the standard calibration and

verification procedure could not be followed because of the enormous amount of unrecorded shore protection activity that has taken place and the recorded erratic movement of the shoreline position (cf., Appendix D). If the time history of all construction and beach fill activity were known, GENESIS could, in principle, incorporate it. As an acceptable alternative, calibration and verification were made for the critical zone of Sandy Hook, which is contiguous with the north end of the project. This section of beach has experienced minimal human intervention, except for occasional placement of beachfill. Dates of major beachfills are believed to be known and could be avoided. Major beachfills were documented in the early 1960's, November 1982 through August 1984, and in 1984 (Slezak et al. 1984). Thus, these intervals were not included in the calibration and verification. Phillips (1985) tentatively concluded that shoreline change at the critical zone could not be explained by any known process information. However, as described below, shoreline change at the critical zone occurring in recent times was readily amenable to quantification by GENESIS.

108. In addition to the direct calibration and verification procedure, two indirect tests of model prediction were made. One was a qualitative check to ascertain that calculated and observed angles and sizes of groin fillets were in general agreement. Typical values of updrift fillet angle obtained from the model were 10-16 deg, whereas measured angles were in the range of 14-16 deg. This is a qualitative verification of the sediment bypass algorithm. The other test (described in paragraphs 121-124) was calculation of the net longshore sediment transport rate at specified locations along the coast.

109. In the calibration and verification procedure, visual comparisons were made by plotting calculated and measured shorelines. In addition, a difference indicator Ydiff was devised to provide a more objective fitting criterion. The difference indicator is defined as the sum of the absolute differences between measured and calculated shoreline positions at each grid point:

$$Ydiff = \sum_{i=1}^{N} |Ymeas - Ycalc|_i \qquad (5)$$

where the summation runs over all grid cells, and

Ymeas = measured shoreline position

Ycalc = calculated shoreline position

i = grid cell number

N = number of grid cells

110. If Ydiff is multiplied by the grid cell width (50 m), the deviation between measured and calculated shoreline positions can be expressed as a total net plan shape area.

Calibration

111. Calibration of the GENESIS model was performed using the measured shorelines for 1971 and 1982, with 1971 data representing the initial shoreline position. After 11 simulated years, the calculated 1982 shoreline position was compared to the measured position.

112. By assigning different values to the transport parameters, K_1 and K_2 in Equation 3, and making numerous calibration trial runs, a minimum difference indicator of Ydiff = 597 m was found between the measured and simulated 1982 shorelines. The resultant optimized values of the transport parameters K_1 and K_2 were 0.41 and 0.10, respectively. A plot of the measured 1971 and 1982 shorelines, and the simulated 1982 shoreline, are shown in Figure 16. These optimal values were obtained for a variable depth of closure (Equation 2) given as a function of the wave conditions at each time step.

113. The average value of the depth of closure from Equation 2, excluding zeros associated with calm days of no longshore sediment transport, was found to be 1.35 m for the 3-year wave hindcast data set. However, in the long term, the beach profile is active to a much greater depth. Kraus and Harikai (1983) have discussed alternative definitions of the closure depth. In the present case, a representative value of the maximum depth of closure calculated from the wave data was found to be 6.0 m. A larger value of the depth of closure requires a larger value of K_1 (and, possibly, K_2) in the calibration to maintain the same time scale of shoreline change. A larger value of K_1 produces a higher longshore sediment transport rate (Equation 3).

114. In order to check the sensitivity of the model to depth of closure, the calibration procedure was twice redone, once with a constant depth of closure of 1.35 m, and again with a constant depth of closure of 6.0 m. These values represent the average and approximate maximum depths of closure, respectively, calculated from the input wave time series and Equation 2. In the case of a constant depth of closure of 1.35 m, the 1982 shoreline was simulated with $K_1 = 0.28$ and $K_2 = 0.15$. The difference indicator for the

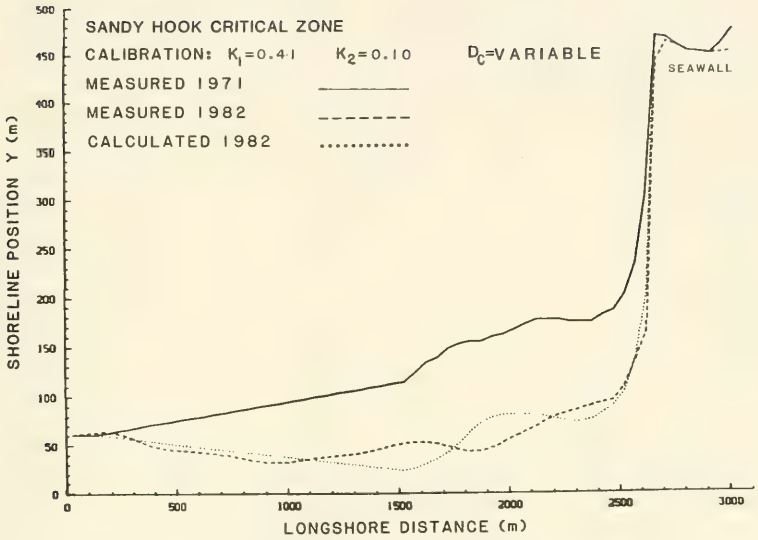

Figure 16. Results of calibration 1971-1982
(variable depth of closure)

measured and simulated 1982 shorelines was 591 m. In the case of a constant depth of closure of 6.0 m, the position of the 1982 shoreline was optimally reproduced with $K_1 = 0.80$ and $K_2 = 0.10$, and the difference indicator was 575 m.

115. A plot of the measured 1971 and 1982 shorelines, and the simulated 1982 shoreline calculated with a constant maximum closure depth, is shown in Figure 17. Calculated 1982 shorelines shown in Figures 16 and 17 both show an acceptable visual fit to the measured 1982 shoreline position. This result indicates that use of either a variable or constant maximum depth of closure will provide a calibrated model for estimating shoreline change in the project area.

116. Although the calibration procedure reproduced the 1982 measured shoreline successfully under both conditions, the longshore sediment transport rate predicted by the two calibrations differs by a factor of about 2. Since the optimal K_1 transport parameter changes from 0.41 to 0.80, the transport rate will increase by the same multiplier to replicate shoreline change over

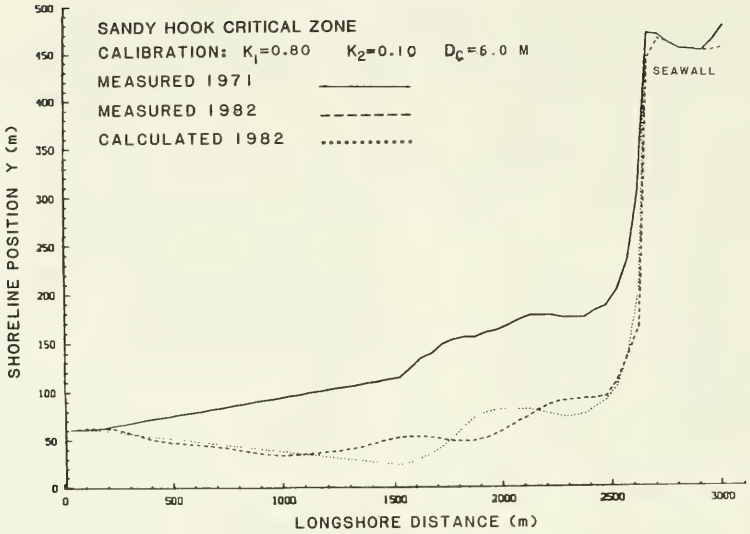

Figure 17. Results of calibration 1971-1982 (maximum constant depth of closure)

the same time interval. It should be noted that a value of $K_1 = 0.80$ is close to the empirical design value of 0.77 given for the CERC formula in the SPM (Chapter 4, p 4-96).

Verification

117. Verification was performed using the measured shorelines for 1932 and 1953. Simulation of shoreline change for this 21-year time period was accomplished in order to provide independent confirmation of the calibration. Transport parameters K_1 and K_2 were determined in the calibration with the three aforementioned procedures for specifying the depth of closure.

118. The three resultant simulated 1953 shoreline positions were then visually compared to the measured 1953 shoreline position and the acceptability of fit indicator Ydiff calculated for each case. Figures 18 and 19 show results obtained for a varying depth of closure and maximum depth of closure, respectively. A minimum Ydiff of 919 m was found between the measured and simulated shorelines for a variable depth of closure. The result using a constant maximum depth of closure was about 10 percent higher.

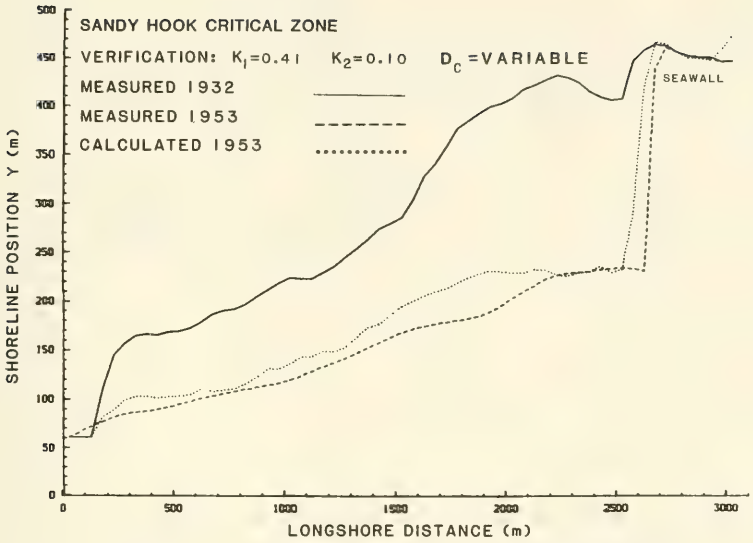

Figure 18. Results of verification 1932-1953
(variable depth of closure)

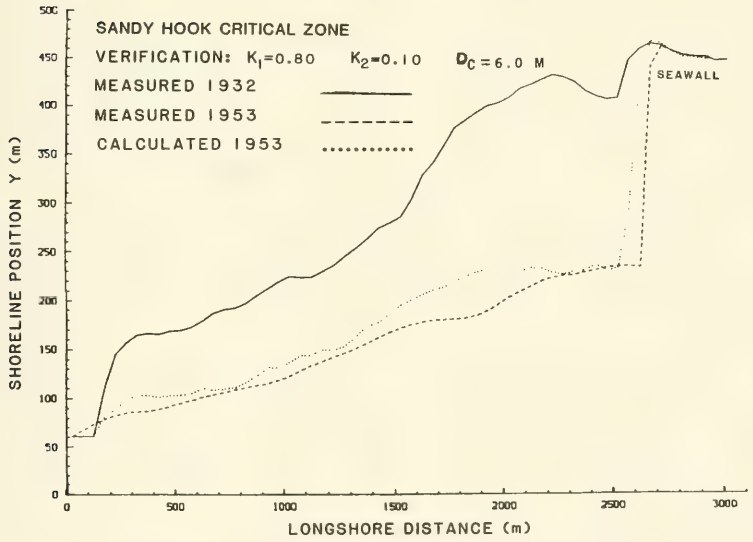

Figure 19. Results of verification 1932-1953
(maximum constant depth of closure)

119. Table 6 summarizes results of the three calibrations and verifications. It is concluded that use of the calibrated model with either a variable or constant maximum depth of closure will produce essentially equivalent results. Longshore sediment transport rates associated with the maximum depth of closure model will be higher by a factor of about 2.

Table 6
Comparison of Calibration and Verification Results

D_c(m)	K_1	K_2	Ydiff for Calibration (m)	Ydiff for Verification (m)
Variable	0.41	0.10	597	919
1.35	0.28	0.15	591	1,317
6.00	0.80	0.10	575	1,094

120. Longshore sediment transport rate capacity. The calibrated model was used to compute the longshore sediment transport rate capacity from Shark River Inlet to Sandy Hook. Transport rate capacity is the potential maximum transport rate assuming infinite sediment supply and no interception or interruption by structures. The transport rate capacity was calculated with GENESIS by removing all groins and the seawall from the 1985 shoreline configuration. The beach could then erode and accrete in response to local breaking wave action only. This situation was run to give an indication of the transport rates which created Sandy Hook, when the coast was in its natural state before implementation of shore protection measures.

121. Calculated longshore sediment transport rate capacities are given in Figure 20. Rates were obtained by averaging yearly volumes of transported sediment obtained from 3 years of simulated shoreline change with the 3-year hindcast wave time series.

122. Transport rate capacities with a constant maximum depth of closure are approximately double those for a variable depth of closure. The magnitudes of these computed transport rate capacities are about one-third those obtained by Caldwell (1966) in his arithmetic budget analysis based on long-term change in shoreline position at Sandy Hook.

123. The computed sediment transport is directed to the north, as expected, but the difference between output and input rates at the ends of the

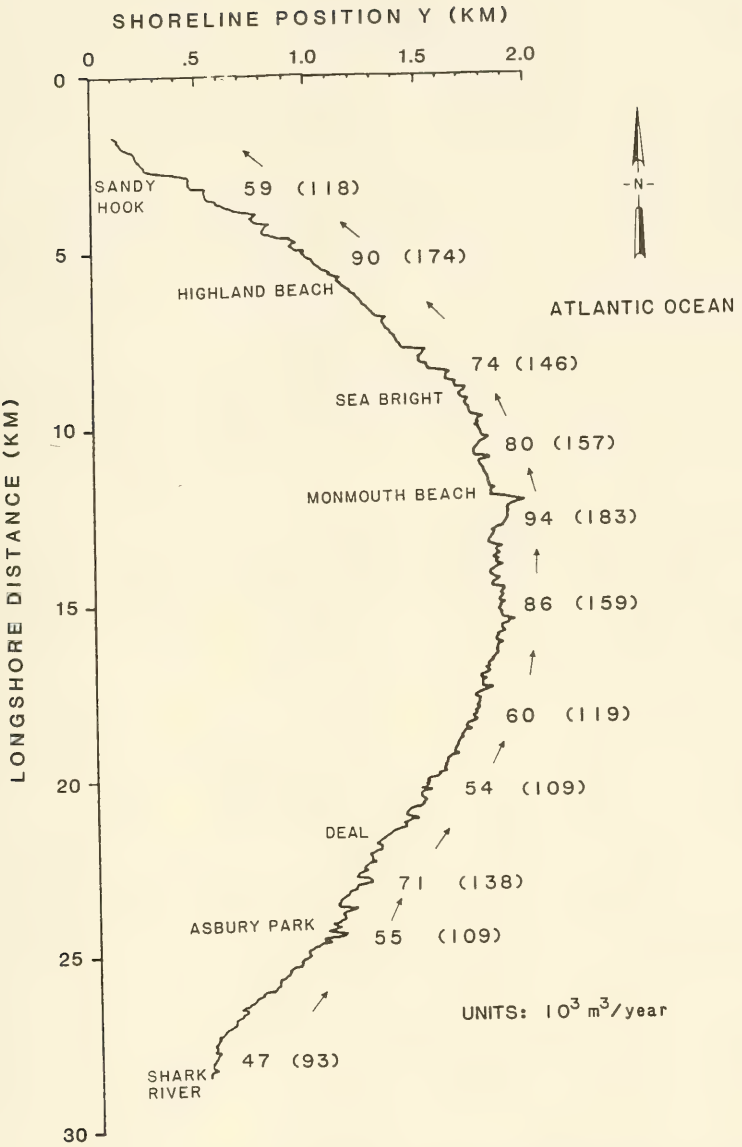

Figure 20. Calculated transport rate capacities using a variable and a constant maximum (in parentheses) depth of closure

grid is small. The small difference means that the only slightly more sediment leaves the grid than enters it, producing a relatively low rate of shoreline erosion. This result is considered to be incorrect in view of the historical trend of shoreline recession. For example, the rates obtained by Caldwell (see Figure 6) indicate a net transport rate out of the project area of approximately 174,000 cu yd/year (493,000 minus 319,000).

124. The suspected cause of the low net transport rate is the limited representation of the shadowing effect of Long Island in the wave refraction modeling. In the refraction study described in Part III, it was assumed that a single WIS hindcast would be sufficient to represent the wave climate over the entire study reach (approximately 16 miles). However, if wave shadowing is proven to be a significant factor, it would be necessary to perform the WIS hindcast at several locations along the reach and develop a methodology to incorporate these individual hindcasts in the nearshore refraction calculation. This level of effort was beyond the scope of the present study.

125. Based on the successful calibration and verification of shoreline change at Sandy Hook, the wave input and shoreline model in their present forms are believed to have restricted applicability for evaluation of the relative merits of beachfill designs. A comparison of alternative designs was not performed in this study.

PART V: STORM-INDUCED BEACH EROSION

Introduction

126. An important goal of this study is development of a quantitative means of investigating the potential impact of storm events on the integrity of an existing beach complex. Specifically, alternative beach fill berm configurations designed to protect the seawall along the open and approximately straight coastal area between Sea Bright and Ocean Township will be the subject of this chapter.

127. This goal can be realized through the development of a one-dimensional numerical model based on certain simplifying assumptions which are particularly appropriate for the project area. These assumptions are described below. The analysis involves development and application of a numerical model to estimate shoreline recession caused by storms of foreseeable intensity.

128. Although modeling procedures have recently been developed for numerically simulating the dynamic response of beaches to storm events, this methodology has not yet been extended for the simulation of storm-induced erosion of beaches protected by vertical seawalls. The purpose of this section is to present the modified model and methodology developed for accomplishing this task. The final product represents the first application of this new technology in a form which will, in the future, be available for District use. It is noted that scour at the foot of a seawall is not addressed in the model.

129. Following a brief description of the basic theory of the storm-induced beach erosion model, a demonstration of the verification of the model will be made. Although appropriate data for this purpose are sparse, comparisons of pre- and post-storm surveys with model predictions demonstrate that the model is capable of producing realistic estimates of both erosion volume and berm recession. This comparison is followed by a description of the approach used to incorporate storm surge model information in the beach erosion model, which results in a means of comprehensively evaluating various beachfill configurations. Design beach profiles are evaluated by assessing each option with respect to a computed beach recession-recurrence interval curve. Included is an empirical estimate of the natural longshore variability

of beach erosion. In this manner, an efficient yet economically feasible beachfill program can be evaluated and realized.

Beach Erosion Numerical Model

Background

130. A numerical modeling scheme for beach and dune erosion developed at the University of Delaware and the University of Florida was selected for modification and enhancement to include the capability of simulating vertical seawalls. The background and application of this model have been reported by Kriebel (1982; 1984a,b), and Kriebel and Dean (1985a,b). A quantitative comparison of this model, referred to as the "Kriebel" model, was made to various existing dune and berm erosion models by Birkemeier et al. (1987).

131. The comparison concluded that the Kriebel model was conceptually superior to other existing models, although, with proper calibration and "tuning," each was capable of predicting approximately similar results with respect to erosion volumes. This is not unexpected since all presently available coastal zone erosion models are empirical in their formulation. It was found, however, that the Kriebel model was less susceptible to user manipulation and yielded realistic results without having to alter coefficients. This is due, in part, to the following desirable features of the model which are not shared by the other investigated models:

a. The model does not require detailed knowledge of the berm or dune geometry or the offshore bathymetry.

b. The model relates the computed offshore sediment transport rate (which is used to compute dune or berm erosion) to several wave and storm parameters. Although the model is still empirical, this feature is viewed as advantageous. Models which neglect this coupling are rendered site specific in that they must be calibrated for each new application.

c. The model is easy and economical to apply. This feature permits the simulation of multiple storm events required for the computation of the final berm (or dune) recession and erosion volume versus recurrence interval plots.

Basic Theory

132. The objective of the beach erosion model is to determine both the volume of material which will be eroded during a specific storm event and the corresponding amount of berm recession which can be expected to occur. These quantities are a function of the existing (pre-storm) berm and subaqueous

beach configuration, storm surge characteristics, and time. The prediction is accomplished by relating relevant characteristics of the storm with offshore sediment transport, which can then be related to erosion and recession. A complete treatment of the basic theory and methodology of the model is presented by Kriebel and Dean (1985a,b) and in the documentation of the original model (Kriebel 1984a,b).

133. As previously noted, one of the primary advantages of the model is its ease of application. This is due, in part, to an assumption that the entire area to be modeled can be schematized into three distinct regions. These regions, shown in Figure 21, are as follows:

a. A dune area defined by a constant height and constant face slope. The distance to the base of the dune face is specified as a distance from an arbitrary reference point.

b. A berm area defined with an initial horizontal width (which can be specified as zero), height, and face slope. This area extends from the base of the dune face to a location equivalent to 0.5 ft (0.15 m) below mean sea level (MSL).

c. An offshore area defined according to the equilibrium beach profile concept in which the depth h monotonically increases with distance offshore x according to the following relationship:

$$h = A\, x^{2/3} \tag{6}$$

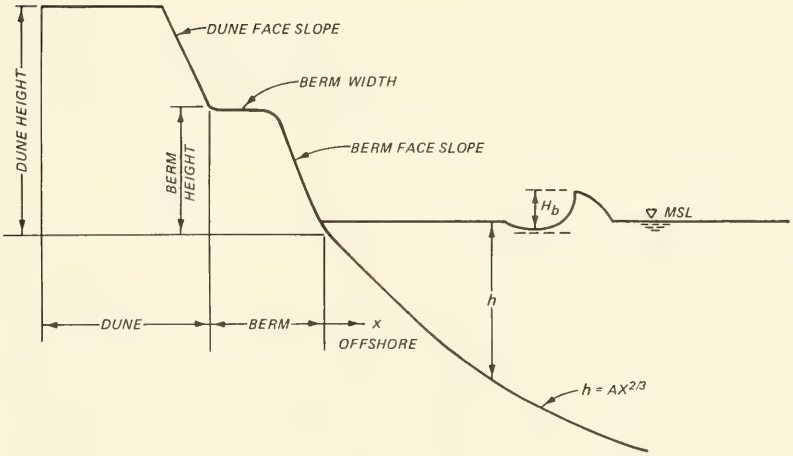

Figure 21. Schematized model area

where the coefficient A , called the "shape parameter," determines the steepness of the offshore profile. This form of the equilibrium profile was first advocated by Bruun (1954) and has subsequently been shown by others (e.g., Dean 1977, Hughes 1978, Moore 1982) to adequately represent the shape of natural offshore profiles. Since steepness is a function of grain size, the value of A can be related to the grain diameter, although the recommended practice is to select an A-value which produces an optimized representation of the existing (pre-storm) profile. If pre-storm conditions are not known, the grain size diameter relationship shown in Figure 22 (Moore 1982) can be used to estimate an A-value. Comparisons of calculated equilibrium profiles and measured profiles at various project sites are given in Appendix D.

134. One apparent disadvantage of this schematization concept is that certain features, such as offshore bars, troughs, navigational channels, or other abrupt irregularities, cannot be represented. Conversely, since the primary purpose of the model is to approximate subaerial beach erosion, an advantage of the model is that detailed bathymetric information is not required for obtaining reliable estimates. An additional advantage is that the

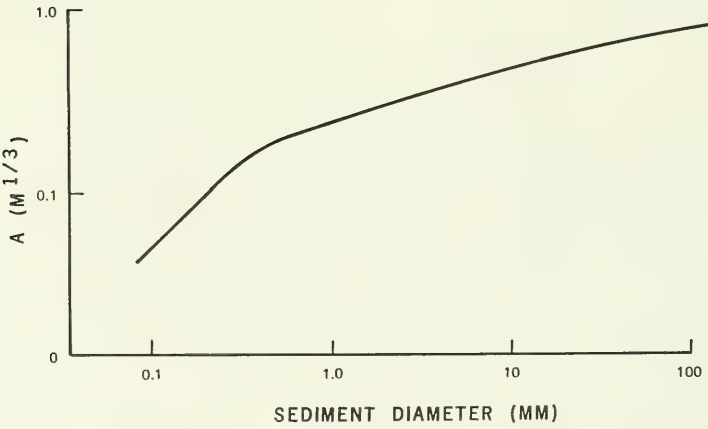

Figure 22. Shape parameter, A , versus sediment diameter (after Moore 1982)

geometrical idealizations of the modeled area are not difficult to justify since the majority of undisturbed beaches (i.e., beaches without jetties, detached breakwaters, or inlets in the immediate vicinity) have well-defined features which can be easily idealized. Beaches which are heavily influenced by natural or artificial boundary conditions cannot be modeled by the present or any other one-dimensional erosion model. Complex cases such as these must be modeled by computationally expensive two-and three-dimensional numerical models which more completely represent the physics of the flow regime. These models are not, with available techniques, economically feasible for studies such as this in which multiple simulations of random storm events are required; additionally, the dune and fluid interaction has not yet been well represented in such models.

Governing equations

135. The governing equations of the model can now be presented. The most important concept of the model, and one which separates it from most other beach erosion models, is the specification of a sediment transport relationship which states that the cross-shore sediment transport rate in the surf zone, Q_c , is a function of the dissipation of wave energy. This is written as

$$Q_c = k\,(D - D_{eq}) \tag{7}$$

where k is an empirical coefficient which was determined by Moore (1982) to have a relatively constant value of 2.2×10^{-6} m^4/N (0.001144 ft^4/lb). The dissipation term, D , is given by

$$D = \frac{1}{h}\frac{dF}{dx} \tag{8}$$

where F represents the energy flux evaluated with linear wave theory. The dissipation D can be reduced to the following simple form:

$$D = \text{const}\;\; h^{1/2}\frac{dh}{dx} \tag{9}$$

in which "const" is the product of known constant factors. The term D_{eq} is defined as the equilibrium dissipation resulting when the offshore profile is in equilibrium according to Equation 6. It has been found that the

equilibrium dissipation is independent of both wave characteristics and water depth to the accuracy of available data (Moore 1982).

136. The relationship between cross-shore sediment transport rate and offshore bathymetric change is described by the one-dimensional continuity equation, written in the following form:

$$\frac{dx}{dt} = - \frac{dQ_c}{dh} \tag{10}$$

in which the distance x to a known contour line is written as a function of the change, or gradient, in the sediment transport rate. For example, if more sediment enters the system than exits, sediment accumulates on the bottom and the distance from a fixed point on the beach to the same contour line increases.

Implementation and Assumptions

137. Equation 10 is numerically solved by an implicit scheme at each time step for the time-dependent surge level to yield a total volume of sediment eroded or deposited in the area bounded approximately by the water line and the breaker line. Recession of the dune and berm is related to the total volume deposited offshore through the assumption that this deposited volume originated from the dune and berm complex. If onshore transport is indicated, the offshore volume of erosion is assumed to accrete uniformly on the berm face. Accretion to the dune face is not allowed.

138. Only cross-shore sediment transport is considered in this one-dimensional approach. This points out an important assumption that alongshore sediment transport is negligible with respect to the cross-shore component during a storm. This is often not a valid assumption, but two-dimensional considerations were beyond the scope of model development. Longshore variations will be introduced through empirical considerations.

139. The input data necessary for simulating the impact of a storm event are as follows:

a. The dune area is specified according to a height, distance to edge of the dune face (from some arbitrary reference point landward of the feature), and slope of the dune face.

b. The berm zone is specified according to a width (if a horizontal transition between the dune face and berm face exists; otherwise, zero), height, and berm face slope.

c. A shape parameter, A, (Equation 6) is defined to provide a best fit to the active portion of the offshore profile.

d. The breaking wave height must be specified. An estimate such as one inferable from WIS is adequate for this purpose.

e. The time history of the storm surge in 0.5-hr increments must be specified.

140. Dune and berm elevations in increments of 0.5 ft were specified in the original model. Material eroded from the dune and berm (or deposited on the berm) is assumed to erode equally from each elevation contour. The internal empirical parameters (such as k in Equation 7 and Q_c in Equation 10) have been shown to produce acceptable results without alteration. The above physical descriptors of the storm event and the areas to be modeled represent all of the data required for the numerical simulation of the interaction processes.

141. To simulate the presence of the seawall in the project area, the Kriebel model was modified by replacing the dune area (shown in Figure 21) with a vertical wall. Material deposited offshore is equally supplied by each berm contour line until recession reaches the seawall. At this point recession ceases and the beach in front of the seawall begins to rapidly erode. Since the model cannot describe the scour process at a wall, the calculation is terminated when the seawall becomes exposed at MSL. Further erosion might result in undermining of the structure. Figure 23 conceptually illustrates shoreline erosion and recession for cases with and without seawalls.

142. Following the completion of modifications to the Kriebel model, testing was performed to verify that the resultant model was capable of simulating the erosion patterns and volumes which were documented to have resulted from an actual storm event. This verification process is described in the following section.

Model Calibration and Verification

143. A quantitative assessment of the predictive capability of the Kriebel model was reported by Birkemeier et al. (1987). Although the range of parameters (storm surge level and duration, and dimensions of the dune and berm) was limited by the available data, comparisons of model output to pre- and post-storm survey data were made for 14 separate profiles representing four different East Coast storm events. Table 7 presents a summary of

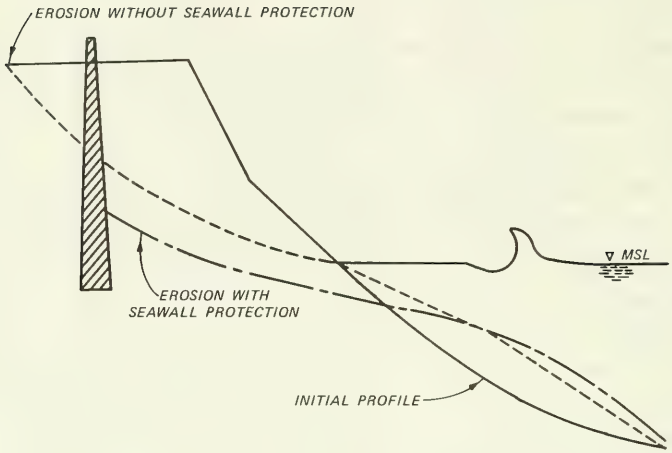

Figure 23. Conceptual seawall effects

the measured and computed volumes of erosion above MSL.

144. The report by Birkemeier et al. (1987) concluded that the Kriebel model is capable of predicting order of magnitude estimates of erosion rates for storm events of known intensity and duration. Limited sensitivity testing was also performed in which the change in computed volumes of erosion resulting from the alteration of certain key model parameters was investigated. Results showed the model to be stable with respect to these parameters if they were specified within reasonable limits. None of the 14 profiles referred to in Table 7 contained a seawall. In order to verify the seawall simulation modification of the model in the present study, additional sets of data were sought which were appropriate for that purpose.

145. The scarcity of pre- and post-storm survey data for locations seaward of a seawall-backed beach is primarily due to the fact that post-storm surveys rarely concentrate on areas where no structural damage took place. Unless a seawall is undermined or experiences failure, quantitative measurements documenting the erosion of the beach directly in front of the seawall are often not made. However, one data set was obtained that was acceptable

Table 7

Measured and Computed Volume Changes (cu m/m)

Storm	Profile	Measured	Computed	Percent of Measured
Westhampton, NY	3	52.8	29.5	56
3 February 1972	4	69.4	23.0	33
	5	51.3	37.9	63
Westhampton, NY	3	26.5	33.9	128
19 February 1972	4	35.2	19.1	54
	5	37.1	21.1	67
Long Beach Is., NJ	14	30.6	38.2	125
19 December 1977	15	26.2	42.5	162
	16*	13.8	35.2	255
	17	34.5	43.4	126
	18*	6.0	41.7	695
Duck, NC	186	31.7	33.4	104
13-14 November,	188	41.3	48.1	112
1981	190	37.4	53.7	143

* Profiles were located in the vicinity of coastal structures

for the purposes of verifying the model (CE 1986). A brief description of the subject area and the associated storm event are presented below.

146. Simulation for Revere Beach. The storm event selected for verification of the beach erosion model with seawall modification was a winter storm of 6-7 February 1978. The area of interest is Revere Beach located in Revere, Massachusetts, approximately 10 miles north of Boston (Figure 24). Onshore profiles and bathymetric surveys were taken prior to the storm during November and December of 1977 and again after the storm. Eight separate survey lines were taken which covered the area from the seawall to a depth of 20-30 ft MLW. A storm summary, prepared by Carol R. Johnson & Associates, Inc. (1978), reported a storm surge in Boston Harbor of approximately 4.0 ft superimposed on a spring tide condition. The two-day event was accompanied by maximum wind velocities of 70 knots. Recorded time histories of the total surge level indicated a maximum elevation of nearly 10.5 ft above the mean. Such documentation of a single storm event and resultant bathymetric change is uncommon.

147. Analysis of the Revere Beach data set was made in order to determine its acceptability for verification of the seawall model. This analysis resulted in the following observations:

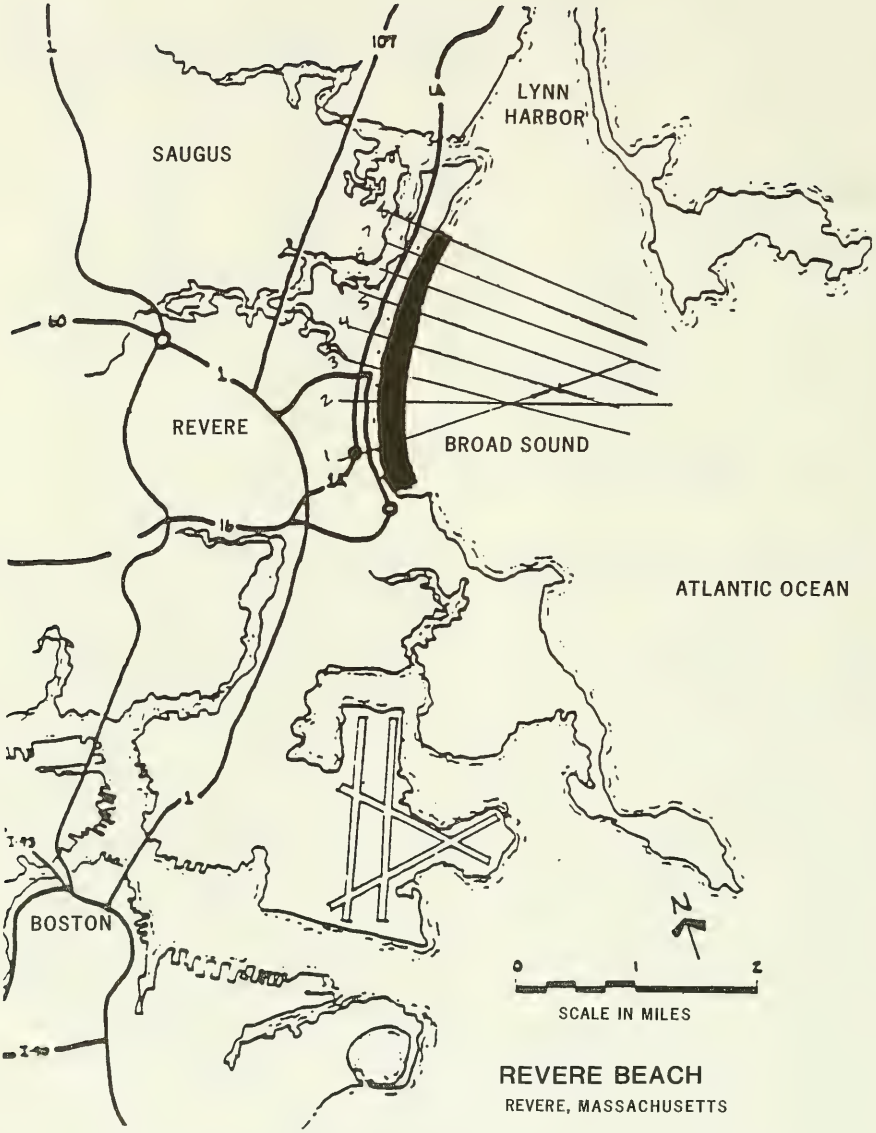

Figure 24. Location map for Revere Beach (from CE 1986)

a. Of the eight profiles surveyed before and after the storm, two were at locations where erosion of the beach in front of the seawall was so severe that protective material was placed in front of the wall during February and March of 1978, before the post-storm profiles were taken (Profiles 2 and 3). Two profiles contained nonvertical barriers (a sloping concrete apron at Profile 4 and a sloping stepped wall at Profile 7) which were inappropriate for the model without further modification. An additional profile (Profile 8) was in a location so protected by land that accretion of the beach was experienced instead of erosion. Obviously, this profile was also inappropriate for a one-dimensional analysis. The remaining three profiles (Profiles 1, 5, and 6) were selected for model simulation.

b. The assumption of one-dimensionality necessary for making this type of analysis economically feasible has been previously mentioned. The present project area is the Atlantic Ocean coast of New Jersey from Sea Bright to Ocean Township. A one-dimensional modeling effort is particularly well suited to this area since it is located on an open coast and has no major structural or natural features which dominate the cross-shore flow regime, invalidating the one-dimensional assumption. Revere Beach, however, is a protected beach which appears to be a highly two-dimensional system. As can be seen in Figure 24, the beach is located within a small bay (Broad Sound), protected to the northeast by a headland. The February storm originated from the northeast quadrant and winds were almost shore parallel during the entire storm event. This is clearly not one-dimensional. This was documented in the storm summary which reported a considerable amount of alongshore transport below NGVD. Use of the Revere Beach data was therefore limited to the area above NGVD where erosion of the dune in front of the seawall was observed. The assumption is therefore made that the offshore two-dimensional effects can be considered to have a negligible effect on erosion of the dune and berm. This implies that, although the predominant transport of sediment seaward of the NGVD shoreline is alongshore, the cross-shore component which governs the one-dimensional model can still be used to compute dune erosion. The conclusion is, therefore, that the Revere Beach data set is acceptable for a limited verification of the model (i.e., examination of dune erosion and not of offshore erosion and deposition patterns). This approach is valid if limitations of the basic model are considered during interpretation of the results.

c. Surge data for the 6-7 February storm event were provided from a tide gage in Boston. The maximum surge level was recorded to be 10.3 ft NGVD. Due to differences in location and degree of sheltering, the surge level at Revere Beach was slightly higher since it was reported that the seawall (elevation of approximately 15 ft NGVD) was overtopped. This difference in surge levels was accounted for in the verification of the model.

d. Each of the post-storm profiles was lacking a survey point at the seawall. It is not known whether or not the berm eroded back to the seawall (although photographs seem to indicate that erosion did extend to the seawall). Since the total volume of eroded material is somewhat dependent on that measurement, a comparison of volumes will not be made. Verification is made by comparing the computed change in elevation at specific distances from the seawall with the measured changes at those locations as shown by the post-storm survey and reported in the storm report.

148. The beach erosion numerical model with seawall modification was used to simulate the storm event for the three profiles described above. Input data for the berm geometry were taken from the surveys, whereas storm data were extracted from the storm report. Results of those simulations are shown in Table 8 and discussed in paragraph 151.

149. Simulation for Sea Bright. To demonstrate that berm recession in the project area could be adequately predicted by the model, a simulation of beach erosion was performed for the November 1953 storm that made landfall in

Table 8

Computed and Measured Elevation Changes at Revere Beach

Profile Number	Distance from seawall ft	Measured elevation change, ft	Computed elevation change, ft
1	75.1	-1.71	-1.05
	187.0	+0.20	-1.05
	236.9	-1.51	-0.46
average		-1.02	-0.85
5	62.3	-1.12	-1.97
	87.6	-1.38	-1.97
	115.2	-2.00	-1.38
	200.1	-2.00	-0.23
average		-1.64	-1.38
6	75.1	-0.69	-0.46
	134.8	-2.00	-0.46
	225.1	-0.49	+0.56
average		-1.05	-0.13

the vicinity of Sea Bright. Detailed comparisons of the impacted area were not made since the precise amount of recession is not known. It was reported (CE 1954, p 48) that "At elevation 10 ft above mean low water recession averaged 98 ft." It was also reported that ". . . selected profiles subsequent to the November 1953 storm indicate recession of from 30 to 85 ft from the summer shore line position" (CE 1954, p D3). It can be inferred that the reported recession was not solely a result of the November storm, but of all storms occurring between the surveys of June - August 1953 and the November post-storm survey. Another major storm event, occurring on 22 October 1953 with an "observed storm tide" of 6 ft MSL (Dendrou, Moore, and Taylor 1981), probably contributed to the erosion documented by the November post-storm survey. The 30-, 85-, and 98-ft recession figures most likely represent an overestimate of the November 1953 storm damage; nevertheless, it is well documented that erosion from this single event was devastating.

150. The storm event was simulated by subjecting the summer 1953 Profile 13 (CE 1954) to the November 1953 storm surge as documented by Pore and Barrientos (1976). The numerical simulation gave a maximum recession of 48.3 ft, within the recession limits reported by CE (1954). Caldwell (1959) presents additional data on the November 1953 storm, which are given in Table 9 and used in the present study to assess longshore variability of beach erosion.

Table 9

Measured Changes in Contours Between Surveys Made in the Summer of 1953 and Immediately after the 6-7 November 1953 Storm, Sea Bright, New Jersey (after Caldwell 1959)

Contour Elevation (ft above MLW)	Landward Retreat of Contour (ft)	
	Average	Maximum
0	65	110
5	63	90
10	98	180
15	53	120

151. Results of the two verifications for seawall-backed beaches indicate that the model acceptably reproduces measured recession of a berm in front of a seawall which occurs in response to a known storm event. Although

the physical situation of Revere Beach violates the one-dimensional assumptions used in developing the model, reasonable results were obtained. Further verification tests should be performed in the future when additional data become available. For the present purpose, the model has been shown to be adequate for estimating berm recession for the Sea Bright to Ocean Township area. The following section will focus on application of the model to determine the amount of recession in front of the project seawall as a result of a stochastic application of both hurricanes and northeasters of known frequency of occurrence.

Storm Simulation

152. The need for an effective beach renourishment program was recognized following the occurrence of the November 1953 storm which caused widespread damage to the project beach area. Three alternate berm width plans (CE 1984), based on post-storm recommendations, were selected for evaluation:

a. A historical maximum width of 100 ft corresponding to the average dune recession measured during the November 1953 storm. The design profile for the 100-ft width is shown in Figure 25.

b. A minimum width of 30 ft recommended by the Beach Erosion Board (BEB) in 1959.

c. An intermediate design of 50 ft (also recommended by the BEB) as a realistic compromise of the two extremes.

153. The beach erosion model was selected as a means of systematically evaluating the effectiveness of a coastal system to withstand a variety of storm events. The methodology used to evaluate the proposed berm width alternatives makes extensive use of the stage-frequency analysis described in Part VI of this report. In that chapter, details on the generation of hurricanes and northeasters are presented. The generated storms are used to develop stage-frequency curves corresponding to both hurricanes and northeasters. Both types of storm events were analyzed because of basic differences in the characteristics of the two; hurricanes tend to have very high surge levels which are relatively short in duration, whereas northeasters are lower in surge level but substantially longer in duration. Each generated hurricane and northeaster is composed of a randomly selected storm surge of known duration superimposed on a randomly selected tidal series. The

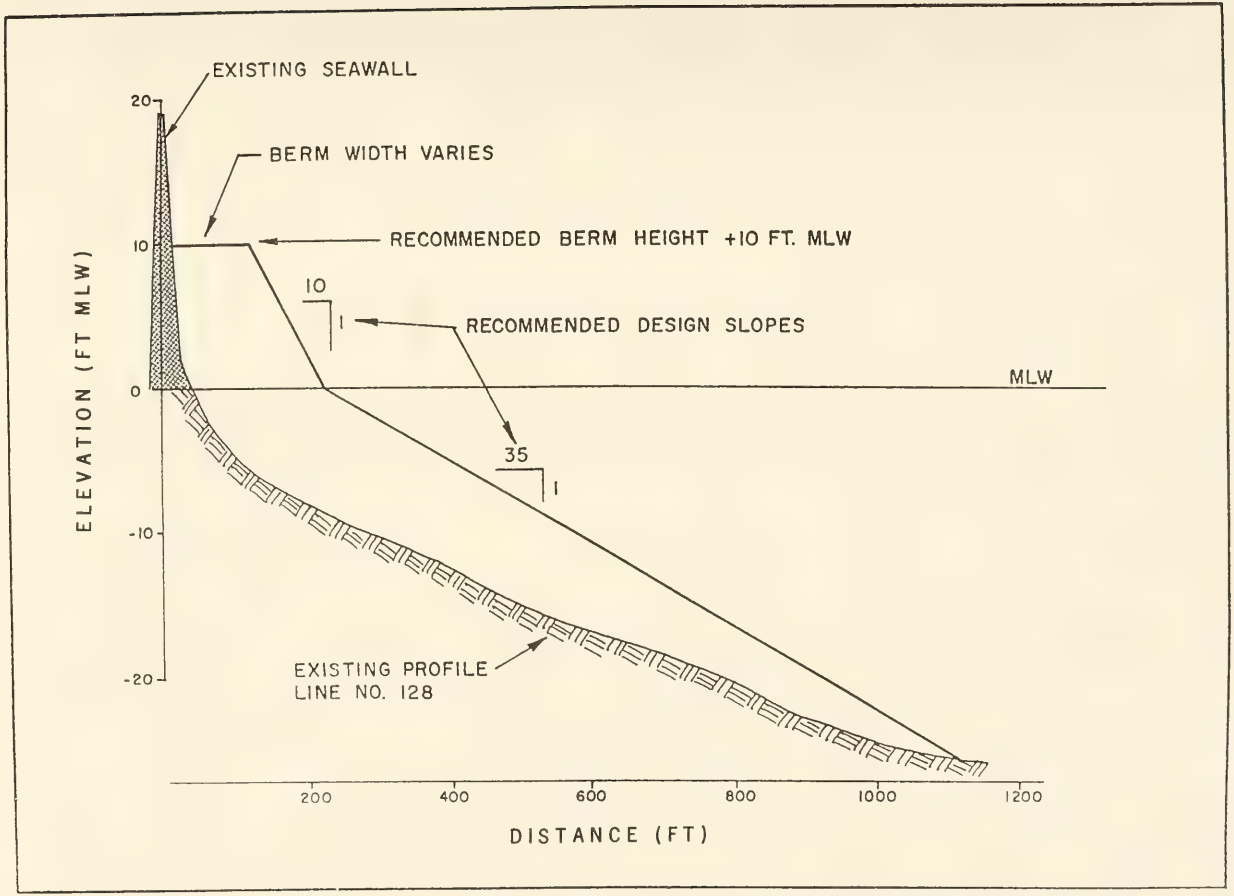

Figure 25. Design profile for the 100-ft berm width (communicated from CENAN 1987)

resulting storm event is identified by a total surge level (storm surge plus tide), a recurrence period (in years) associated with the basic storm event, and a numerical identifier uniquely associated with each generated storm. This identifier is used to reconstruct the time history of each generated storm for subsequent input to the beach erosion model.

154. The reconstruction of each randomly selected storm event from the storm identifier results in the development of an event of known return period and surge height, but of variable duration. Erosion of dune and berm areas has been shown (Birkemeier et al. 1987) to be highly dependent on storm duration as well as surge level; two storms of equivalent return period and surge level do not necessarily produce the same amount of erosion and recession. For this reason, multiple storm simulations were made for both hurricanes and northeasters.

155. The procedure for generating hurricane and northeaster storm events and the methodology for using these events to calculate berm recession versus recurrence interval relationships were specifically developed for this project. Fifty-five hurricanes were randomly selected, reconstructed, and generated corresponding to discrete maximum total surge (storm plus tide) elevations ranging from 4.0 ft to 14.8 ft NGVD at 0.2-ft increments. Similarly, 24 northeasters were generated for total surges ranging from 5.0 ft to 9.6 ft NGVD at 0.2-ft increments. All storm events were based on stage-frequency curves (for both hurricanes and northeasters) computed for Monmouth Beach, New Jersey (see Part VI).

156. Due to differences in both erosion and recession produced by storms of equal surge level but different duration (and distribution of the surge peak within each storm event), the random storm selection was performed five times in order to create a large comprehensive data base of storm events of known total surge level, duration, and return period. This approach resulted in the generation of 275 hurricanes and 120 northeasters which are individually input to the beach erosion model for evaluation of the desired berm configurations. The approach provides a reliable data base for comparing potential storm-associated damage as a function of erosion resulting from storm events with frequencies of occurrence ranging from several years to over 1000 years.

Evaluation of Existing Conditions

157. An evaluation of existing conditions was requested by CENAN in order to document the necessity for developing a beach fill protection plan for the project beach complex. An investigation was therefore made of four existing profile locations specified by CENAN to be representative of the Sea Bright to Ocean Township area. Locations of the profiles are shown in Figure 26. Detailed information related to profile locations and shoreline change is contained in Appendix D.

158. Case A. Profile 160, shown in Figure 27, was selected to represent a typical cross-section characterized by an existing beach backed by a protective seawall. Profile 160 is located in Block 15, the Long Branch south block (Figure D1), along which the average rate of shoreline change from 1953-1985 was +0.39 m/year (Table D18). The average measured grain size for this block is in the range of 0.33-0.37 mm (Table D19). Analysis of the offshore profile indicated that the value of the shape parameter A of Equation 6 was equal to 0.176 $m^{1/3}$, corresponding to a sediment diameter of 0.40 mm.

159. Case B: Profile 82, shown in Figure 28, was selected to represent the case of a narrow beach in front of the seawall. This profile is located in Block 5 in the Navesink Beach-Normandie Beach area. The average rate of shoreline position change for this area was -0.31 m/yr between 1953 and 1985 (Table D18). Grain size measurements are not available for Navesink Beach, but Normandie Beach average grain size varies between 0.35 and 0.60 mm for the 1953 and 1985 surveys respectively (Table D19). Data from Normandie Beach also show a trend of increasing grain size with distance offshore (Table D19). For the 1985 survey, the mean diameter reaches 1.05 mm at the -30-ft contour. Analysis of the offshore profile data yielded an A-value of 0.283 $m^{1/3}$, corresponding to a sediment diameter of approximately 1.40 mm. This large diameter is characteristic of a surf zone subjected to steep waves which remove much of the small-diameter sediment. In addition, the possible absence of an adequate supply of fine sediment to replace that lost offshore as a result of wave action is indicated. Note that a small subaerial beach area is specified as an initial condition; a finite beach initial boundary condition is required by the model to give an initial source of material for offshore sediment deposition.

160. Case C. Profile 140, shown in Figure 29, was selected to

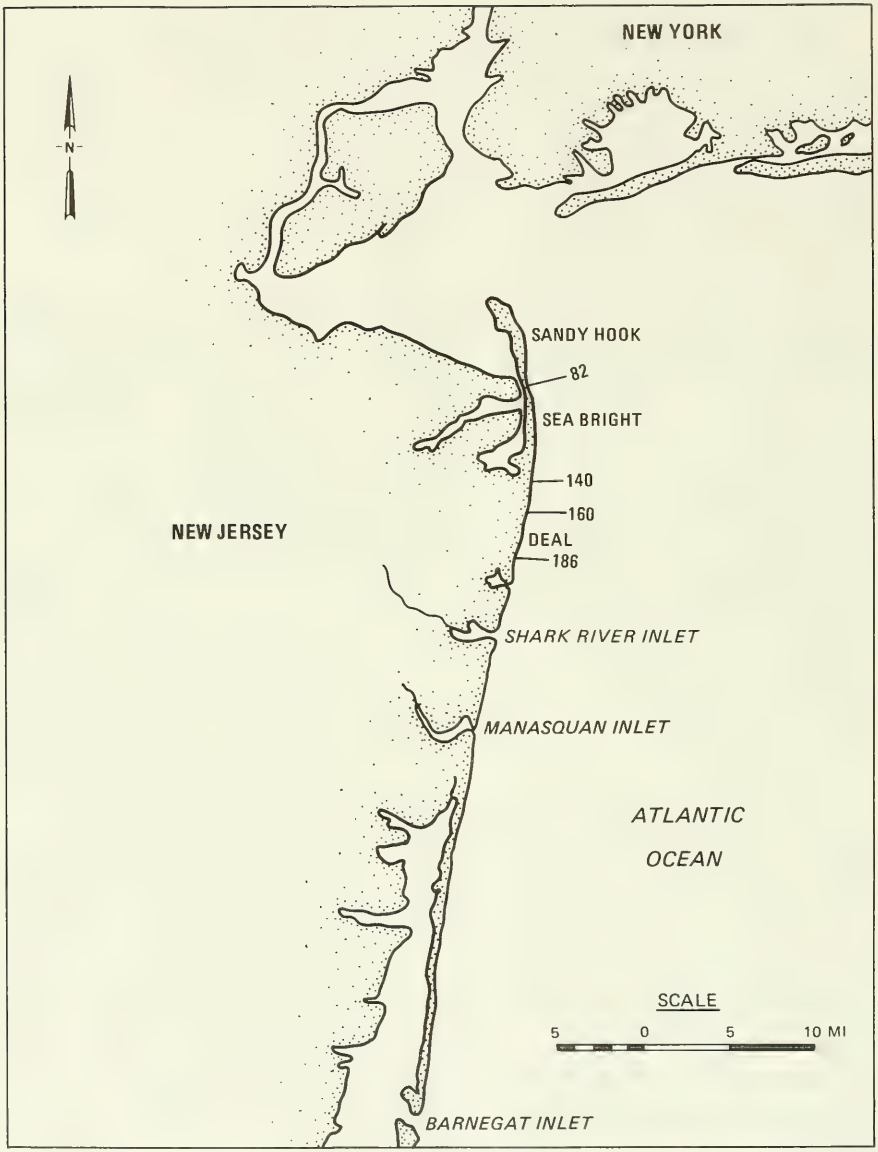

Figure 26. Location map of selected profiles in the Sea Bright to Ocean Township project area

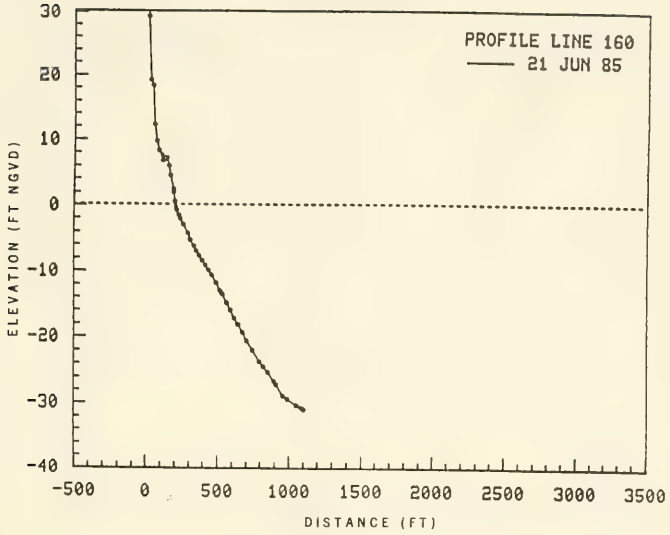

Figure 27. Profile 160

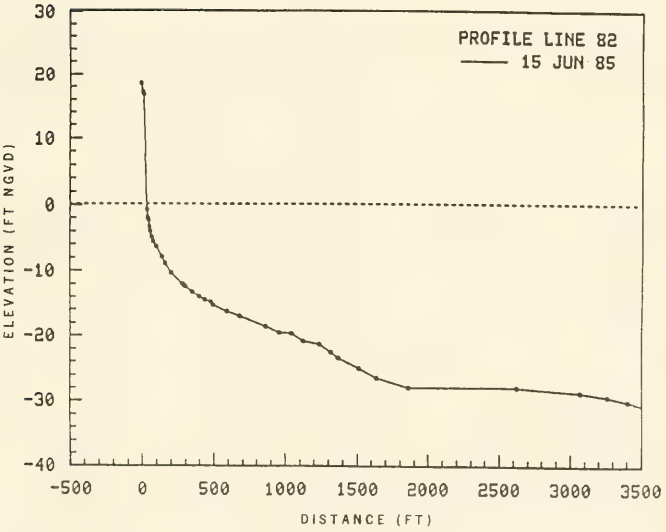

Figure 28. Profile 82

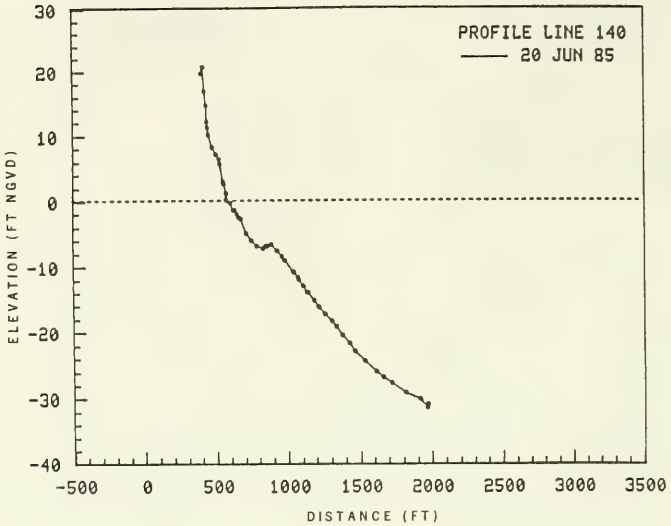

Figure 29. Profile 140

represent a beach with a high dune but with no protective seawall. This case was utilized to demonstrate the possibility of unrestricted dune recession. Profile 140 is located in Block 12 (North Long Beach). The average rate of shoreline position change in this area (-1.18 m/yr) exceeds that of all other blocks for the 1953-1985 time period (Table D18), suggesting that beach material has been available for transport. Average grain size is 0.34 mm for both the 1953 and 1985 surveys (Table D19). A coefficient of A = 0.136 $m^{1/3}$ was computed from offshore profile data. This value corresponds to a sediment diameter of 0.28 mm.

161. Case D. Profile 186, shown in Figure 30, was selected as an example of a low-elevation dune unprotected by a seawall. This profile is located in the Deal south block, along which the average rate of shoreline position change (1953-1985) was -0.44 m/yr (Table D18). Average grain sizes of Block 19 for the 1953 and 1985 surveys were in the range of 0.28-0.31 mm (Table D19), indicating the availability of sediment for transport. An A-value of 0.135 $m^{1/3}$ was computed for this profile, corresponding to a sediment diameter of 0.29 mm.

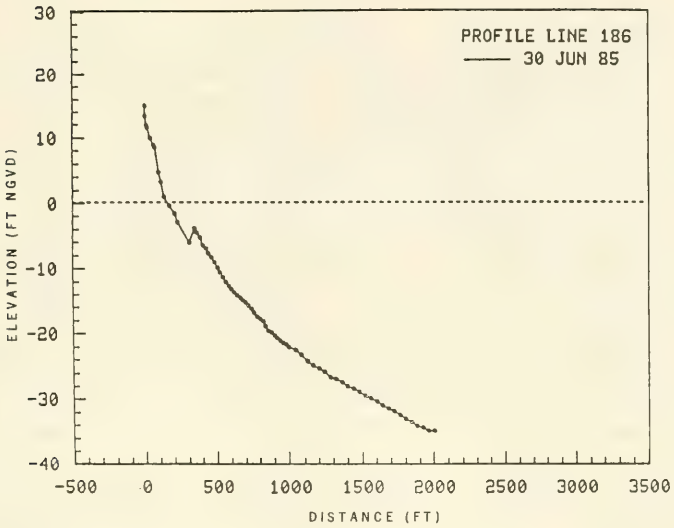

Figure 30. Profile 186

162. All water levels and profile elevations were adjusted to MSL for input to the beach erosion model. The relationships between datums used for this conversion are MSL = (NGVD + 0.57 ft) = (MLW + 2.2 ft) as determined by telephone conversation with the National Ocean Service (NOS) of NOAA in January 1987.

163. Evaluation of the existing-condition cases was accomplished by subjecting the four individual profiles to each of the 275 hurricanes and 120 northeasters in a total of five separate runs. A value was then computed which corresponds to the maximum computed recession of any contour line between the the dune crest and MSL during the entire storm event of known recurrence interval. Maximum recession does not usually occur at the end of a storm, during which time beach recovery may be in progress. Therefore, the maximum was selected as a reliable indicator of storm-related damage.

164. Recession-recurrence diagrams. The recession-recurrence interval plots represent the computed recession resulting from each of the stochastically generated storm events. These plots demonstrate the natural variability in recession which occurs as a result of storms of equal surge. For the

present numerical investigation, these differing recession values are attributed to the fact that storms of equal surge level result in varying volumes of erosion due to differences in total surge duration. In order to develop a single design curve descriptive of the overall relationship, an upper envelope line is provided for each plot. In each case, a small number of points lie above this line. These points were considered to be atypical in that they were found to result from generated storms of unusually long duration.

165. The resulting straight line recession-recurrence interval relationships for both hurricanes and northeasters were combined to produce a final single curve for each representative profile. This design curve was generated by adding the frequency of occurrence (reciprocal of the recurrence period) corresponding to a given envelope curve recession value for both the hurricanes and northeasters and taking the reciprocal of the sum to produce a return period for the combination. Both the individual storm simulations and the combined storm design curves are presented in the following analysis of existing condition profiles for the Sea Bright area. This procedure is not considered rigorous, but is believed to give a reasonable first-order estimate.

166. Case A-Profile 160. The recession-recurrence interval curves corresponding to hurricanes and northeasters for Profile 160 are shown in Figures 31 and 32. The computed spread in recession values can readily be seen in each plot. As an example, one 400-year storm shown in Figure 31 indicates a recession of 67 ft. Analysis of the generated total surge shows that this event has a duration of 33.0 hr whereas the average generated surge duration is on the order of 18-20 hr. For this reason, this point was allowed to fall outside the design envelope. The combined hurricane-northeaster design curve is shown in Figure 33.

167. Case B-Profile 82. The recession-recurrence interval calculations for Profile 82 indicate that all storm events (both hurricanes and northeasters) result in erosion of the entire beach to the seawall. Although recovery of the beach often follows a storm event, the present calculations are made for maximum recessions only. An implication of this analysis is that even a 10 to 20-year event could severely jeopardize the integrity of the seawall. The use of a smaller shape parameter, indicating a smaller grain size than first used, also resulted in complete erosion of the beach fronting the seawall. Since prediction of scour at the toe of a seawall is beyond the

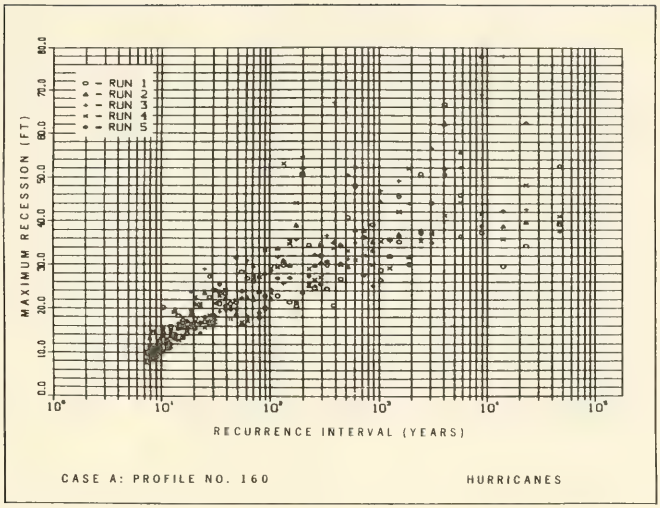

Figure 31. Hurricane recession-recurrence plot for Profile 160

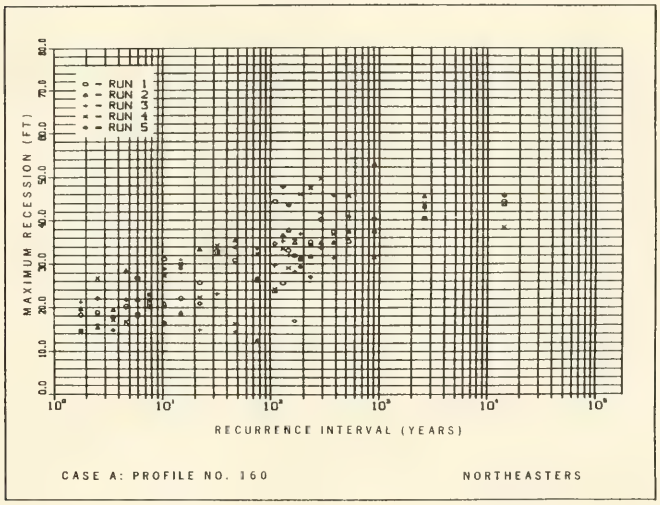

Figure 32. Northeaster recession-recurrence plot for Profile 160

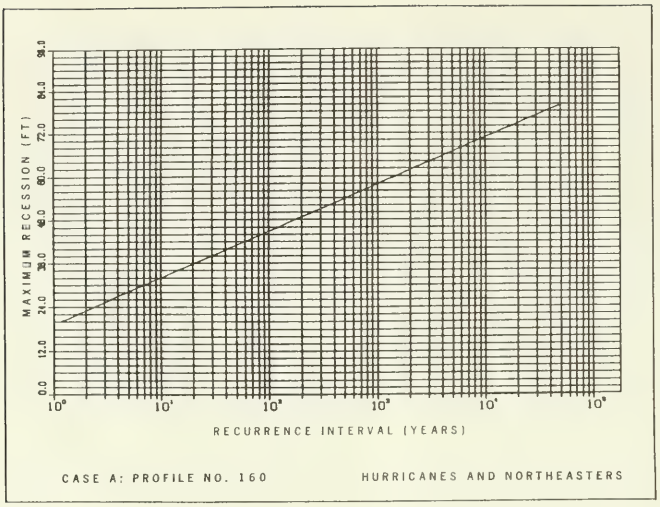

Figure 33. Maximum recession-recurrence design curve for combined hurricanes and northeasters for Profile 160

capability of this or any known model, no further analysis of Profile 82 was made.

168. Case C-Profile 140. Calculations for Profile 140 illustrate the protection afforded by a relatively high dune. This example profile has a berm crest elevation of approximately 20 ft. Recession-recurrence curves for hurricanes (Figure 34) and northeasters (Figure 35) indicate maximum recessions of less than 30 ft for a 500-year storm. The model indicates that recession rarely exceeds 30 ft regardless of the intensity of the storm event. These results are consistent with the observed tendency for a dune to afford protection to the beach by eroding and thereby making material available for transport offshore. This results in a decrease in surf zone depth which forces incident waves to break further offshore, dissipating their energy over a wider beach and causing less erosion of the dune. The combined hurricane-northeaster curve for Profile 140 is shown in Figure 36.

169. Case D-Profile 186. Profile 186 was selected as an example of an unprotected beach with a low dune, in contrast to the Profile 140 high-dune case. Maximum recession curves for hurricanes and northeasters are shown in

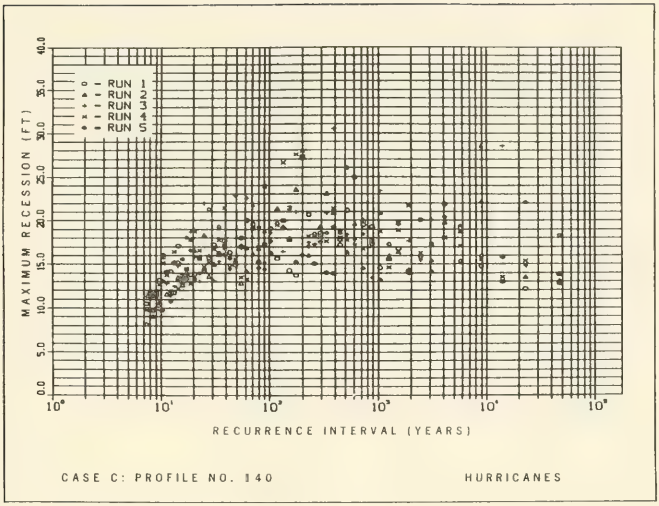

Figure 34. Hurricane recession-recurrence plot for Profile 140

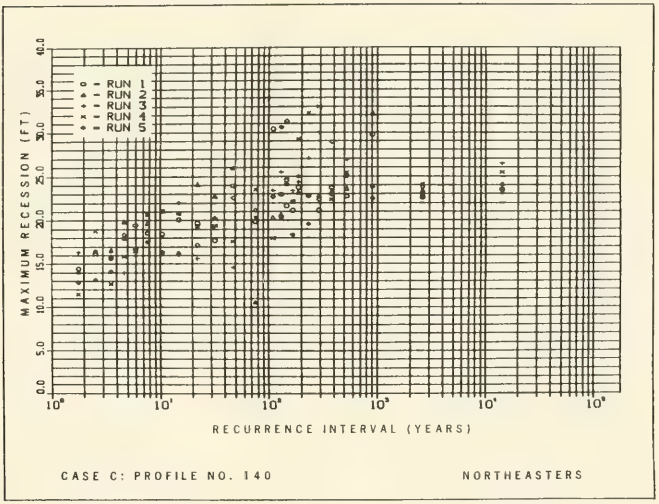

Figure 35. Northeaster recession-recurrence plot for Profile 140

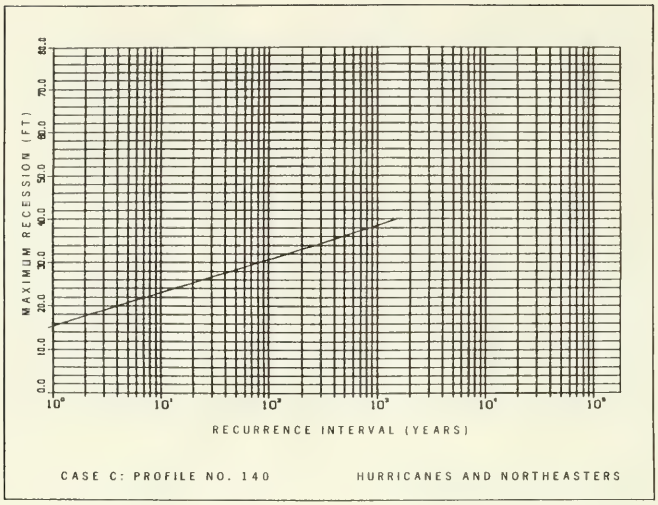

Figure 36. Maximum recession-recurrence design curve for combined hurricanes and northeasters for Profile 140

Figures 37 and 38. Recessions of 50 ft are indicated on the combined curve for recurrence intervals of 500 years (Figure 39).

170. Analysis of typical profiles for the Sea Bright to Ocean Township area shows that storms with recurrence intervals on the order of 500 years can result in maximum recessions on the order of 30 to 50 ft. For seawall-backed beaches (Profiles 160 and 82) recession of the berm crest extends to the seawall, possibly resulting in substantial undermining of the structure. For unprotected beaches with low dunes, such as those typified by Profile 186, this amount of recession could result in breaching of the dune at several locations alongshore, since many dunes are less than 50 ft wide at the crest. Results of this investigation indicate that protective measures are necessary for the beach complex in the project reach; three of the four profiles examined indicate either the possibility of breaching or undermining of the seawall as a result of a single major storm event. This situation would be severely compounded if several storms were to occur in one year or between beach renourishments. The recommended fill designs are therefore evaluated as a means of providing a desirable level of protection.

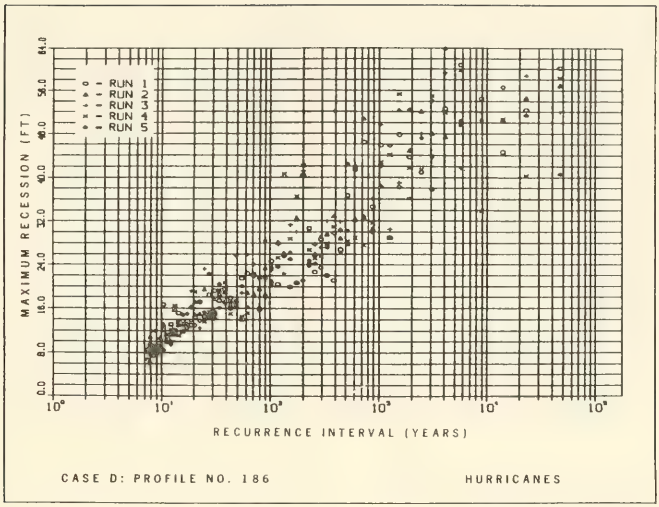

Figure 37. Hurricane recession-recurrence plot for Profile 186

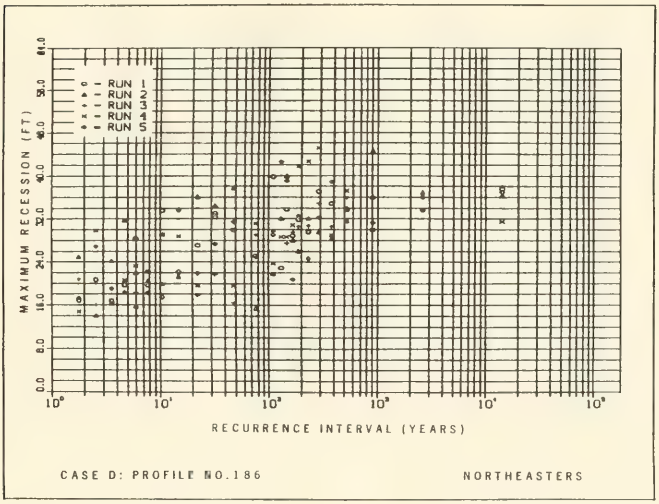

Figure 38. Northeaster recession-recurrence plot for Profile 186

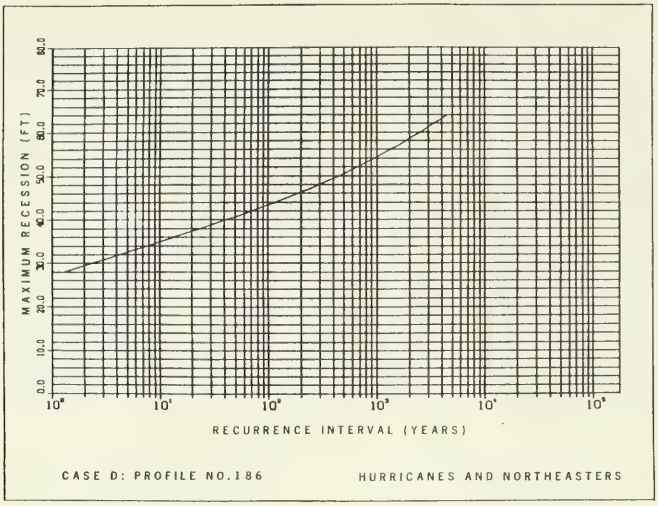

Figure 39. Maximum recession-recurrence design curve for combined hurricanes and northeasters for Profile 186

Evaluation of Alternative Beach Fill Designs

171. The beach erosion model with seawall modification was used to evaluate the effectiveness of the three alternative beach fill designs. The basic berm and profile configuration, shown in Figure 25, is as follows:

a. Berm height of 10.0 ft MLW

b. Seawall fronted by berm widths of 30, 50, and 100 ft

c. Berm slope of 1:10 to MLW

d. Offshore slope (from MLW) of 1:35

The design wave height was taken to be 12 ft, a representative maximum value for the coast (Table 1). The shape parameter for the design beach fill should be selected to be representative of a wide beach area (such as Case C or D), not one controlled by a seawall as in Case B. Survey data for Cases C and D indicate a mean sediment diameter in the range of 0.28-0.34 mm. Calculations of the shape parameter for the 1:10 and 1:35 slopes adjusted to MSL resulted in a value of 0.149 $m^{1/3}$, corresponding to a mean diameter of approximately 0.31 mm. Since this value is consistent with the 1953 and 1985 surveys, it

was employed in the design evaluation. All designs were subjected to the total number of hurricane and northeaster storm events.

172. Design A: 100-ft berm width. Recession-recurrence plots for Design A are shown in Figures 40 (hurricanes) and 41 (northeasters). The combined design curve is shown in Figure 42. The combined computations indicate maximum recession values of 60 ft corresponding to a frequency of occurrence of approximately 100 years. This value is comparable to the average of the reported recessions for the November 1953 northeaster (Table 9), although it has previously been noted that the measured recessions are most likely the product of multiple storms. Assuming the 98-ft average recession value for the +10 ft contour (CE 1954) is an overestimate for the single November storm, the 100-ft berm width design would appear to provide protection to the degree that computed recessions would only reach the seawall as a result of storms with recurrence intervals greater than 100 years.

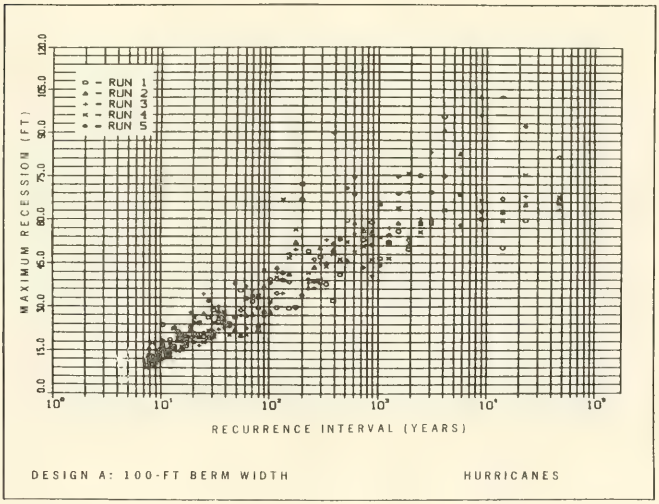

Figure 40. Hurricane recession-recurrence plot for Design A: 100-ft berm width

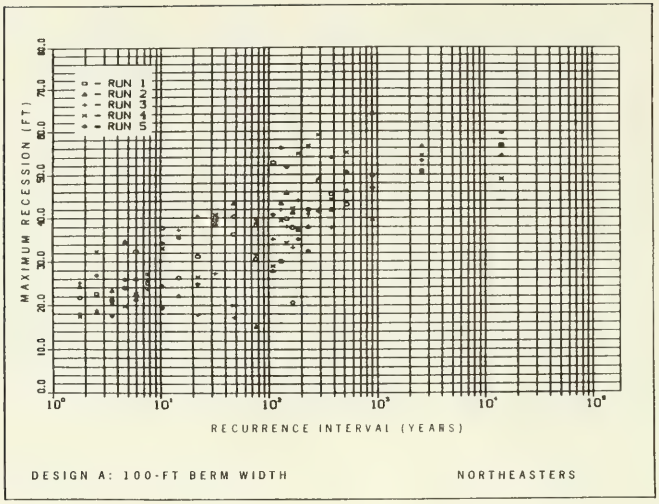

Figure 41. Northeaster recession-recurrence plot for Design A: 100-ft berm width

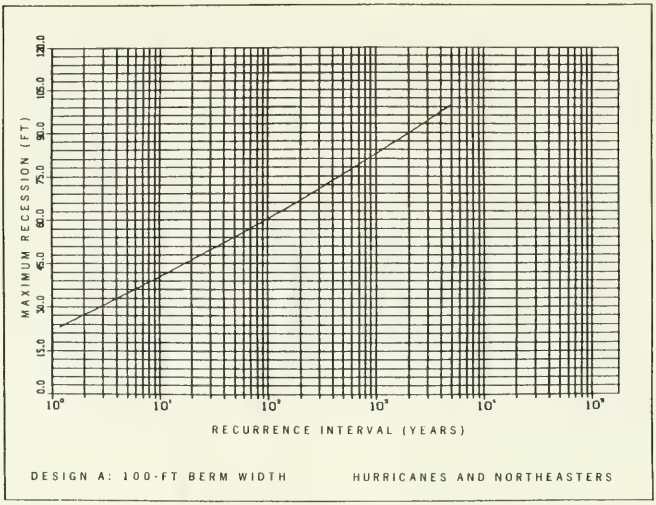

Figure 42. Maximum recession-recurrence design curve for combined hurricanes and northeasters for Design A: 100-ft berm width

173. Design B: 50-ft berm width. The recession-recurrence interval plots for Design B are shown in Figures 43 and 44, and the combined curve is shown in Figure 45. The combined storm analysis indicates that maximum recessions of 50 ft can occur with recurrence intervals of about 30 years. This amount of erosion would completely eliminate the flat protective berm region fronting the seawall, continued erosion would uncover the face of the seawall, rendering it increasingly vulnerable to scour.

174. Design C: 30-ft berm width. The recession-recurrence interval relationships and the combined design curve for Design C are shown in Figures 46-48. Results of the combined design curve indicate that maximum recessions to the seawall can occur in as short a time as two years. This severe recession indicates the vulnerability of the 30-ft design to storms of relatively short recurrence intervals.

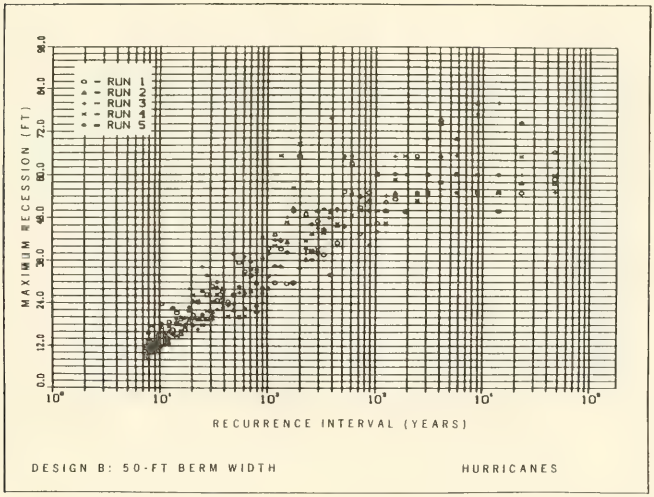

Figure 43. Hurricane recession-recurrence plot for Design B: 50-ft berm width

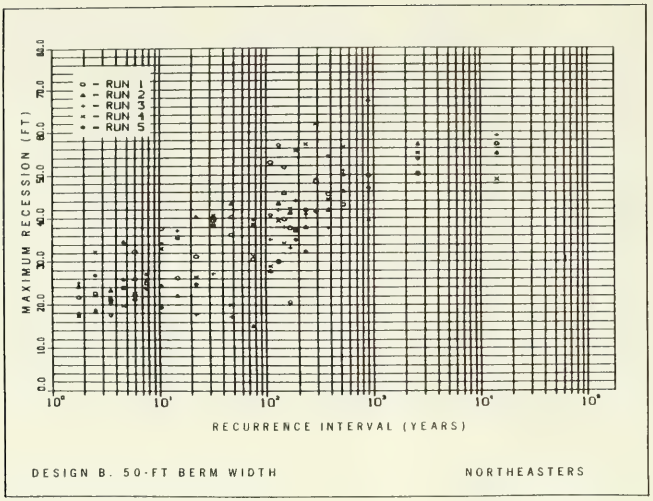

Figure 44. Northeaster recession-recurrence plot for Design B: 50-ft berm width

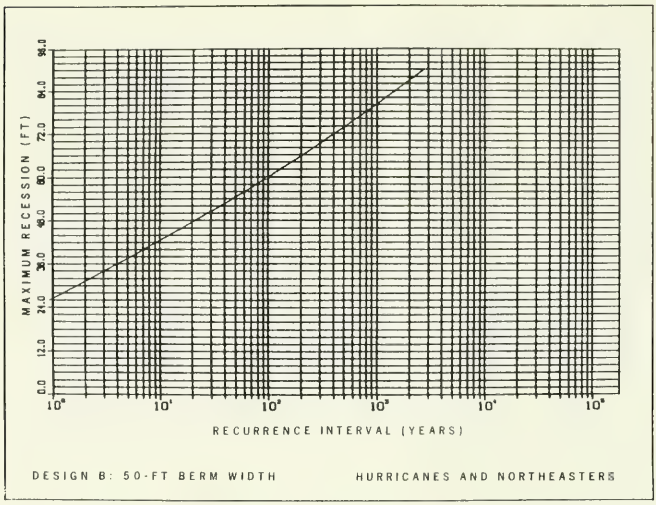

Figure 45. Maximum recession-recurrence design curve for combined hurricanes and northeasters for Design B: 50-ft berm width

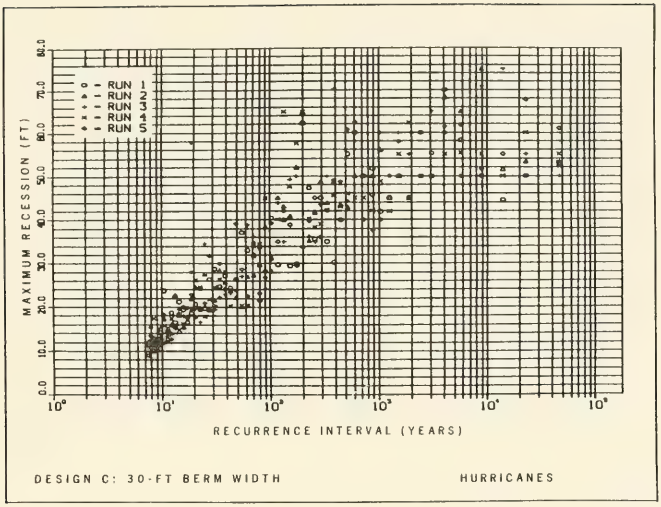

Figure 46. Hurricane recession-recurrence plot for Design C: 30-ft berm width

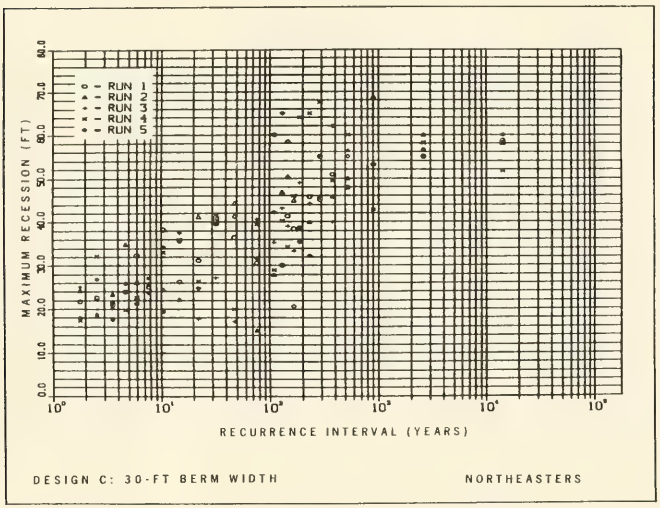

Figure 47. Northeaster recession-recurrence plot for Design C: 30-ft berm width

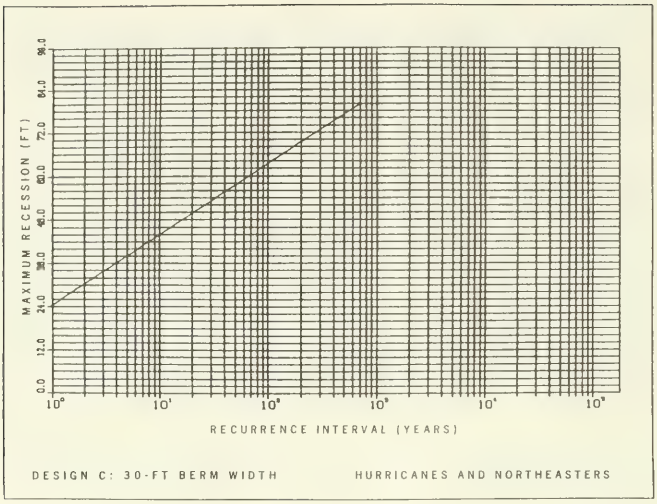

Figure 48. Maximum recession-recurrence design curve for combined hurricanes and northeasters for Design C: 30-ft berm width

Variability Factor

175. The recession-recurrence analysis procedure developed for this project treated storm descriptors in a stochastic (random) manner. The beach was idealized as having a known cross-section, and longshore variability of the beach profile was neglected. In nature, the hydraulic eroding forces and the beach profile will individually exhibit longshore variability. These separate variabilities are site-dependent and also change in time. Therefore, it is impossible to quantify, in a deterministic manner, the mesoscale detail of the longshore variation in erosion potential due to storm action.

176. Although an estimate of the longshore variability in storm erosion potential cannot be calculated at present, it is possible to arrive at an estimate based on measured variations. Birkemeier et al. (1987) and Savage and Birkemeier (1987) examined the variation in erosion associated with 588 different profiles at seven East Coast localities for 13 storms. A variability factor was defined to encompass 75 percent of the observed change. This value can be interpreted as the multiplier of the median required to include

volumetric erosion expected to occur on 75 percent of the shoreline. The so-defined variability factor was determined to have the value 2.0. Assuming that the results computed in the present study are median values, multiplication by the factor 2.0 would encompass 75 percent of the expected recession of the shoreline. It should be noted that the data set compiled by Savage and Birkemeier does not include events greater than the 100-year storm.

177. There are limited data available for the project site with which to test the variability concept. Caldwell (1959) provides average and maximum values of landward retreat of selected contours above MLW for the New Jersey Storm of 6-7 November 1953 (Table 9). A total of 20 profiles spaced over approximately 40 miles of the north New Jersey coast were averaged in the comparison, omitting measurements which were believed to be influenced by the presence of the seawall. This information is a good source with which to examine longshore variability in recession at the site (subject to considerations of storm sequence given in the next paragraph). Data presented in Table 9 are compatible with a variability factor of 2.0 as discussed above.

178. There is an ambiguity associated with the data given in Table 9. As discussed above, at least one other storm is known to have impacted the area in the interval between profile surveys. Caldwell (1959) takes note of this and states "... it is believed that the greater part of the indicated erosion took place during the (6-7 November 1953) storm itself."

179. The methodology and recommendations given here were developed to estimate beach erosion resulting from a single event. A natural shore experiences several annual erosive events of various strengths, continual shoreline evolution caused by longshore sediment transport, and accretion under summer swell conditions. Given the long-term trend of the project coast to erode, consideration of multiple erosive events and natural longshore variability indicate that a variability factor on the order of 2.0 should be incorporated in the protective berm design.

180. Incorporation of the variability factor is made by determining the frequency of occurrence of maximum recession equivalent to one-half the design berm width. This approach gives a conservative estimate of the minimum recurrence interval for complete erosion of the flat portion of the design berm. Initial computed recession values can not be doubled for the variability analysis because recession is limited by the presence of the seawall; continued erosion beyond the design width would result in scour at the face of

the wall. Following this approach, 50 ft of recession for the 100-ft design would have a frequency of occurrence of approximately 35 years. Recurrence intervals on the order of years are indicated for complete recession of the flat berm with the 50-ft and 30-ft designs. Because the continued lowering of the beach is nonlinearly related to the computed maximum recession frequency of occurrence curves, further comparisons of the 50- and 30-ft designs cannot be made without additional analysis. The results indicate, however, that both the 30- and 50-ft berm width designs provide far less protection to the seawall face than does the 100-ft design.

181. Consideration of the potential recession experienced by the 30- and 50-ft design profiles leads to the conclusion that both berm widths would provide insufficient shore protection in the project area. Present model results quantitatively substantiate a recommendation for a 100-ft design berm width.

PART VI: STAGE FREQUENCY RELATIONSHIPS

Introduction

182. The products of this portion of the study are stage-frequency curves which relate the elevation of flood waters to the average waiting time between floods of equal or greater severity. The ordinate of these curves is stage, measured in feet NGVD, and the abscissa is return period expressed in years.

183. Flooding in the study area is caused by the combination of storm-induced water level and astronomical tide. Storm-induced water level has two main components, storm surge and wave-induced water level. Storm surge is composed of the combined effects of storm winds piling water along the shore and low barometric pressure raising the water surface. The wave component is produced by breaking waves; a portion of the momentum of the waves is transformed into a rise in water level called wave setup. This project is primarily concerned with the combined effects of storm surge and tide. However, an estimate is made of the contribution due to wave setup in areas where this effect is considered important.

184. Two distinct classes of storms affecting the study area are northeasters and hurricanes. Northeasters, named after the predominant direction of the associated winds, are large-scale, low pressure disturbances which usually occur from late September through April. Wind speeds associated with a northeaster are generally less than those of a hurricane. Although gusts can reach hurricane strength in a very severe northeaster, sustained wind speeds are rarely greater than 50 knots. Flood damage caused by a northeaster is a function of the storm's duration and intensity. Storms of longer duration are more likely to destroy both natural and engineered flood protection features. Also, since a northeaster may last several days, the possibility of a storm occurring simultaneously with a spring tide increases, thereby increasing potential flood damage. An average of 2.4 northeasters per year with maximum storm surges greater than 2.5 ft affect the study area (Prater, Hardy, and Butler in preparation). The maximum recorded northeaster storm surge near the study area was 8.5 ft, which occurred during the November 1950 storm.

185. Hurricanes are a rarer occurrence in the study area. By the time hurricanes approach the latitudes of the northern New Jersey coast, they are

usually in a stage of rapid decay and are far out to sea on a path that is curving away from the coast. The average waiting time between hurricanes passing within approximately 100 n.m. of the study area was found to be 5.7 years (0.175 hurricanes per year) (Prater, Hardy, and Butler in preparation). Despite their infrequent occurrence, hurricanes have the potential to cause devastating flooding in the study area because of the large storm surge caused by high wind speeds and low pressures. The duration of a hurricane is typically shorter than that of a northeaster.

186. Stage-frequency curves were developed using a probability model in conjunction with a numerical storm surge model. The calculation technique can be outlined as follows (Figure 49):

a. The probability model selected storms and assigned probabilities to each (no tide) to create separate northeaster and hurricane ensembles.

b. Surge level time-histories at the boundary of the study area were obtained either from gage data or numerical simulations from the FIMP study.

c. Each storm surge time history in the two ensembles was combined with a large number of tide time-histories to create two very large ensembles of synthetic northeaster and hurricane surge plus tide events.

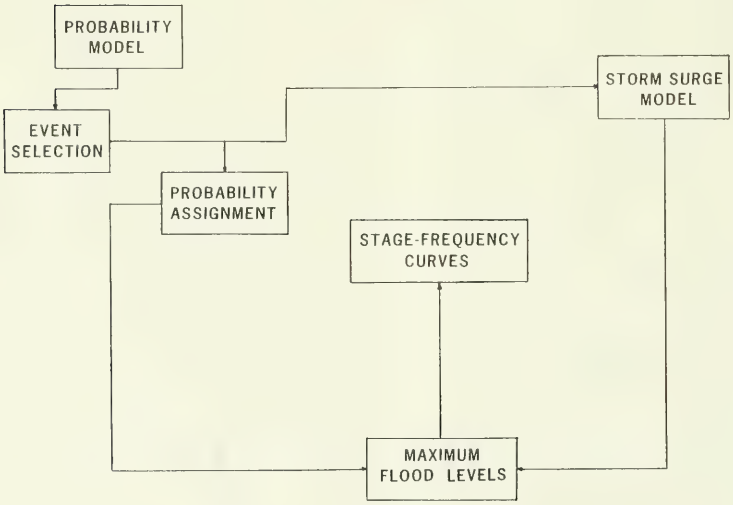

Figure 49. Flow chart of project technique

d. Events were selected from each of the ensembles to be simulated by the storm surge model.

e. The storm surge model was calibrated and verified for the study area.

f. Each of the selected northeaster and hurricane events was simulated by the storm surge model to produce a time history of surge plus tide water levels throughout the study area.

g. At various locations throughout the study area the maximum still water level produced by each simulated event was assigned the probability represented by that event. After all selected events were simulated, the resultant maximum total water levels and corresponding event probabilities were used to create stage-frequency curves.

Review of the FIMP Study

187. Since the present study area lies within the geographical boundaries of the FIMP study, this previous project served as a "parent" study. The present study used techniques from FIMP to refine and extend results into areas which were outside the initial FIMP study area (New Jersey coast) or not modeled in FIMP (Shrewsbury and Navesink River basins). Due to the dependence of the present study on FIMP, the following short review will be provided.

188. The FIMP study investigated the frequency of storm plus tide water levels along the coast and within the bays of southern Long Island, New York. In order to model storm surge it is customary to extend the computational grid beyond the edge of the continental shelf into deep water. Since it is also desirable to have small cell sizes in areas of interest, a large number of grid cells may be necessary to model a study area using a single grid. Consequently, in regions with a wide continental shelf, as in FIMP, a two-grid system is often developed. A global grid with coarse resolution extends throughout the study area and past the edge of the continental shelf while a nearshore grid, with a much finer resolution, covers only the immediate study area. A storm is first simulated on the global grid. Then, using water surface fluctuation time-histories computed on the global grid as boundary values for the nearshore grid, the storm event simulation is made for the immediate study area. For FIMP, the global grid covered the New York Bight from a point south of Atlantic City, New Jersey, to beyond Cape Cod, Massachusetts, including New York Harbor and Long Island Sound. The global grid encompassed the present study area but did not resolve the Shrewsbury and Navesink Rivers.

The FIMP nearshore grid covered only the coast and bays of southern Long Island.

189. The scarcity of historical water level records for southern Long Island required a synthetic modeling approach to generate the large number of independent events (water levels) needed for construction of stage-frequency curves. For hurricanes, the joint probability method (JPM) (Meyers 1970) was used to create synthetic storms. An individual hurricane can be represented by five parameters: central pressure deficit (DP), forward speed (FS), radius of maximum winds (RM), track angle (TA), and landfall point (LP). Probability was assigned to an individual storm by determining the probability of each parameter value in that storm. If the parameters are independent, the storm probability is the product of the probability of each component parameter. However, in the New York Bight, not all parameters were found to be independent. There were two "dependency limbs," one involving DP above and below 2 in. Hg, and one involving bypassing storm tracks. A total ensemble of 918 synthetic hurricanes was generated from all possible combinations of selected parameter values within each dependency limb as shown in Table 10.

Table 10

Construction of Synthetic Hurricane Ensemble for FIMP Study

Dependency Limb	Parameter Combinations					Total
	DP	RM	FS	TA	LP	
Landfalling Storm Tracks						
High Pressure	2	3	3	3	5	270
Low Pressure	4	3	3	3	5	540
Bypassing Storm Tracks	6	3	3	2	1	108
Total						918

190. Northeasters are more difficult to parameterize than are hurricanes; therefore, historical data were used to establish a northeaster storm ensemble for FIMP. Twenty-seven storms were selected as representative of the 41-year period of 1940 through 1980. Water level data, after the subtraction of predicted tide, were used to develop a partial duration stage-frequency curve of northeaster surge levels at Sandy Hook, New Jersey. Probabilities

were assigned to the 27-member storm ensemble according to the portion of the stage-frequency curve that they represented.

191. The interaction of surge and tide is significantly nonlinear in shallow water. Also, the contribution to flooding in back-bay areas from the overtopping and breaching of barrier islands is a highly nonlinear process. For these two reasons, in shallow water, surge and tide cannot be separately modeled and then added together to produce a combined water level. However, in FIMP, the boundary of the nearshore grid was in relatively deep water and far enough away from the barrier islands so that it was unaffected by the above-mentioned nonlinearities. Therefore, it was possible to simulate surge without tide on the global grid, and then linearly add tidal time histories to the surge time histories. By combining multiple tides with each storm, a large number of synthetic surge plus tide events were created. This process created more than 600,000 hurricane and 18,000 northeaster surge plus tide time-histories.

192. With the assumption that a storm has an equal probability of starting at any point during a tidal cycle, stage-frequency curves were constructed for surge plus tide water levels. This was done on the boundary of the nearshore model as well as at several open-coast locations such as Sandy Hook.

193. It was not feasible to model on the FIMP nearshore grid any but a small portion of the large ensemble of events created by the convolution of global results with tide. A procedure was therefore devised to select events to be modeled. A total of 51 hurricane plus tide and 40 northeaster plus tide events were simulated. The stage-frequency curve at the nearshore boundary was discretized by height with a single event selected at each height interval to represent all events having maximum water levels falling in that interval. At these discrete locations on the global stage-frequency curve, the maximum water level occurring during each selected event was assigned a probability equal to the probability mass of its interval of the stage-frequency curve. After the event was simulated on the nearshore grid, this probability was assigned to the maximum water level caused by the event at various locations throughout the study area. Thus, stage-frequency curves were created for multiple locations throughout the FIMP nearshore grid.

Adapting FIMP Ensembles and Results to the Present Study

194. The present study area is located southwest of the FIMP area. Considering the relatively small spatial scale of hurricanes, it was necessary to alter the FIMP hurricane storm ensemble for use in the present study. All 918 original synthetic storms were retained and one additional landfall point accompanied by a track angle was added. This additional storm track was patterned after the 1903 hurricane which made landfall near Barnegat Inlet on the south New Jersey coast. After these new LP- and TA-values were combined with the six DP, three FS, and three RM values from FIMP, an additional 54 synthetic hurricanes resulted. The additional 54 hurricanes were simulated on the FIMP global grid. The hurricane storm ensemble for the present project is shown in Table 11. Surge time-histories from a numerical gage located at Sandy Hook were used to create the hurricane surge plus tide ensemble for these 972 simulations.

Table 11

Parameter Values of Synthetic Hurricanes

	DP	RM	FS	TA	LP	
					X	Y
No.	(in. Hg)	(n.m.)	(Knots)	(Deg)*	(n.m.)**	(n mi)**
1	0.9	20	12	54.5	7.4	13.2
2	2.1	36	19	34.5	25.4	17.3
3	1.1	50	27	-0.5	45.4	23.0
4	1.4			69.5	64.2	28.0
5	1.7			14.5	88.9	32.9
6	2.3			-28.5	94.1	8.2
7					-10.0	49.4

* Referenced clockwise from north; direction toward which the storm is traveling.

** The landfall point was defined as the distance in nautical miles from the origin of the numerical grid of this study (40°18' N, 74°06' W) to where the storm landed.

195. Considering the relatively large spatial extent of northeasters, the 27 historical northeasters from FIMP were assumed to be adequate for the present study. The Sandy Hook tidal gage operated by NOS is located at the boundary of the present study area. Gage data were available for all 27 storms in the northeaster ensemble. After subtracting the predicted tide,

these data were used to create the synthetic northeaster events in place of the results from the FIMP global simulations. The maximum surge (total water level minus predicted tide) for each historical storm is listed in Table 12.

196. Astronomical tides were predicted at Sandy Hook using tidal constituents provided by NOS. A 19-year tidal cycle was generated for each of the two storm types. Hurricane season was defined as May to October and northeaster season as October to April. Tides for hurricanes were predicted at 20-minute intervals, and tides for northeasters were predicted at 60-minute intervals.

197. To develop a data base for boundary conditions to drive the project model, two separate sets of surge plus tide event ensembles (northeaster and hurricane) were created by convolving each storm time-history from the global FIMP model with a tide time-history. The convolution process entailed the superposition of each surge time-history on a predicted seasonal tide record at Sandy Hook, starting at the beginning of the storm season and continuing through the season advancing the starting position by one hour. The maximum total water level during the surge event is recorded for each hour shift. To reduce the amount of data to be handled, a random selection procedure was developed to select 500 tide combinations for each northeaster (13,500 events) and 100 tide combinations for each hurricane (97,200 events). The recorded maximum water levels for each ensemble (keeping hurricane and northeaster events separate) were ranked by magnitude.

198. Just as in FIMP, these two very large event ensembles could not be simulated by the storm surge model. Therefore, events were selected according to maximum water level from the ranked files described in the preceding paragraph. These selections were made to duplicate the separate stage-frequency curves that were created in FIMP for northeaster and hurricane surge plus tide at Sandy Hook (Figure 50). The probability of a selected event is equal to the proportion of the probability mass which it represents. Events were selected in sets of 20; two sets of hurricane and two sets of northeaster events. By simulating the two sets of a storm type separately and creating separate stage-frequency curves, a measure of the variation in the selection process can be determined.

Table 12

Historical Northeasters Used to Generate Synthetic Surge Plus Tide Events

No.	Date	Maximum Surge (ft)
1	7-9 Nov 1947	3.2
2	19-21 Dec 1948	2.5
3	22-24 Mar 1950	2.9
4	23-29 Nov 1950	8.5
5	4-5 Mar 1952	2.3
6	19-23 Nov 1952	3.5
7	6-7 Nov 1953	5.3
8	14-15 Dec 1954	2.9
9	8-11 Jan 1956	3.9
10	8-9 Apr 1957	1.8
11	18-21 Mar 1958	3.4
12	11-13 Mar 1959	2.8
13	18-19 Feb 1960	4.0
14	3-5 Feb 1961	4.2
15	5-8 Mar 1962	4.8
16	4-7 Dec 1962	3.2
17	12-14 Jan 1964	3.9
18	24-25 Feb 1965	2.9
19	22-24 Jan 1966	4.5
20	26-28 Jan 1967	3.4
21	13-15 Jan 1968	3.0
22	9-11 Nov 1968	5.2
23	25-27 Dec 1969	3.6
24	25-27 Jan 1971	2.1
25	17-20 Feb 1972	4.2
26	21-22 Mar 1973	2.1
27	8-10 Dec 1973	3.1

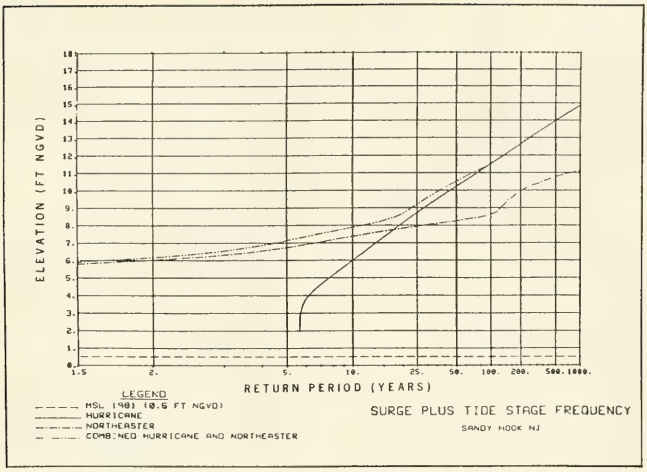

Figure 50. Still-water level stage-frequency curves - Sandy Hook, New Jersey

Storm Surge Model

199. The WES Implicit Flooding Model (WIFM) was used as the hydrodynamic storm surge model. The numerical and hydrodynamic features of WIFM are discussed in Butler (1978) and the application of WIFM to coastal studies is demonstrated in numerous reports, including Butler (1983). WIFM solves the vertically integrated, dynamic, shallow-water wave equations of fluid motion using an alternating direction, implicit, finite difference algorithm. The model allows subgrid barriers (which can be non-overtoppable, overtoppable, or submerged) to be included in the grid. An important feature of WIFM is the capability for using an exponentially stretched numerical grid, which permits concentration of grid resolution in areas of interest. Also included in the code is the capability to flood or dry individual cells during a simulation.

Numerical grid

200. The computational grid for this project contains 1,938 cells, with 34 cells along the vertical axis and 57 cells along the horizontal axis. The grid covers the area from Sandy Hook Coast Guard Station to Long Branch and the tidal regions of the Navesink and Shrewsbury River basins. Cell size

ranges from 178 ft × 540 ft in the high-resolution region of the Shrewsbury River, to 2,720 ft × 3,180 ft along the landward boundary of the grid. The nearshore grid used in the surge model is illustrated in Figure 51.

201. Water depths and land elevations were assigned to grid nodes based on information obtained from:

a. A topographic map (1954, photorevised in 1981) of Sandy Hook and Long Branch, New Jersey.

b. NOAA Nautical Chart No. 12324 (edition 22, January 1984).

c. Shrewsbury River map (May 1985) supplied by CENAN.

Water depths and land elevations used in the calibration are shown in Figure 52.

202. Channel bathymetries were sparsely marked on both the topographic map and nautical chart. The 1985 field survey was only conducted for a few channel sections: the downstream reach of the Shrewsbury River; the Barley Point Reach; and the lower part of the Long Branch Reach. The lack of accurate data on channel bathymetry from Highland Beach to Sea Bright made channel simulation more complicated and difficult than anticipated.

Calibration

203. Before conducting water level simulations, the model was calibrated and verified using data obtained from the study area to ensure the accuracy of model results. Tide gages were installed at the following five locations (Figure 53): Sandy Hook Bay Marina (TG1), Red Bank (TG2), Rumrunner Restaurant (TG3), Mariner's Emporium at Manhasset Creek (TG4), and Locust Point Bridge (TG5). Unfortunately, data from TG5 were lost and only a small portion of the data from TG4 was available due to mechanical malfunction of the gages.

204. A 35-hr period, from 0700 26 May to 1800 27 May, 1985, was chosen for calibration since usable data were available at gages TG1, TG2, and TG3 and wind data indicated low wind speeds. To account for wind effects during the calibration period, field data from TG1 were used to drive the boundary of the storm surge model. Previous simulations showed negligible differences between the boundary and gage data from the Sandy Hook Bay Marina gage (TG1). The model was calibrated and verified by adjusting depths, frictional coefficients (Manning's n), channel sizes, and back-bay volumes. Values of the coded friction array and Manning's n used in the calibration are shown in

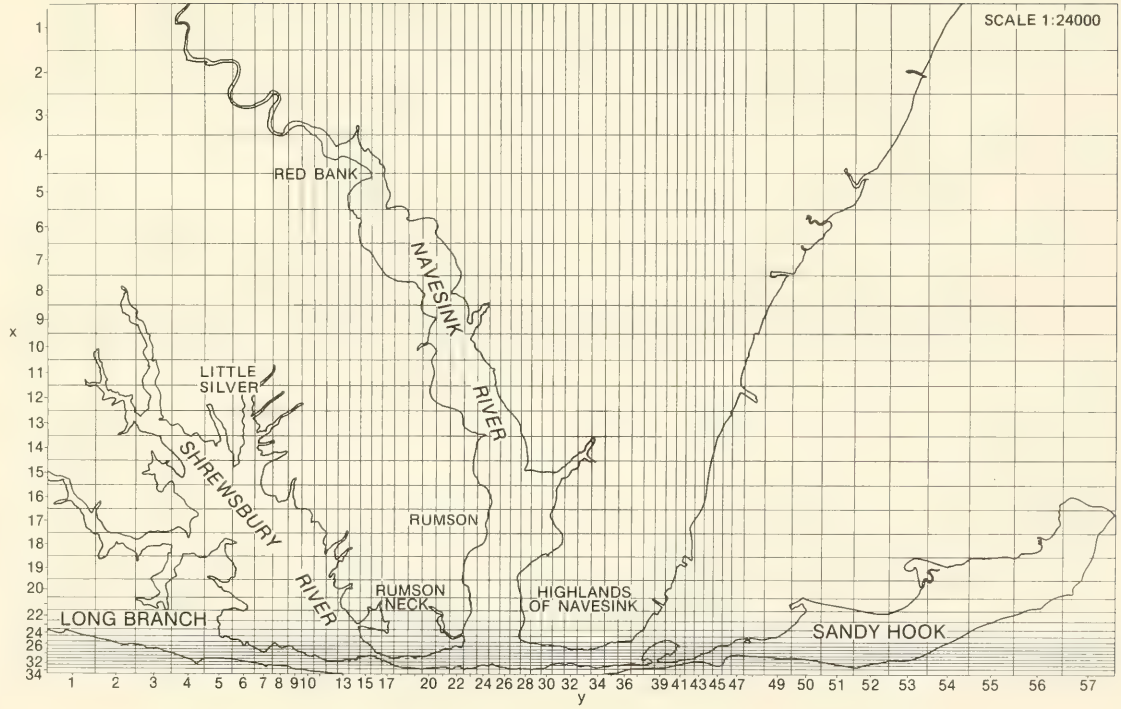

Figure 51. Numerical grid for nearshore storm computations

Figure 52. Water depths and land elevations used in calibration of tides
(depths given in ft MLW; elevations given in ft NGVD)

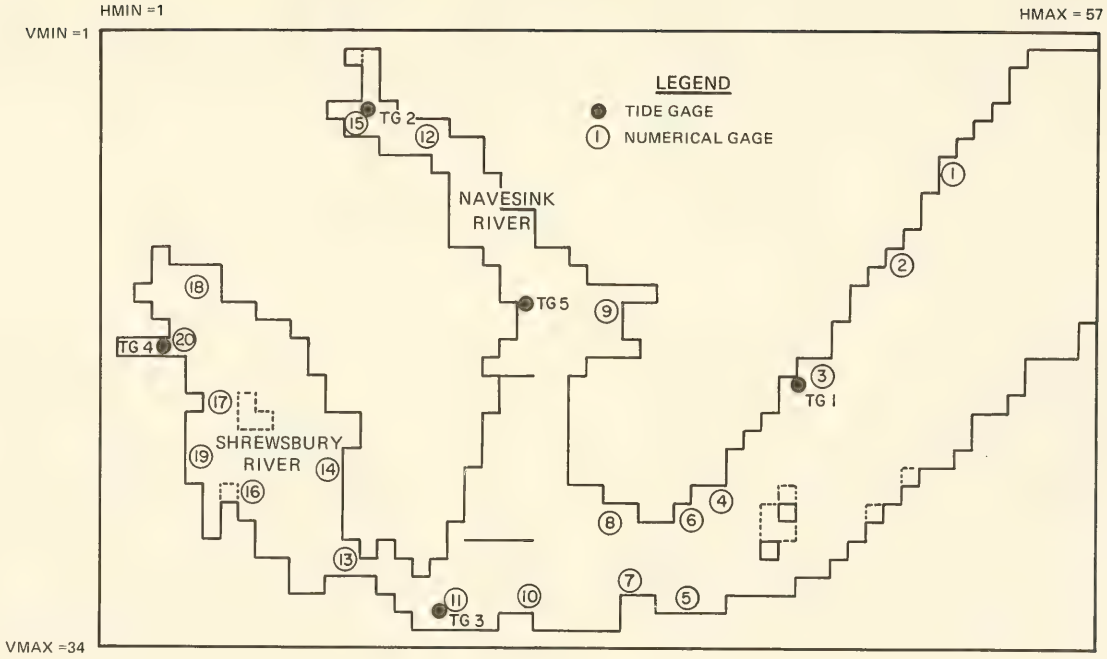

Figure 53. Locations of tide gages and numerical gages

Figure 54. The computed gage data were compared with field data for gages TG1, TG2, and TG3 (Figures 55-57).

205. An excellent match in phase and range was obtained between model and recorded tides at Sandy Hook Bay Marina (TG1). This was expected since TG1 gage data were used as boundary conditions. Good results at high tides were obtained at Red Bank (TG2) and Rumrunner Restaurant (TG3). Differences between tide gage data and model results at gages TG2 and TG3 were less than 0.10 ft and 0.15 ft, respectively. The model predicted a later and higher low tide, 7.5 min and 0.1 ft, respectively, at Rumrunner than was indicated in field gage data; however, this discrepancy had little significance in this project.

206. Although a small difference between calculated and measured water level is indicated at hour 39 for Red Bank (Figure 56), the computed peaks follow a pattern similar to that predicted in the NOAA Tide Tables (1985) for the given time period. The discrepancy may be related to error in the gage data and/or a meterological factor which was neglected in the calibration process.

Verification

207. The calibrated model was verified for a time interval of 39 hr, from 0400 June 3 to 1900 June 4 1985. The results, presented in Figures 58 through 60, show the model adequately predicted the tide gage data during this period.

208. Two historical storms, the March 1962 northeaster and Hurricane Donna (1960), were simulated on the nearshore grid. Data from the Sandy Hook tide gage were used to supply the boundary condition to drive the storm surge model. Wind speed and direction data were obtained from the Standard Project Hurricane (SPH) windfield model (National Weather Service 1979) for Donna and FIMP for the March 1962 storm.

209. The most accurate method for calibration and verification of the historical storm would involve using historical inlet and channel configurations. However, this was beyond the scope of this project, and present-day bathymetry was used instead.

210. Results of both historical simulations are compared with water levels reported in "Flood Mark Determination for Selected Storms" prepared by VEP Associates, Inc. (1985). The comparisons, given in Tables 13 and 14 for the 1962 storm and Donna, respectively, show a good match between the computed

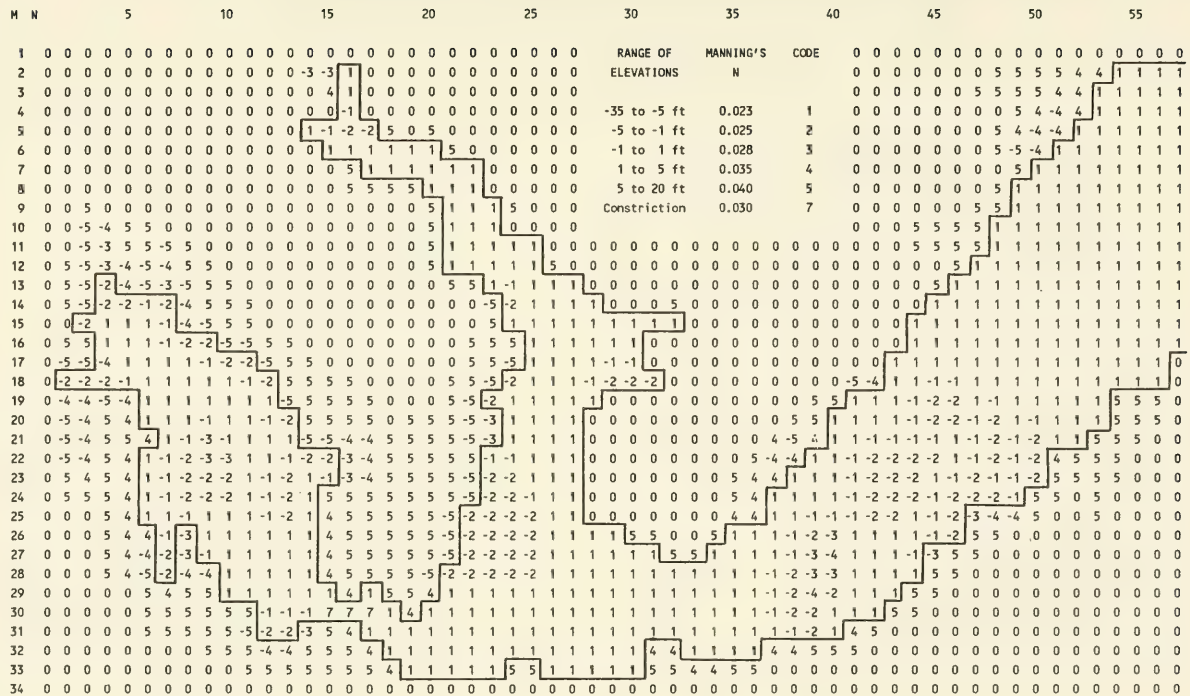

Notes: 0 value represents upland cells

Negative sign (-) denotes cells which can be either flooded or dry

Figure 54. Values of the coded friction array and Manning's n coefficients used in the calibration of tides

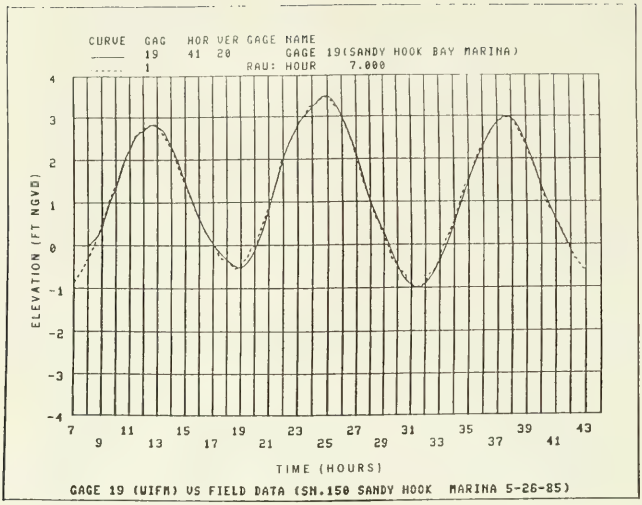

Figure 55. Tide calibration data - Sandy Hook Marina (TG1)

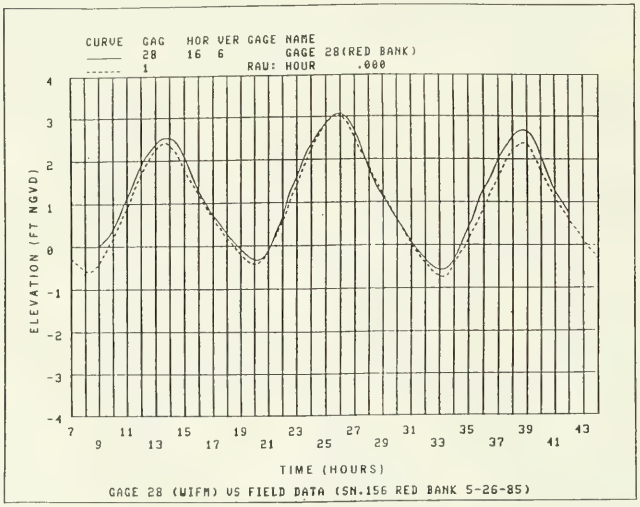

Figure 56. Tide calibration data - Red Bank (TG2)

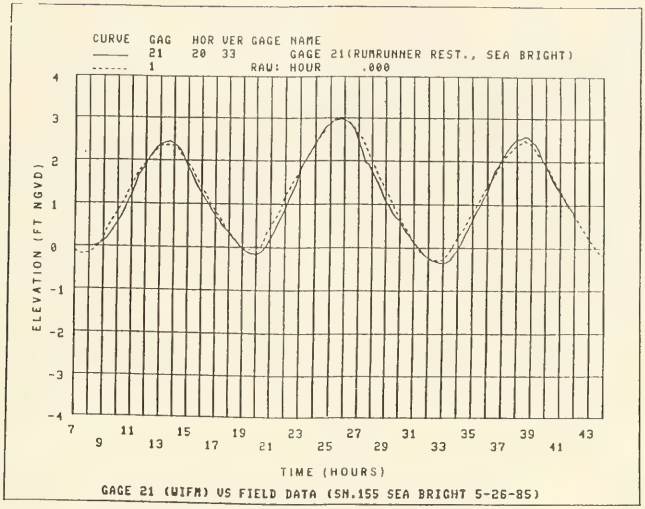

Figure 57. Tide calibration data - Rumrunner Restaurant, Sea Bright (TG3)

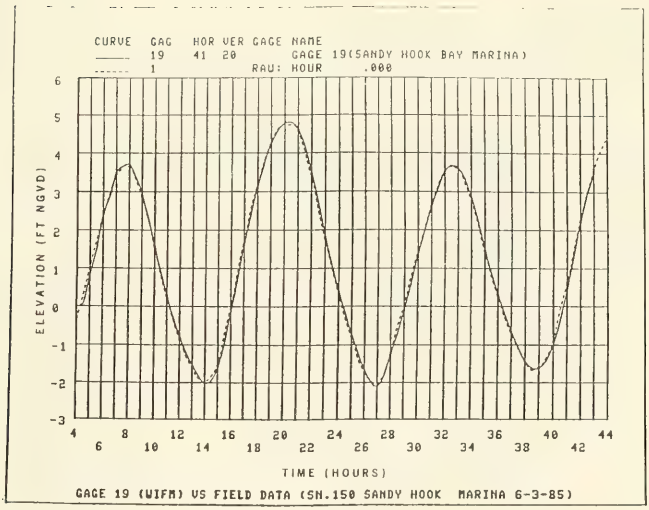

Figure 58. Tide verification data - Sandy Hook Marina (TG1)

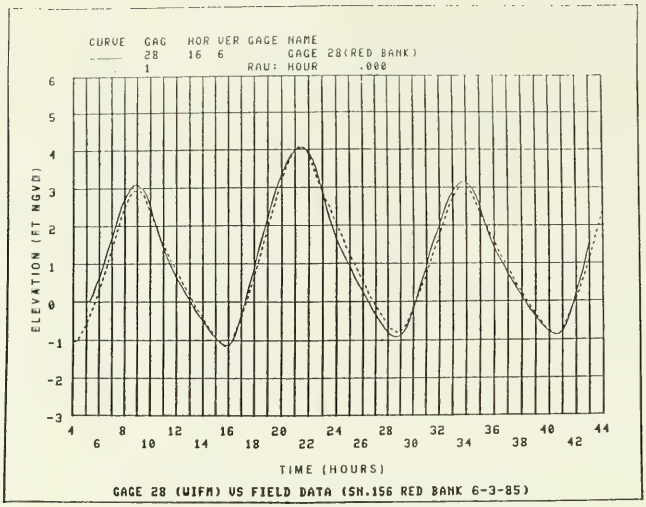

Figure 59. Tide verification data - Red Bank (TG2)

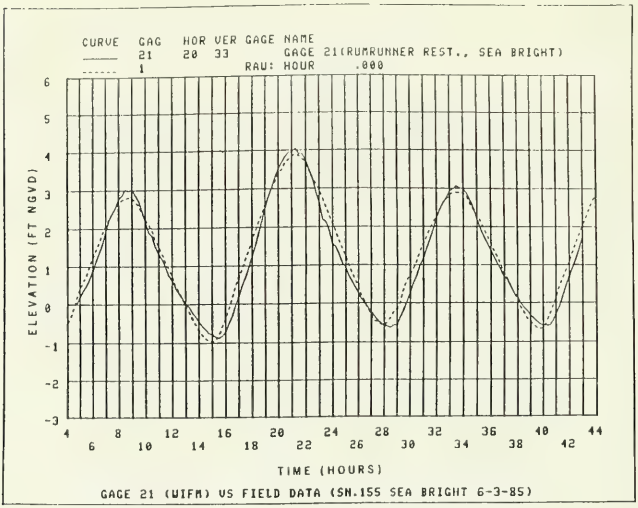

Figure 60. Tide verification data - Rumrunner Restaurant, Sea Bright (TG3)

Table 13

Flood Mark Comparison for the March 1962 Northeaster

Point* No.	Location*	Grid Cell (Y,X)	Flood* Mark (ft)	WIFM Max. Elev. (ft)	WIFM Max. Wave Effects (ft)
33	Highland - Beetle's Drug Store, Corner of Miller St. & Bay Ave.	(36,26)	7.8	8.2	-
34	Highland - Bay Ave. in front of Katz's Confectionary Store	(37,24)	8.5	8.2	-
35	Highland - Intersection of Bay Ave. & Miller St.	(36,26)	7.3	8.2	-
36	Red Bank - Marine Park, at Bulkhead	(15, 6)	9.1	7.0	4.5
37	Red Bank - Marine Park, at Bulkhead	(15, 6)	10.6	7.0	4.5
40	Little Silver - at residence on Point Rd.	(6,14)	9.4	6.6	3.9
41	Little Silver - Gooseneck Point Rd.	(4,15)	5.4	6.8	3.9

* From "Flood Mark Determination for Selected Storm Events," prepared by: VEP Associates, Inc., (1985).

Table 14

Flood Mark Comparison for Hurricane Donna, September 1960

Point* No.	Location*	Grid Cell (Y,X)	Flood* Mark (ft)	WIFM Max. Water Elev. (ft)
25	Highland - Bay Ave. & Valley St. by Katz's Confectionary Store	(36,26)	7.0	9.1
26	Highland - Bay Ave. at Katz's Confectionary Store	(36,26)	9.0	9.1

(Continued)

* From "Flood Mark Determination for Selected Storm Events," prepared by: VEP Associates, Inc., (1985).

Table 14 (Concluded)

Point* No.	Location*	Grid Cell (Y,X)	Flood* Mark (ft)	WIFM Max. Water Elev. (ft)
28	Rumson - Intersection of Waterman Ave. & Grant Ave.	(17,29)	10.4	6.9
29	Red Bank - Marine Park, at Bulkhead	(15, 6)	8.6	7.7
30	Red Bank - Marine Park, at Bulkhead	(15, 6)	9.8	7.7

and reported water levels at locations 33, 34, and 35 for the 1962 storm and locations 26 and 29 for Hurricane Donna.

211. Model results at Red Bank and Little Silver, in the upper reaches of the Navesink and Shrewsbury basins, respectively, are typically much lower than observed water levels. These areas are susceptible to significant increases in water level due to wave setup and wave crest overtopping. As described above, wave setup is not included in model calculations and is considered insignificant in most of the modeled area. To include these effects, procedures similar to those used in the FIMP study were adopted. These procedures reflect the physical principles involved, but are greatly simplified. The maximum wave setup is shown to be 0.15 times the significant wave height. Maximum significant wave heights for the gages in question are approximately 7 and 6 ft, respectively, resulting in wave setups of 1.0 and 0.9 ft. An effective flood elevation, or wave crest elevation, can be expressed as the surge plus tide plus wave setup elevation plus an additional 0.5 times the significant wave height. This calculation allows a total maximum water level of 4.5 and 3.9 ft above the model surge level at Red Bank and Little Silver, respectively. The reader is cautioned to interpret the results with care. These additional levels represent a maximum wave effect occurring at the peak surge plus tide level. However, the difference noted between observed and calculated results is expected since additional water level due to wave effects is not included in the model.

212. Results for the Highland area (near VEP gage points 25 and 26) are good for Hurricane Donna. The 2-ft discrepancy between the flood mark at

gage 25 and that at gage 26 cannot be supported. The 9.1-ft model elevation is representative of the entire lower Sandy Hook Bay area. The comparison at Red Bank can be explained by the omission of wave effect impacts. Winds associated with Donna blew straight down the Navesink basin, peaking at 60 knots just prior to the arrival of the peak surge level. The duration of these winds was much shorter than those experienced during the 1962 northeaster, and consequently the additional water level due to wave setup and wave crest overtopping should be significantly less than that shown in Table 13.

213. The location of VEP gage 28 (Rumson) is on the south side of the entrance to the Shrewsbury basin. As shown in tidal simulations, a significant hydraulic loss occurs across this entrance. Surge plus tide levels in the south Navesink basin are approximately 7.5 ft. With a loss across the entrance and southerly winds blowing, it seems highly unlikely that water levels could reach 10.4 ft as reported by VEP.

214. To make an additional check on the accuracy of using Sandy Hook data to drive the nearshore model and to add confidence to the augmented JPM curve developed for Sandy Hook, a comparison of the Sandy Hook stage-frequency curve with historical data was made. The comparison, presented in Figure 61, confirms that procedures used in the JPM process and boundary condition data are appropriate.

Simulation of Storms

215. Two sets of 20 hurricanes each were simulated on a Cyber 205 computer using the calibrated and verified storm surge model. Boundary conditions for each surge plus tide event were generated from the FIMP data base. The time from the start of hurricane simulation to the time of landfall was computed within WIFM based on the ratio of RM to FS. Faster moving storms require less time for simulation than do slower ones, and hurricanes with large spatial extent require more execution time than smaller storms. The fastest storm was simulated for 18 hr, beginning 12 hr before landfall and ending 6 hr after. For the slowest storm, the simulation was initiated 24 hr before landfall and continued for 10 hr afterward, for a total of 34 hr. For each of the 40 surge hurricane plus tide event time-histories, all maximum still-water levels greater than 6.5 ft NGVD were included in the development of the stage-frequency curves. A time step of 60 sec was used for lower

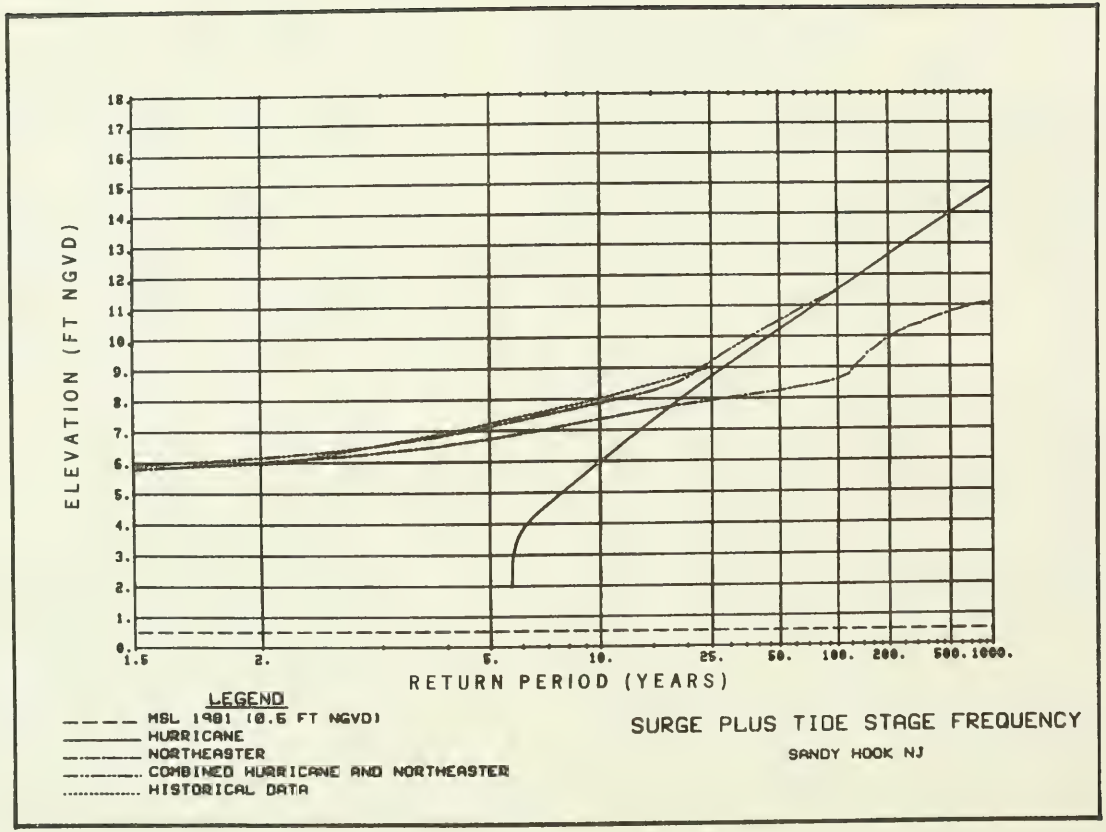

Figure 61. Comparison of JPM results with historical data at Sandy Hook, New Jersey

intensity storms, whereas a 30-sec step was required for accurate simulation of high-intensity events.

216. Figures 62 through 63 display example wind field patterns and isovelocities for synthetic storm No. 847 for simulation hours 9 and 12. This storm had the following parameters: DP = 2.3 in. Hg, RM = 36.0 n.m., FS = 19 knots, TA = -0.5 deg, and LP = (64.2 n.m., 28.0 n.m.). Similar data were developed on file for each storm.

217. Two sets of 20 selected northeasters were also simulated. Simulation time for the storms ranged from 14 to 26 hr. A constant time step of 60 sec was used for all northeaster simulations.

Development of Stage-Frequency Curves

218. The method used to develop the stage-frequency curves is similar to the one used by Hardy and Crawford (1986). For each numerical gage, an array of stage intervals each with a width of 0.1 ft was created. The probability of each storm event was added to the interval bracketing the maximum water level computed for that event. The exceedance, or cumulative probability, for each interval was calculated by adding its probability to the cumulative probability of the next higher interval whose stage is one increment greater.

219. Exceedance was calculated separately for each of the two sets of hurricanes and northeasters producing four separate raw stage-exceedance curves. To smooth these raw stage-frequency curves, linear regression was performed on the cumulative probabilities to compute a straight line through the data. Most linear regression lines resulted in minimum correlation factors of 0.98 for the hurricane sets and 0.96 for the northeaster sets. Figure 64 contains a plot of both raw and regressed stage-frequency curves for the numerical gage at the west end of the I-36 bridge (gage 6).

220. Confidence in the results is obtained by analyzing the variability in the stage frequencies generated by each set of hurricanes and northeasters. Results of this analysis for gages at the entrance to the back-bay river system (gage 6) and in the upper reach of the Navesink basin (gage 12 near Red Bank) are displayed in Figures 65 through 68. By averaging the two sets of regressed curves for both hurricanes and northeasters, a single, more accurate regressed curve for each gage is obtained. These stage-frequency curves for

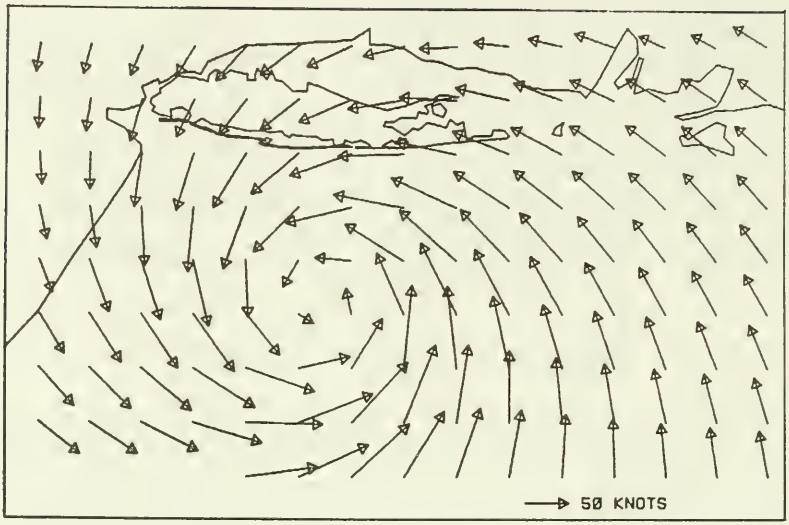

(A) WINDFIELD

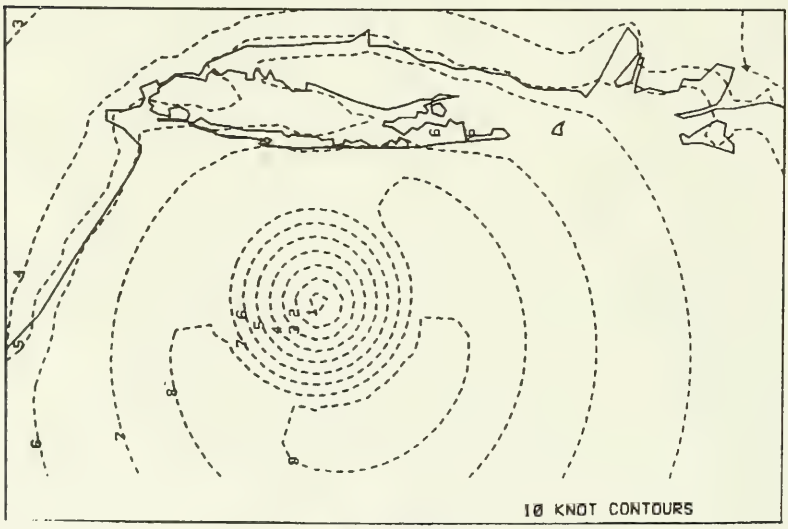

(B) ISOVELS

Figure 62. Wind field and isovelocities, design storm No. 847, hour 9

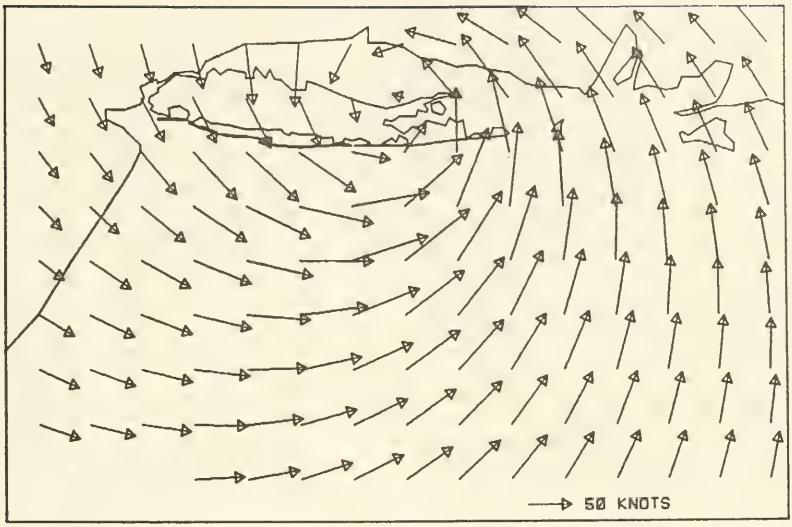

(A) WINDFIELD

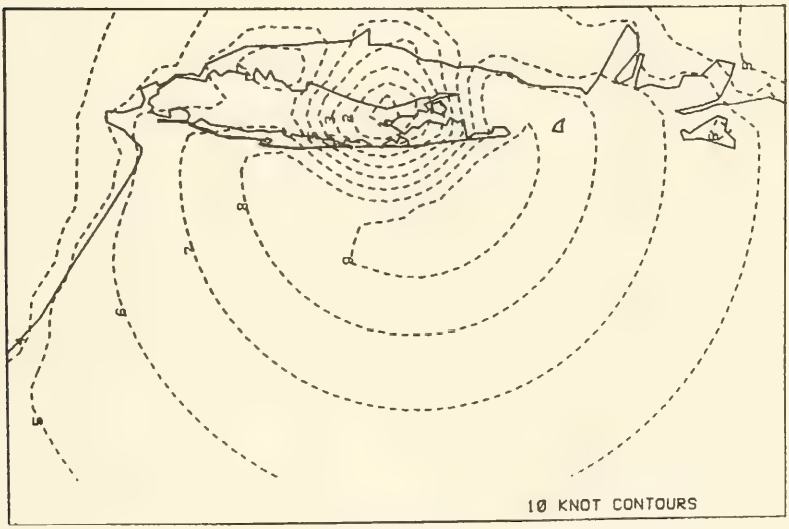

(B) ISOVELS

Figure 63. Wind field and isovelocities, design storm No. 847, hour 12

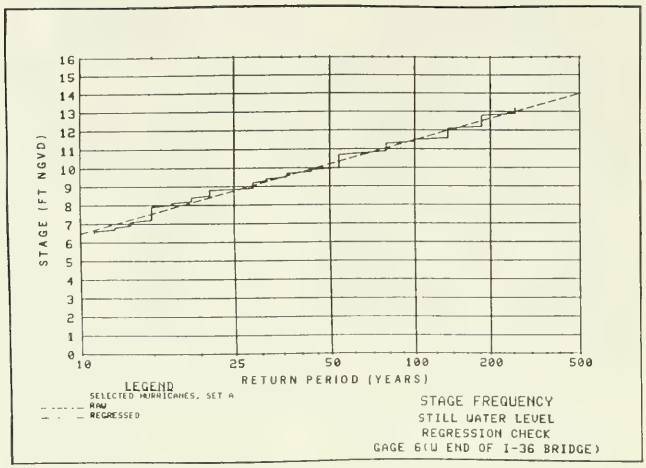

Figure 64. Example of raw and regressed stage-frequency curves

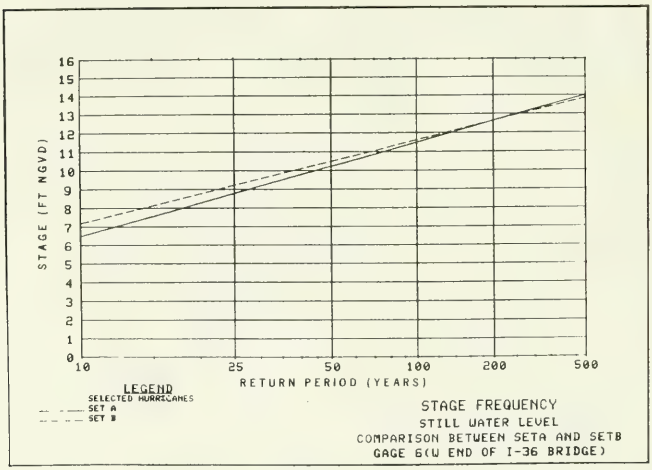

Figure 65. Variability in stage frequency for the two hurricane data sets at gage 6

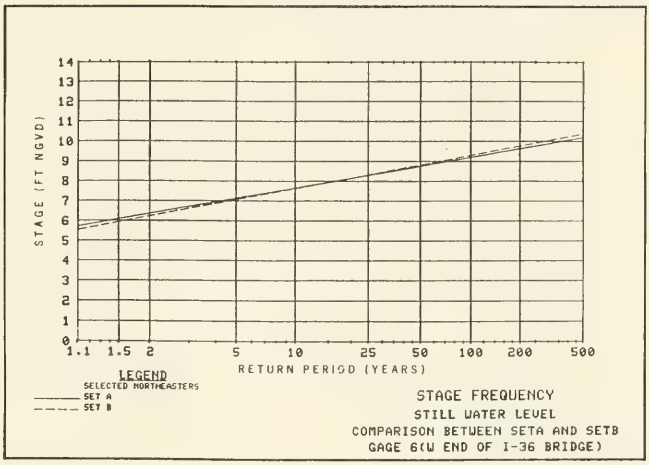

Figure 66. Variability in stage frequency for the two northeaster data sets at gage 6

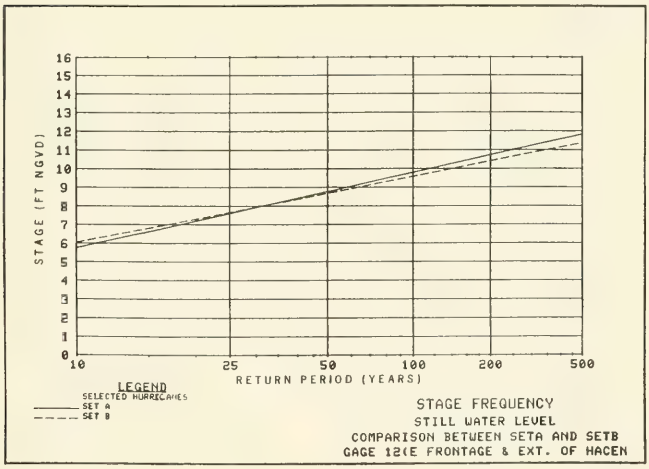

Figure 67. Variability in stage frequency for the two hurricane data sets at gage 12

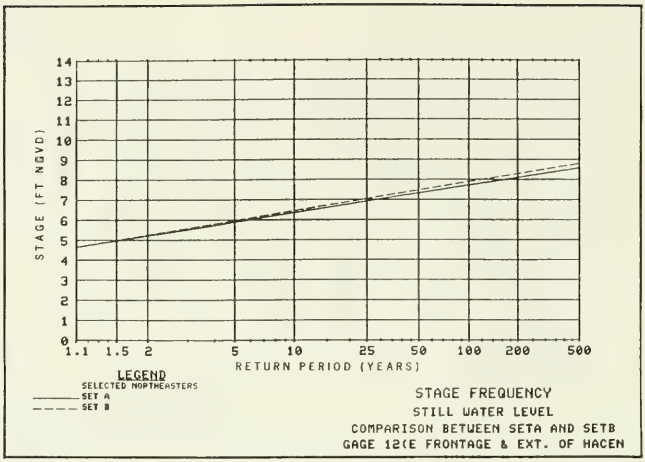

Figure 68. Variability in stage frequency for the two northeaster data sets at gage 12

hurricanes and northeasters are presented in Appendix G for each of the 20 numerical gages. Locations of all gages are shown in Figure 53.

221. The required final product is a single stage-frequency curve for the combined hurricane- and northeaster-induced water level. This combined frequency curve was obtained by adding the exceedance probabilities of hurricanes and northeasters at each stage increment. Combined regressed frequency curves for gages 6 and 12 are shown in Figures 69 and 70; curves for all 20 numerical gages are presented in Appendix G.

222. The combined stage-frequency curves discussed above do not include any additional still-water level increase due to wave setup or wave crest overtopping. Most channels within the river system are narrow and do not provide adequate fetch lengths for these processes to occur. However, the upper reaches of the Navesink and Shrewsbury basins are susceptible to such wave impacts. Standard methods given in the SPM (1984) were applied to estimate the maximum wave setup and wave crest elevation that can be expected in these areas. Results for these estimates are shown in Figures 71 and 72 for numerical gages 15 and 18.

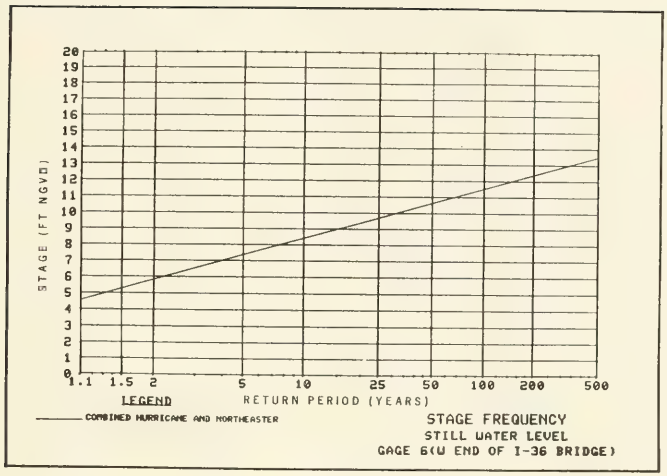

Figure 69. Stage frequency for the combined hurricane- and northeaster-induced water level at gage 6

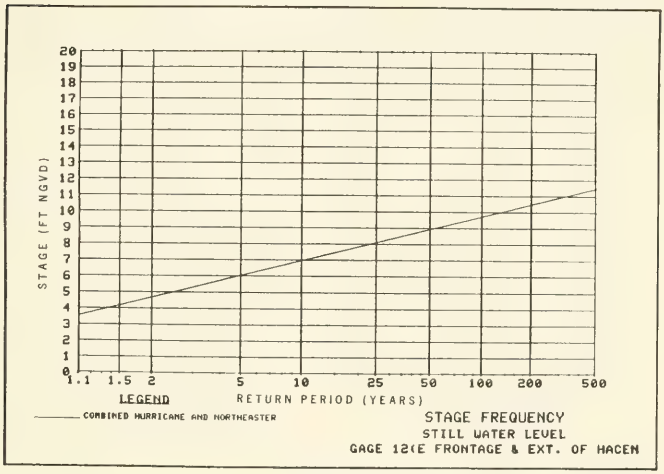

Figure 70. Stage frequency curve for the combined hurricane- and northeaster-induced water level at gage 12

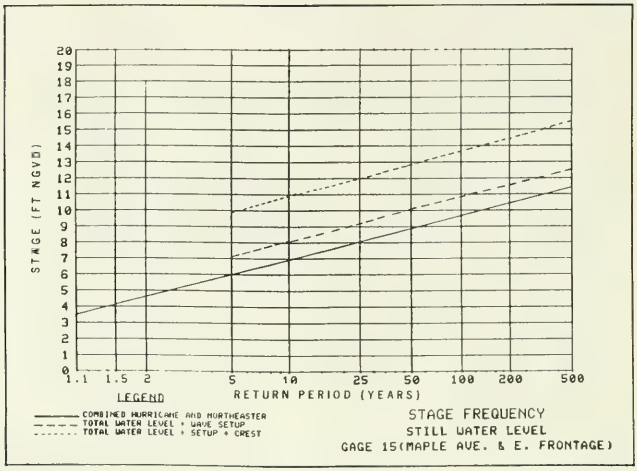

Figure 71. Estimation of maximum wave effects in the upper Navesink basin (gage 15)

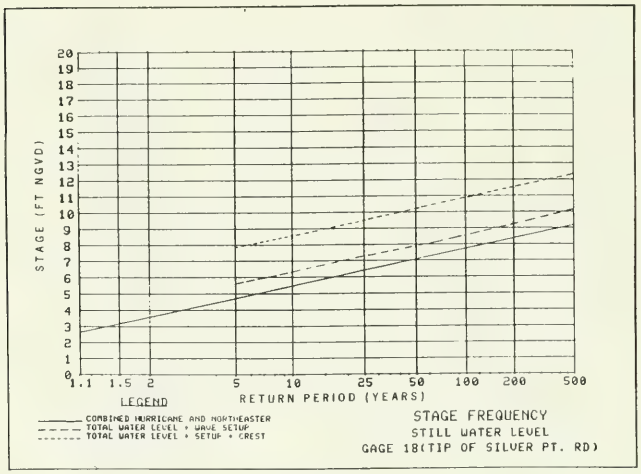

Figure 72. Estimation of maximum wave effects in the upper Shrewsbury basin (gage 18)

Stage frequency at Monmouth Beach

223. Stage-frequency results for the Monmouth Beach gage are representative of the open-coast stage frequency in the entire project area. Results for the Monmouth Beach gage were reported in the FIMP study; however, the set of hurricane parameters chosen for the FIMP study did not account for some storms which may impact the New Jersey coast. As previously discussed, 54 storms were modeled to augment those in the FIMP project. The stage-frequency curve at Sandy Hook was not significantly altered in the new analysis. The curve derived from the new analysis for Monmouth Beach is shown in Figure 73.

224. Wave setup is not included in the surge modeling, and the wave effect contribution to total water level can be significant. To include this effect at Monmouth Beach, the same procedures used in the FIMP study were adopted (as discussed earlier). The frequency curve for Monmouth Beach was discretized into seven intervals according to flood heights. All storms contributing to a given part of the stage-frequency curve were analyzed and an average maximum wind speed (and, hence, an average significant wave height) was assigned to the mid-point of each interval. Wave setup was calculated for each interval and curves were fitted through these data points to display wave effect contributions. The resulting curves are also presented in Figure 73.

225. The accuracy of wave effect results (Figures 71-73) suffers because of the simplifying assumptions made as well as a lack of information available as to the physical processes involved. These results do give a good indication of the magnitude of wave influence on back-bay and open-coast stage frequencies.

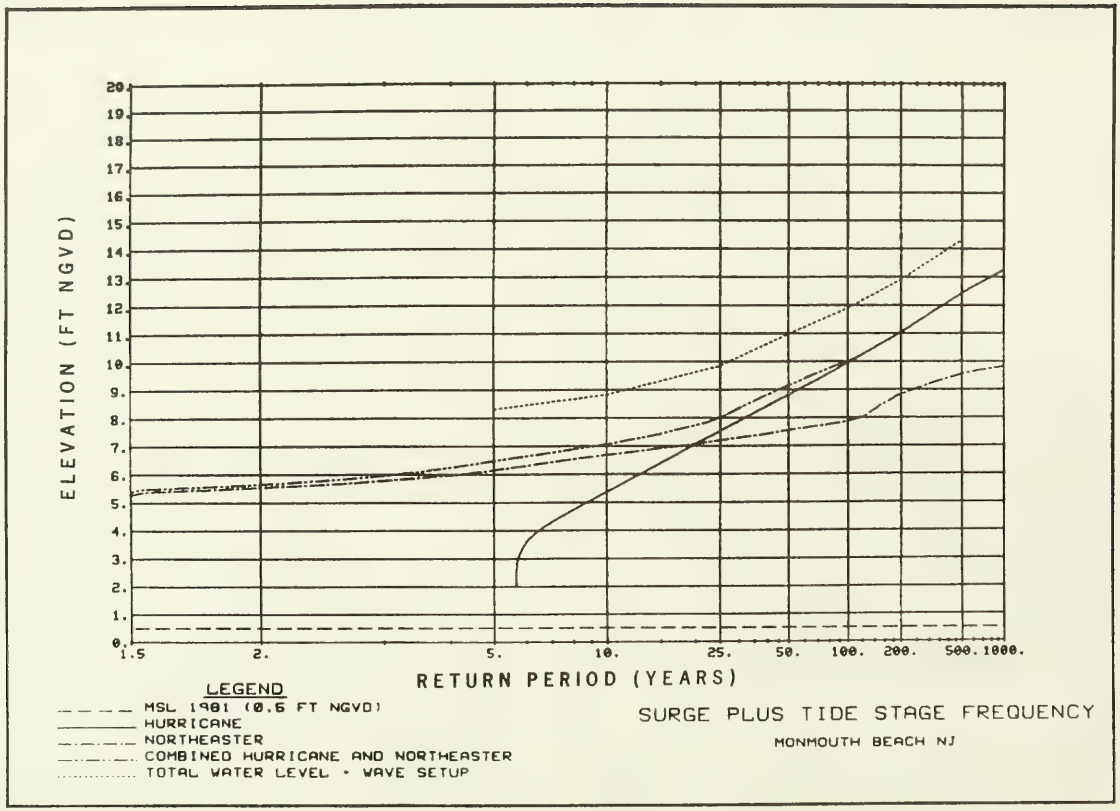

Figure 73. Stage frequencies at Monmouth Beach, New Jersey

Allen, J. R. 1981a. "Beach Erosion as a Function of Variations in the Sediment Budget, Sandy Hook, New Jersey," Earth Sciences Processes, Vol 6, pp 139-150.

_____. 1981b. "Theoretical Model of Shoreline Dynamics at Sandy Hook, N.J.," Northeastern Geology, Vol 3, pp 243-251.

_____. 1985. "Field Evaluation of Beach Profile Response to Wave Steepness as Predicted by the Dean Model," Coastal Engineering, Vol 9, pp 71-80.

Allen, J. R., and Nordstrom, K. F. 1977a. "Beach Form Changes in the Lee of Groins at Sandy Hook, N.J.," Proceedings of Coastal Sediments '77, American Society of Civil Engineers, pp 33-47.

_____. 1977b. "A Computer Simulation Model of Shoreline Dynamics for Sandy Hook, New Jersey," Committee on Marine Geography, Proceedings of the Marine Geography Specialty Committee, Association of American Geographers, pp 290-300.

Alpine Ocean Seismic Survey. November 1985. "Sand Inventory Investigation Proposed for the Offshore Area of New Jersey, Between Sea Bright and Ocean Township," unpublished Revised Final Report, prepared for US Army Engineer District, New York.

_____. February 1986. "Remote Sensing of Proposed Offshore Sand Borrow Areas," unpublished Draft Report for Atlantic Coast of New Jersey Sea Bright to Ocean Township, prepared for US Army Engineer District, New York.

Ashley, G. M., Halsey, S. D., and Buteux, C. B. 1986. "New Jersey's Longshore Current Pattern," Journal of Coastal Research, Vol 2, pp 453-463.

Birkemeier, W. 1984. "A User's Guide to ISRP: The Interactive Survey Reduction Program," Instruction Report CERC-84-1, US Army Engineer Waterways Experiment Station, Coastal Engineering Research Center, Vicksburg, Miss.

Birkemeier, W. A., Kraus, N. C., Scheffner, N. W., and Knowles, S. C. 1987. "Feasibility Study of Quantitative Erosion Models for Use by the Federal Emergency Management Agency in the Prediction of Coastal Flooding," Technical Report CERC-87-8, US Army Engineer Waterways Experiment Station, Coastal Engineering Research Center, Vicksburg, Miss.

Bruun, P. 1954. "Coast Erosion and the Development of Beach Profiles," TM-44, US Army Corps of Engineers, Beach Erosion Board.

_____. 1962. "Sea-Level Rise as a Cause of Shore Erosion," Journal of Waterways and Harbor Division, American Society of Civil Engineers. Vol 88, pp 117-130.

Butler, H. L. 1978. "Coastal Flood Simulations in Stretched Coordinates," Proceedings of the 16th International Conference on Coastal Engineering, American Society of Civil Engineers, pp 1030-1048.

_____. 1983. "Lake Pontchartrain and Vicinity Hurricane Protection Plan, Report 3, Numerical Model Investigation of Plan Impact On the Tidal Prism of Lake Pontchartrain," Technical Report HL-82-2, US Army Engineer Waterways Experiment Station, Vicksburg, Miss.

Butler, H. L., and Prater, M. D. 1987. "Innovative Determination of Nearshore Flood Frequency," Proceedings of the 20th Coastal Engineering Conference, American Society of Civil Engineers, pp 2463-2476.

Caldwell, J. M. 1959. "Shore Erosion by Storm Waves," Miscellaneous Paper No. 1-59, US Army Corps of Engineers, Beach Erosion Board.

_____. 1966. "Coastal Processes and Beach Erosion," Journal of the Society of Civil Engineers, Vol 53, No. 2, pp 142-157. (Also reprinted with an abstract and errata as Reprint Report I-67, US Army Coastal Engineering Research Center, Corps of Engineers, 1967.)

Carol R. Johnson & Associates, Inc. 1978. "Storm Report, Revere Beach Reservation," unpublished report prepared for US Army Engineer Division, New England.

Coastal Planning and Engineering, Inc. Undated. "Sea Bright to Ocean Township, N.J. Groin Inspection Sheets," Boca Raton, Fla.

Corps of Engineers. 1954. "Atlantic Coast of New Jersey, Sandy Hook to Barnegat Inlet," US Army Engineer District, New York, Beach Erosion Control Report on Cooperative Study (Survey), Serial No. 38.

_____. 1964. "A Pictorial History of Selected Structures Along the New Jersey Coast," US Army Coastal Engineering Research Center, Miscellaneous Paper No. 5-64, 99 pp.

_____. 1984. "Reanalysis of The Federally Authorized Project Atlantic Coast of New Jersey Sandy Hook to Barnegat Inlet with Emphasis on Sea Bright to Monmouth Beach," US Army Engineer District, New York.

_____. 1986. Unpublished data on storm erosion at Revere Beach, Massachusetts, US Army Engineer Division, New England.

Dean, R. G. 1977. "Equilibrium Beach Profiles: U.S. Atlantic and Gulf Coasts," Ocean Engineering Report No. 12, Department of Civil Engineering, University of Delaware, Newark, Del.

Dendrou, S. A., Moore, C. I., and Taylor, R. S. December 1981. "New York City Flood Insurance Study, Report No. 6, Northeaster Methodology and Analysis," Camp Dresser and McKee, Inc.

Ebersole, B. A., Prater, M. A., and Cialone, M. A. 1986. "Regional Coastal Processes Numerical Modeling System; Report 1 RCPWAVE - A Linear Wave Propagation Model for Engineering Use," Technical Report CERC-86-4, US Army Engineer Waterways Experiment Station, Coastal Engineering Research Center, Vicksburg, Miss.

Fairchild, J. C. 1966. "Correlation of Littoral Transport with Wave Energy Along Shores of New York and New Jersey," Technical Memorandum No. 18, US Army Engineer Waterways Experiment Station, Coastal Engineering Research Center, Vicksburg, Miss.

Farrell, S. C. 1981. "An Evaluation of Longshore Sand Transport at Manasquan Inlet, New Jersey," unpublished report prepared for US Army Engineer District, Philadelphia.

Gares, P. A. 1981. "Historical Analysis of Shoreline Changes at Sandy Hook Spit," in Assessment of Management Problems and Management Strategies for the Shoreline of Sandy Hook Spit, Gateway National Recreational Area, Vol II, Technical Appendices, Center for Coastal and Environmental Studies, Rutgers University, New Brunswick, N. J., pp 15-50.

Gorman, L. T. 1988. "Geomorphic Development of Northern New Jersey Beaches, Sea Bright to Ocean Township, with Annotated Bibliography," US Army Engineer Waterways Experiment Station, Coastal Engineering Research Center, Vicksburg, Miss.

Hallermeier, R. F. 1979. "Uses for a Calculated Limit Depth to Beach Erosion," Proceedings of the 16th Coastal Engineering Conference, American Society of Civil Engineers, pp 1493-1512.

_____. 1983. "Sand Transport Limits in Coastal Structure Designs," Proceedings Coastal Structures '83, American Society of Civil Engineers, pp 703-716.

Hanson, H. 1987. "GENESIS - A Generalized Shoreline Change Numerical Model for Engineering Use," unpublished PhD Dissertation, Department of Water Resources Engineering, Lund University, Lund, Sweden.

Hanson, H., and Kraus, N. C. 1986. "Seawall Boundary Condition in Numerical Models of Shoreline Evolution," Technical Report CERC-86-3, US Army Engineer Waterways Experiment Station, Coastal Engineering Research Center, Vicksburg, Miss.

_____. In preparation. "Generalized Shoreline Simulation System, Report 1, GENESIS--A Shoreline Change Numerical Simulation Model for Engineering Use," US Army Engineer Waterways Experiment Station, Coastal Engineering Research Center, Vicksburg, Miss.

Hardy, T. A., and Crawford, P. L. 1986. "Frequency of Coastal Flooding at Roughans Point, Broad Sound, Lynn Harbor, and the Sangus-Pines River System," Technical Report CERC 86-8, US Army Engineer Waterways Experiment Station, Vicksburg, Miss.

Helle, J. R. 1958. "Surf Statistics for the Coasts of the United States," Technical Memorandum No. 108, US Army Corps of Engineers, Beach Erosion Board.

Heritage Studies. August 1985. "A Cultural Resources Reconnaissance for the New Jersey Shore from Highland Beach, Sea Bright to Deal Lake: Loch Arbour Boroughs of Sea Bright and Monmouth Beach, City of Long Branch, Boroughs of Deal and Allenhurst, Village of Loch Arbour, Monmouth County, New Jersey," unpublished report prepared for US Army Engineer District, New York.

Hicks, S. D. 1978. "An Average Geopotential Sea Level Series for the United States," Journal of Geophysical Research, Vol 83, No. C3, pp 1377-1379.

Hicks, S. D., Debaugh, Jr., H. A., and Hickman, Jr., L. E. 1983. "Sea Level Variations for the United States 1855-1980," National Oceanic and Atmospheric Administration, Rockville, Md.

Horikawa, K., Sasaki, T., and Sakuramoto, H. 1977. "Mathematical and Laboratory Models of Shoreline Changes due to Dredged Holes," Journal of the Faculty of Engineering, Vol XXXIV, No. 1, The University of Tokyo, Tokyo, Japan, pp 49-57.

Hughes, S. A. 1978. "The Variation in Beach Profiles When Approximated by a Theoretical Curve," unpublished M.S. Thesis, Coastal and Oceanographical Engineering Department, University of Florida, Gainesville, Fla.

_____. 1984. "The TMA Shallow-Water Spectrum Description and Applications," Technical Report CERC 84-7, US Army Engineer Waterways Experiment Station, Coastal Engineering Research Center, Vicksburg, Miss.

Jensen, R. E. 1983. "Methodology for the Calculation of a Shallow Water Wave Climate," Wave Information Study Report No. 8, US Army Engineer Waterways Experiment Station, Coastal Engineering Research Center, Vicksburg, Miss.

Kondolf, G. M. 1978. "Genesis and Development of Sandy Hook, New Jersey," unpublished Senior Thesis, Department of Geological and Geophysical Sciences, Princeton University, Princeton, N. J.

Kraus, N. C. 1983. "Applications of a Shoreline Prediction Model," Proceedings of Coastal Structures '83, American Society of Civil Engineers, pp 632-645.

Kraus, N. C., and Dean, J. L. 1987. "Longshore Sediment Transport Rate Distributions Measured by Trap," Proceedings Coastal Sediments '87, American Society of Civil Engineers, pp 881-896.

Kraus, N. C., and Harikai, S. 1983. "Numerical Model of the Shoreline Change at Oarai Beach," Coastal Engineering, Vol 7, No. 1, pp 1-28.

Kraus, N. C., Gravens, M. B., and Mark, D. J. 1988. "Coastal Processes at Sea Bright to Ocean Township, Report 2: Appendices," US Army Engineer Waterways Experiment Station, Coastal Engineering Research Center, Vicksburg, Miss.

Kraus, N. C., Hanson, H., and Harikai, S. 1985. "Shoreline Change at Oarai Beach: Past, Present and Future," Proceedings of the 19th Coastal Engineering Conference, American Society of Civil Engineers, pp 2107-2123.

Kriebel, D. L. 1982. "Beach and Dune Response due to Hurricanes," unpublished M.S. Thesis, Department of Civil Engineering, University of Delaware, Newark, Del.

_____. 1984a. "Beach Erosion Model (EBEACH) Users Manual, Volume I: Description of Computer Model," Beaches and Shores Technical and Design Memorandum No. 84-5-I, Division of Beaches and Shores, Florida Department of Natural Resources.

_____. 1984b. "Beach Erosion Model (EBEACH) Users Manual, Volume II: Theory and Background," Beaches and Shores Technical and Design Memorandum No. 84-5-II, Division of Beaches and Shores, Florida Department of Natural Resources.

Kriebel, D. L., and Dean, R. G. 1985a. "Beach and Dune Response to Severe Storms," Proceedings of the 19th Coastal Engineering Conference, American Society of Civil Engineers, pp 1584-1599.

_____. 1985b. "Numerical Simulation of Time-Dependent Beach and Dune Erosion," Coastal Engineering, Vol 9, pp 221-245.

Kughler Co., Inc. Undated. "Vibracore Photos, Penetration Graphs, Geological Descriptions, Monmouth Beach - Sea Bright - Belmar Aread (sic)," unpublished report prepared for US Army Engineer District, New York.

Le Mehaute, B., and Soldate, M. 1980. "A Numerical Model for Predicting Beach Changes," Miscellaneous Report No. 80 (6), US Army Corps of Engineers, Coastal Engineering Research Center, Vicksburg, Miss.

Meyers, V.A. 1970. "Joint Probability Method of Tide Frequency Analysis Applied to Atlantic City and Long Beach Island, N.J.," ESSA Technical Memorandum WBTM HYDRO 11, US Department of Commerce, Environmental Science Services Administration, Weather Bureau, Silver Springs, Md.

Moore, B. 1982. "Beach Profile Evolution in Response to Changes in Water Level and Wave Height," unpublished M.S. Thesis, Department of Civil Engineering, University of Delaware, Newark, Del.

Motyka, J. M., and Willis, D. H. 1975. "The Effect of Wave Refraction Over Dredged Holes," Proceedings of the 14th Coastal Engineering Conference, American Society of Civil Engineers, pp 615-625.

National Oceanic and Atmospheric Administration. 1985. "Tide Tables 1985 - High and Low Water Predictions - East Coasts of North and South America," US Department of Commerce, NOS, Rockville, Md.

National Weather Service. September 1979. "Meteorolgical Criteria for Standard Project Hurricane and Probable Maximum Hurricane Windfields, Gulf and East Coasts of United States," NOAA Technical Report NWS 23, US Department of Commerce, Washington, DC.

Nordstrom, K. F. 1975. "Beach Response to Cyclic and Seasonal Wave Regimes at Sandy Hook, N.J.," Marine Science Center Technical Report No. 75-3, Rutgers University, New Brunswick, N. J., 57 pp plus appendices.

Nordstrom, K. F., Allen, J. R., Sherman, D. J., Psuty, N. P., Nakashima, L. D., and Gares, P. A. 1982. "Applied Coastal Geomorphology at Sandy Hook, New Jersey," in Assessment of Management Problems and Management Strategies for the Shoreline of Sandy Hook Unit, Gateway National Recreation Area, Vol I, Center for Coastal and Environmental Studies, Rutgers University, New Brunswick, N. J., 88 pp.

Ozasa, H., and Brampton, A. H. 1980. "Mathematical Modeling of Beaches Backed by Seawalls," Coastal Engineering, Vol 4, No. 1, pp 47-64.

Phillips, J. D. 1985. "Headland-Bay Beaches Revisited: An Example from Sandy Hook, New Jersey," Marine Geology, Vol 65, pp 21-31.

Phillips, J. D., Psuty, N. P., and McCluskey, J. M. 1984. "The Impact of Beach Nourishment at South Beach, Sandy Hook, New Jersey," Final Report, Center for Coastal and Environmental Studies, Rutgers University, New Brunswick, N. J., 30 pp.

Perlin, M., and Dean, R. G. 1979. "Prediction of Beach Planforms with Littoral Controls," Proceedings of the 16th Coastal Engineering Conference, American Society of Civil Engineers, pp 1818-1838.

_____. 1983. "A Numerical Model to Simulate Sediment Transport in the Vicinity of Structures," Miscellaneous Report No. 83-10, US Army Engineer Waterways Experiment Station, Coastal Engineering Research Center, Vicksburg, Miss.

Pore, N. A., and Barrientos, C. S. 1976. "Storm Surge," New York Sea Grant Institute, Albany, N. Y.

Prater, M. D., Butler, H. L., and Hardy, T. A. In preparation. "Fire Island to Montauk Point, New York, Storm Surge Model Study, Report 1, Model Calibration and Verification," Technical Report, US Army Engineer Waterways Experiment Station, Vicksburg, Miss.

Prater, M. D., Hardy, T. A., and Butler, H. L. In preparation. "Fire Island to Montauk Point, New York, Storm Surge Model Study, Report 2, Stage Frequency Calculations," US Army Engineer Waterways Experiment Station, Coastal Engineering Research Center, Vicksburg, Miss.

PRC Harris, Inc. 1980. "Manasquan Inlet, Special Study of Sand By-Passing," unpublished final report prepared for US Army Engineer District, Philadelphia.

Price, W. A., Tomlinson, K. W., and Willis, D. H. 1973. "Predicting the Change in Plan Shape of Beaches," Proceedings of the 13th Coastal Engineering Conference, American Society of Civil Engineers, pp 1321-1329.

Sasaki, T. 1975. "Simulation of Shoreline and Nearshore Current," Proceedings of Civil Engineering in the Oceans III, American Society of Civil Engineers, pp 179-196.

Sasaki, T. O., and Sakuramoto, H. 1978. "Field Verification of a Shoreline Numerical Model," Proceedings of the International Conference of Water Resources Engineering, International Association of Hydraulic Research, pp 501-518.

Savage, R. J., and Birkemeier, W. A. 1987. "Storm Erosion Data from the United States Atlantic Coast," Proceedings of Coastal Sediments '87, American Society of Civil Engineers, pp 1445-1459.

Saville, T., Jr. 1954. "North Atlantic Coast Wave Statistics Hindcast by Bretschneider-Revised Sverdrup-Munk Method," Technical Memorandum No. 55, US Army Corps of Engineers, Beach Erosion Board.

Shore Protection Manual. 1984. 4th ed., 2 Vols. US Army Engineer Waterways Experiment Station, Coastal Engineering Research Center, US Government Printing Office, Washington, DC.

Slezak, W. F., Phillips, J. D., Allen, J. R., and Psuty, N. P. 1984. "Sediment Recycling and Beach Nourishment for Sandy Hook, N.J.," Proceedings of Dredging '84, American Society of Civil Engineers, pp 1072-1080.

VEP Associates, Inc. 1985. "Flood Mark Determination for Selected Storm Events," unpublished report prepared for US Army Engineer District, New York.

Weggel, J. R. 1986. "Economics of Beach Nourishment Under Scenario of Rising Sea Level," Journal of Waterway, Port, Coastal and Ocean Engineering, American Society of Civil Engineers, Vol 112, No. 3, pp 418-426.

Willis, D. H., and Price, W. A. 1975. Trends in the Application of Research to Solve Coastal Engineering Problems, In: J. Hails and A. Carr (eds), Nearshore Sediment Dynamics and Sedimentation, Wiley, New York, N. Y., pp 111-121.

APPENDIX A: NOTATION

a	Sand porosity
A	Parameter determining equilibrium beach shape
B	Sand bypassing factor
C_{gb}	Wave group velocity at breaking given by linear wave theory
D	Wave energy dissipation in the surf zone
D_c	Depth of closure
D_{eq}	Equilibrium wave energy dissipation in the surf zone
D_g	Depth at seaward end of groin
DP	Pressure deficit of a synthetic hurricane
F	Wave energy flux by linear wave theory
FS	Forward speed of a synthetic hurricane
h	Water depth
H_b	Breaking wave height
H_{mo}	Energy-based wave height
H_s	Significant wave height
H_{savg}	Average significant wave height
H_{smax}	Maximum significant wave height
i	Grid cell number
k	Empirical coefficient in cross-shore transport rate equation
K_1, K_2	Calibration parameters in shoreline change model
LP	Landfall point of a synthetic hurricane
L_s	Deep water wavelength
n	Manning's roughness
Q	Volume rate of longshore sand transport
Q_c	Volume rate of cross-shore sand transport
RM	Radius of maximum wind of a synthetic hurricane
S	Ratio of sand density to water density
t	Time
$\tan(\beta)$	Beach slope
TA	Track angle of a synthetic hurricane
T_p	Peak spectral wave period
x	Coordinate direction
y	Coordinate direction
Ycalc	Calculated shoreline position

Ydiff	Difference indicator of shoreline position
Ymeas	Measured shoreline position
θ_{bs}	Breaking wave angle to the shoreline